# METHODS FOR CATHODIC INHIBITOR EVALUATION IN NEUTRAL COOLING WATER SYSTEMS

BY

DAVID FERREDAY

A DOCTORAL THESIS

Submitted in partial fulfilment of the requirements for the award of Doctor of Philosophy of the Loughborough University of Technology, August 1992.

SUPERVISOR: Dr P.J. Mitchell

SPONSOR: S.E.R.C. and
Grace Dearborn Chemicals Ltd.

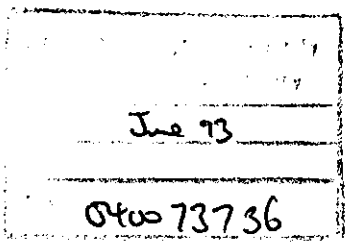

The work described in this thesis has not been submitted in full, or in part, to this or any other institution for a higher degree.

## ACKNOWLEDGEMENTS

My thanks go to my Supervisor, Dr. P.J. Mitchell for his continued help, encouragement and patience throughout the duration of my project, but most of all for his friendship. May it continue in the years ahead.

I am grateful to Grace Dearborn Ltd. for their financial support and advice.

The lads in 'the group' deserve much more than just a mention. I would like to thank them all for their help and friendship through-out.

My greatest thanks go, however, to Lesley-Jane for her understanding, patience and love.

## DEDICATION

*To my Mother and Father .....*

*for their love, encouragement and support.*

*THANKYOU.*

## SUMMARY

Water soluble corrosion inhibitors are acknowledged as the most effective and cost efficient method for protecting mild steel cooling water systems. However, before an inhibitor is used, it's effectiveness must be ascertained. This is usually accomplished using long term rig tests. These are simplified, scaled down versions of industrial systems, in which cooling water conditions are closely simulated. Corrosion rates are calculated from weight loss measurements. These take weeks or even months to complete. Hence with shorter product deadlines, rig tests often prove too lengthy to satisfy commercial pressures.

The objectives of the work reported in this thesis were to investigate and develop methods for quick, yet accurate inhibitor evaluation, with the view to replacing, or at least supplementing traditional weight loss techniques. The study of cathodic inhibitors, was emphasised as being particularly important because of their increased use in new commercial formulations.

The problems associated with conventional oxygen reduction studies at a rotating disc electrode are discussed in detail. The development of three alternative techniques are then considered. First, a concentration step method for cathodic inhibitor evaluation. Second, the use of a differential aeration cell for both anodic and cathodic inhibitor monitoring, and finally the use of a potentiostat controlled flow-through cell.

The concentration step method proved useful for comparing cathodic inhibitors, but gave little mechanistic detail and no kinetic data. The differential aeration cell proved more useful for mechanistic studies on both anodic and cathodic inhibitor systems, and gave some interesting information regarding the dual nature of certain well known inhibitors. The flow-through cell proved the best evaluative technique and was useful for studies on both pre-corroded and clean surfaces. The results obtained gave good correlation with those from rig tests in a fraction of the time.

# CONTENTS

## LIST OF SYMBOLS

| | | |
|---|---|---|
| a | Tafel Intercept | - |
| A | Electrode area or Amperes | $m^2$ or A |
| $A_{f,b}$ | Arrhenius constant for forward/backward reaction | - |
| b | Tafel slope | V/decade |
| C | Capacity of an electrode or concentration | F or mol $m^{-3}$ |
| $C_{dl}$ | Double layer capacitance | F |
| $C_c$ | Differential capacitance of compact layer | F $m^{-2}$ |
| Cd | Differential capacitance of diffuse layer | F $m^{-2}$ |
| $C_o^b, R^b$ | Bulk concentrations of oxidised/reduced species | mol $m^{-3}$ |
| $C_o^s, R^s$ | Surface concentrations of oxidised/reduced species | mol $m^{-3}$ |
| $C_j$ | Concentration of species j | mol $m^{-3}$ |
| $D_{o,R}$ | Diffusion coefficient of oxidised/reduced species | mol $m^{-3}$ |
| $D_j$ | Diffusion coefficient of species j | mol $m^{-3}$ |
| e | The electron | - |
| e | Electronic charge (1.604 x $10^{-19}$ C) | C |
| E | Electrode potential | V |
| $E^\theta$ | Standard electrode potential | V |
| $E_{corr}$ | Corrosion potential | V |

| | | |
|---|---|---|
| $E_i$ | Initial electrode potential | V |
| $E_f$ | Final electrode potential | V |
| $E_p$ | Peak potential | V |
| $E_r$ | Reversible potential | V |
| $E_z$ | Potential of zero charge | V |
| f | Frequency | revs $s^{-1}$ |
| F | The Faraday constant (96487 C $mol^{-1}$) | |
| G | Gibbs Free energy | J $mol^{-1}$ |
| I | Current density | A $m^{-2}$ |
| i | Current | A |
| $i_{corr}$ | Corrosion current | A |
| $i_o$ | Exchange current | A |
| $i_p$ | Peak current | A |
| $i_L$ | Limiting current | A |
| $i_{f,b}$ | Cathodic, anodic partial current | A |
| $i_\infty$ | Current at infinite rotation speed | A |
| $J_j$ | Flux of species j | mol $m^{-2}$ $s^{-1}$ |
| $k_{f,b}$ | Cathodic, anodic rate constant | m $s^{-1}$ |
| $k^o$ | Standard rate constant | m $s^{-1}$ |
| M | Molar | - |
| n | number of electrons | - |
| O | Oxidised species | - |
| Pr | Prandtl number | - |

| | | |
|---|---|---|
| q | Flux | C |
| R | Reduced species | - |
| Rp | Polarisation resistance | ohm |
| R | Gas constant (8.314 J $K^{-1}mol^{-1}$) | |
| t | time | s |
| T | Temperature | K |
| Uo | fluid velocity | $m^2\ s^{-1}$ |
| V | Volts | V |
| v | Vector operation | - |
| $\underline{v}$ | velocity profile | - |
| x | Distance | m |
| $\alpha$ | Charge transfer coefficient | - |
| $\delta$ | Diffusion boundary layer thickness | m |
| $\delta o$ | Prandtl layer thickness | m |
| $\eta$ | Charge transfer overpotential | V |
| $\upsilon$ | Sweep rate<br>or Kinematic viscosity | $V\ s^{-1}$<br>$m^2\ s^{-1}$ |
| $\mu$ | viscosity | $m^2\ s^{-1}$ |
| $\omega$ | Angular frequency | $rad\ s^{-1}$ |

# CHAPTER 1

# INTRODUCTION.

Industrial cooling water systems are often fabricated from mild steel. Steel is used because of it's good mechanical properties, relative low cost and availability. Water is used as an industrial coolant because it is readily available, cheap and easily handled. It can carry a large quantity of heat per unit of volume and does not significantly expand or compress within the temperature ranges normally encountered. However, when these two materials are used in conjunction with each other, corrosion occurs. In the near neutral pH conditions encountered in industrial cooling systems, water is aggressive towards iron/steel. This can prove costly in terms of replacement and time lost due to shut down of the industrial plant.

One method of anti-corrosion protection most commonly used in cooling water systems involves the use of water soluble inhibitors. These are chemical compounds, or mixtures of compounds which reduce the rate of the corrosion processes when added to the feedwater.

Before an inhibitor is used in a cooling water system, it's effectiveness must be ascertained. At present the conditions encountered in a cooling water system are simulated using long term rig tests. These are simplified, scaled down versions of industrial systems. Mild steel 'coupons' are used to simulate industrial piping. The subsequent loss in weight of the coupons is then used to indicate the extent of corrosion.

Unfortunately weight loss techniques are not without their problems. Complications arise when localised attack, particularly pitting, occurs. Without optical inspection, weight loss will not reveal this dangerous condition. Other problems of a commercial nature arise due to the extended period (often weeks), over which rigs must be run to

obtain meaningful data. With shorter product deadlines, the pressure for quick results is often intense.

The object of the work reported in this thesis was to investigate and develop methods for quick, yet accurate inhibitor evaluation. These methods may be used to supplement, or possibly replace traditional weight loss techniques. The study of cathodic inhibitors was emphasised as being particularly important because of their increased use in new commercial formulations.

The problems associated with conventional oxygen reduction studies at a rotating disc electrode are discussed in detail. The development of three alternative techniques are then considered. First, a concentration step method for cathodic inhibitor evaluation. Second, the use of a differential aeration cell for both anode and cathode monitoring. Finally, the use of a potentiostat controlled flow-through cell for both anodic and cathodic studies on clean and pre-corroded surfaces.

# CHAPTER 2

# TESTS FOR SIMULATING COOLING WATER SYSTEMS

## 2.1 INTRODUCTION

In practice, three types of cooling water systems are encountered in industrial plants:

Once-through
Open Evaporative Recirculating
Closed Recirculating

### 2.1.1 ONCE-THROUGH

In 'once-through' systems the cooling water passes through the heat exchange equipment only once prior to discharge. Their operation is extremely wasteful in terms of water, and since the outflow is often discharged to a natural water-course, may lead to pollution. With large systems of this type the use of chemical corrosion inhibitors is often cost-prohibitive. Therefore, to prevent corrosion, once-through systems are generally constructed from expensive inert materials. Because of these disadvantages, once-through systems have been replaced where possible by recirculating systems.

### 2.1.2 OPEN EVAPORATIVE RECIRCULATING

In these systems, the water is continuously recycled and re-used. Hence, the mineral content of the water increases due to the concentrating effect of evaporation. The water is cooled after passing the heat exchanger by the evaporative process at the cooling tower.

### 2.1.3 CLOSED RECIRCULATING

Closed systems normally undergo minimal water loss, and hence negligible mineral concentration. With these systems radiators, refrigeration equipment or heat exchangers are used to cool the water.

For the reasons already discussed, and due to difficulties in obtaining adequate quantities of cooling water, the usage of open recirculating cooling towers has greatly increased. Therefore, these systems will be concentrated upon in the following work.

## 2.2 OBJECTIVES OF COOLING WATER TREATMENT

Industrial cooling systems lose efficiency due to corrosion and fouling. This inefficiency causes a decline in product output and hence economic losses. Thus, the primary objective of cooling water treatment is to maintain transfer efficiency by:

a) preventing corrosion of the heat transfer surfaces and associated pipework.
b) preventing fouling.

Firstly, the factors affecting both corrosion and fouling must be understood and are briefly discussed:

### 2.2.1 CORROSION

The factors affecting the rate of corrosion in cooling water systems are many and diverse, but the principal ones are:

1) Dissolved Oxygen
2) pH
3) Temperature
4) Dissolved Carbon Dioxide
5) Dissimilar Metals
6) Dissolved Solids

7) Water Flow Rate
8) Metal Composition
9) Stability of the oxide film on the metal surface
10) Stress

### 2.2.2 FOULING

Fouling may be split into three distinct types; scaling, general fouling and microbiological fouling:

Scale Formation

The formation of scale during the operation of a cooling water system depends upon the level of hardness salts in the water. Hardness results from the presence of dissolved calcium and magnesium salts, and can be classified as either temporary (carbonate hardness) or permanent. Temporary hardness arises from carbonate, or bicarbonate, whilst permanent hardness is due to the combination of calcium and magnesium with non-carbonate salts eg. sulphates and chlorides. Scale is detrimental to heat exchanger performance since it forms an insulating layer over the surface, causing a loss in heat transfer efficiency. It also adds to plant maintenance and pumping costs by blocking and reducing the flow rate in the pipe network.

Calcium carbonate is probably the most common form of scale encountered in cooling waters. Soluble bicarbonate salts are converted into much less soluble carbonates under the influence of heat, at the exchanger surface, and scale firmly adhers to the underlying metal (see Section 3.3 - Cathodic inhibitors).

In summary, the principal factors affecting the formation of scale in cooling water systems are:

1) Calcium and magnesium content of the water.
2) pH of the water - the higher the pH the lower the solubility of calcium carbonate.

3) Temperature - the higher the temperature the lower the solubility of calcium carbonate.
4) High concentration of dissolved salts.

General Fouling

General fouling, or sedimentation fouling arises from the presence of suspended solids in the cooling water. Constant recirculation causes agglomeration of small suspended particles into larger, heavier particles which then form a sediment on metal surfaces. Accumulation generally occurs at points of reduced flow eg. sump of the cooling tower. Sedimentation arises due to:

1) Corrosion - metallic oxides are insoluble and form particulate matter.
2) Contamination of water supplies with foreign particles.
3) Contamination via air-born particles at the cooling tower.

Microbiological Fouling

Microbiological fouling results from the excessive growth and development of lower forms of plant life - algae, fungi and bacteria, within the cooling water system. These microbiological growths cause plugging of filters and lines, along with the corrosion of metals and deterioration of cooling tower timbers. The rate of microbiological fouling arises from:

1) Sunlight - algal growth requires sunlight and usually occurs in sections of the cooling tower exposed to sunlight.
2) Oxygen - fungi require oxygen to grow and are therefore generally found above the water line.
3) Minerals - bacteria, depending upon the species, require sulphur containing compounds and/or oxygen to grow.

To develop a way of screening inhibitor formulations for use in a full scale plant, a reliable and valid laboratory test must be employed. The requirements of an effective test are rigorous, and must take into account all the variables involved in the corrosion and fouling processes.

## 2.3 RIG TESTS

Long term laboratory tests, taking the form of rig tests have been employed for many years, and still prove the most reliable and consistent method for inhibitor evaluation. A rig is a scaled down model, representative of the industrial plant, where conditions can be closely simulated and test variables easily controlled. As a result, they do not suffer from the inconsistency of some accelerated tests, and are often found to be more reliable than actual service tests.

Figure 2.1 shows a schematic diagram of a typical modern cooling water rig. Water is pumped from an open reservoir through a network of glass pipes. Within this network, water flows through a heat exchanger, coupon chamber, over a cooling tower and then back to the reservoir. Any inhibitor additions can be easily made to the open reservoir, where any loss of water through evaporation (causing an increase in mineral concentration of the water) is replaced from a headertank. Temperature and pH are continuously monitored throughout the run.

Corrosion testing takes the form of weight loss measurements. Coupons of the material under consideration (ie. mild steel) and of known weight are inserted into the rig assembly at various points within the solution flow. After a certain period of time (generally about two weeks, depending upon economic deadlines) the test is stopped and the coupons removed. Any corrosion products are then removed and the coupons re-weighed. The rate of corrosion is directly related to the loss in coupon weight.

Corrosion products are removed both mechanically and chemically. Initially, large particles are dislodged with a brush or by ultrasonic cleaning. The last few layers of material must then be removed by chemical methods. A 'stripping solution' or 'inhibited pickler' is used, which dissolves the corrosion products but not the underlying metal.

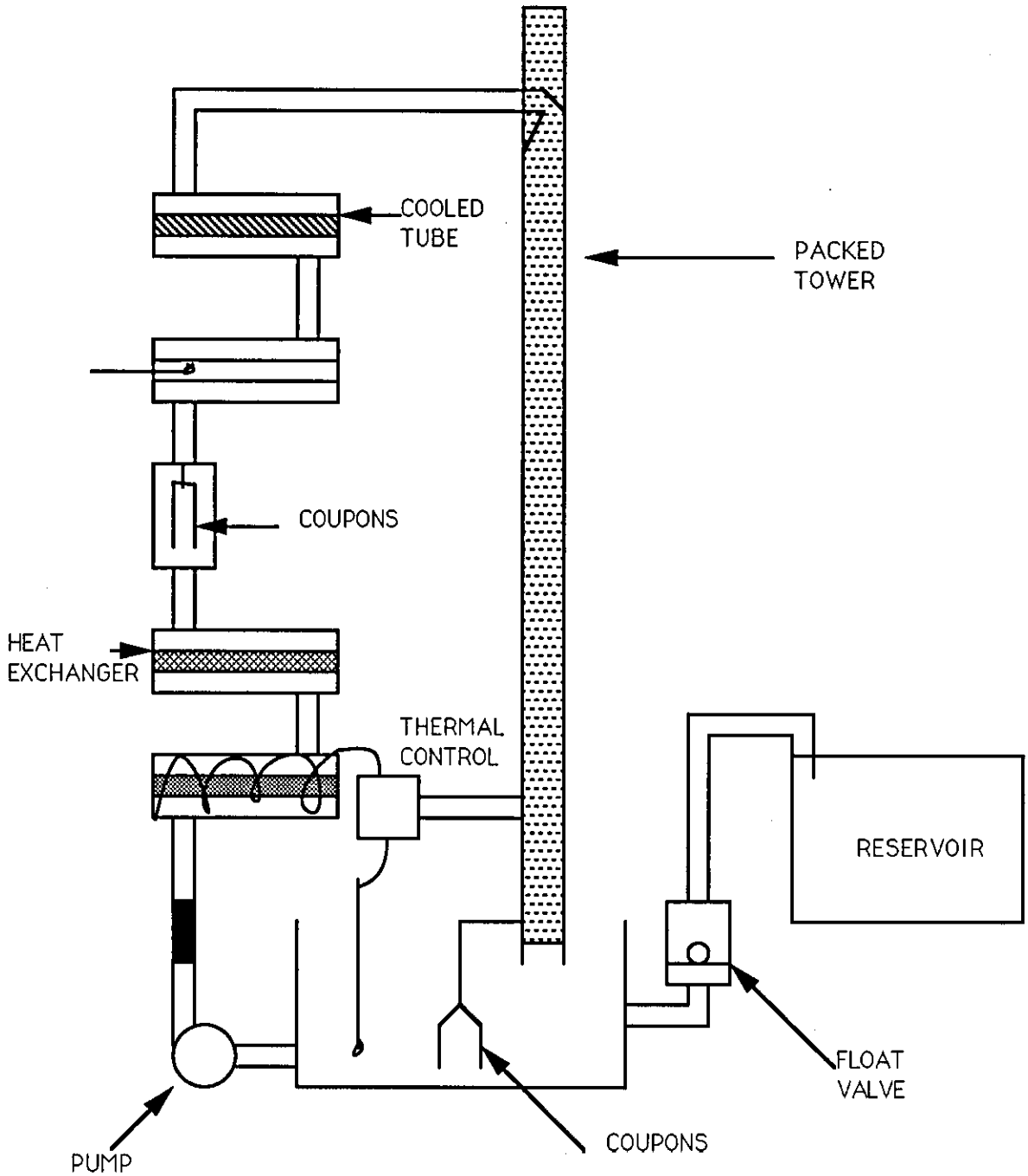


FIG. 2.1 - SCHEMATIC DIAGRAM OF A TYPICAL RIG TEST ASSEMBLY.

Very often the solution contains hydrochloric acid as the 'stripping' component along with an amine as the inhibitor.

Weight loss is a 'destructive' technique, as the sample can no longer be regarded as representative of a 'real' situation once the corrosion products are removed. This was proven by Fisher[1], who compared the results of tests run over two-day and nine-day periods, and found that the build-up of corrosion products caused corrosion rates to decrease markedly with time. Therefore, once the experiment has been terminated, it cannot be restarted.

Rig tests are also time consuming, and may be an unreliable basis for evaluating an anodic inhibitor if underdosing takes place[2]. This leads to localised attack which cannot be distinguished from general corrosion when weight loss measurements are employed alone.

Further, parameters such as scale thickness and the degree of fouling can be measured by temperature and pressure changes. This has been successfully achieved on a pilot plant scale[3], but has proved somewhat inaccurate on laboratory rig tests[1].

## 2.4 ACCELERATED TESTS

A number of accelerated laboratory tests have been developed for corrosion inhibitor evaluation. One or more corrosion factors are intensified in order to obtain a shorter test period. The duration of the technique varies from days to hours or even minutes, depending upon the specific technique.

Weight loss techniques have been accelerated using spinner tests[4,5]. Robitaille[6,7] reduced the test period down to 48hrs, by spinning immersed steel coupons in an aerated solution in order to evaluate molybdate inhibition.

Due to the electrochemical nature of corrosion, a number of electrochemical measurement techniques, both A.C. and D.C. can be

applied to determine corrosion rate. The advantages over direct methods are, the relatively short measuring time, the possibility of continuous monitoring and the absence of restrictions caused by adherent corrosion product formation. The disadvantage of electrochemical methods is that the system must be perturbed by applying an external polarisation. This causes changes at the surface i.e. in surface structure, roughness, formation of surface layers, sorption of inhibitors etc.

The electrochemical techniques most commonly encountered are polarisation resistance measurements, the extrapolation of Tafel lines and A.C. impedance measurements. These are briefly discussed below. A comprehensive description can be found in the review by Lorenz and Mansfeld[8].

### 2.4.1 POLARISATION RESISTANCE METHOD

There is a linear relationship between the applied current I and polarisation $\eta$, for small polarisations (up to 20 mV) from the corrosion potential. The slope of this straight line is given by:

$$\frac{d\eta}{di} = +/- \frac{ba.bc}{2.303\ (ba + bc)\ i_{corr}}$$

where $d\eta/di$ is defined as the polarisation resistance $R_p$ (i.e. the Tangent of the curve at $E_{corr}$) and ba and bc are the slopes of the anodic and cathodic Tafel lines respectively. The experimental determination of $d\eta/dI$ allows calculation of $i_{corr}$. The beauty of this technique is that it may be applied to a passive metal (ba=infinity) or situations where the cathodic reaction is diffusion controlled (bc=infinity).

### 2.4.2 EXTRAPOLATION OF TAFEL LINES

For greater overpotentials i.e. $\eta$ > 50mV the corrosion rate can be determined by extrapolation of the Tafel line for the anodic or cathodic reaction to the corrosion potential. The corrosion current

$i_{corr}$ can be obtained from the point of intersection of the two Tafel lines.

### 2.4.3 A.C. IMPEDANCE

A.C Impedance techniques have an advantage over D.C. techniques in that they can be conducted in relatively low conductivity electrolyte with no loss of accuracy. Mechanistic information can also be obtained from the shape of the impedance diagram. However, direct interpretation is only applicable to simple systems and $R_P$ is the only parameter that is readily obtainable. Interpretation of complex corroding systems is often very difficult.

In general, accelerated tests of aqueous systems correlate well with weight loss determinations. However, a knowledge of the electrochemical system prior to investigation is desirable.

# CHAPTER 3

# LITERATURE REVIEW: INHIBITORS FOR IRON UNDER NEUTRAL ELECTROLYTE CONDITIONS

## 3.1 INTRODUCTION

In order to evaluate the performance of a specific technique for inhibitor evaluation, we must first understand the conditions and mechanisms by which various inhibitors act. As described in Chapter 1, inhibitors may generally be classed as either anodic or cathodic, depending upon the partial reaction they suppress.

The corrosion of iron, under neutral pH conditions can be separated into two partial reactions, oxidation and reduction. Oxidation of iron occurs as the anodic reaction, with the dissolution of iron to produce ferrous ions:

$$Fe \text{ --------> } Fe^{2+} + 2e^- \qquad \text{ANODIC REACTION}$$

The corresponding reduction involves the gain of electrons by dissolved oxygen, to form hydroxyl ions, shown as :

$$1/2\ O_2 + H_2O + 2e^- \text{ -----> } 2OH^- \qquad \text{CATHODIC REACTION}$$

(N.B. Oxygen reduction occurs via a number of intermediate steps)

The overall reaction is a combination of the two partial reactions:

$$Fe + H_2O + 1/2\ O_2 \text{ ------> } 2OH^- + Fe^{2+} \text{----->} Fe(OH)_2 \text{ --->} Fe_2O_3$$

If one or both of these partial reaction rates is decreased, then corrosion will be reduced. Inhibitors are frequently classified by the electrochemical terms anodic and cathodic[9]. An anodic inhibitor

reduces the oxidation reaction, in this case iron dissolution, whilst a cathodic inhibitor reduces the reduction reaction, in this case oxygen reduction.

## 3.2 ANODIC INHIBITORS

These are often defined as substances which increase the anode polarisation, and thus move the corrosion potential in a positive direction. They do so by either decreasing the rate of transfer of metal ions into solution, or by reducing the active part of the electrode by passivation.

As a rule, anodic inhibitors are anions which migrate to anode surfaces, and in neutral water systems cause passivation[10]. Some anions, notably nitrite and chromate, are able to inhibit corrosion in the absence of oxygen, whilst with others e.g. phosphate, silicate and molybdate, oxygen is essential for successful inhibition[11]. Chromate and nitrite are strong oxidising agents and this has been proposed as the reason why they inhibit in de-oxygenated solutions. However, other strong oxidising agents e.g. chlorate and permanganate show no tendency to inhibit corrosion. Concentration is an important factor, as nearly all anions in very low concentrations show aggressive behaviour, and at high concentration some aggressive species have been shown to be inhibitive[12].

### 3.2.1 CHROMATES

Chromates have long been recognised as highly protective and efficient inhibitors, particularly in cooling water systems. However their use is in decline due to their highly toxic nature, and stricter legislation upon the use of toxic chemicals. The mechanism by which they function is not completely understood, but it is believed that ferrous ions are oxidised by chromate at the metal surface, to give a protective ferric oxide layer. Within this $\gamma Fe_2O_3$ layer, chromic oxide, chromates and even a small amount of chromium[13] have been discovered. Their exact function is unknown, but it has been

proposed that the inhibitor has a healing effect on any mechanical defects within the film. Rozenfeld[14] disagrees with this theory, proposing evidence for the formation of a chemisorbed layer of chromates.

In practice, chromate is a good inhibitor for both ferrous and non-ferrous metals. After exceeding a threshold chromate concentration ($7.0 \times 10^{-4}$ M for steel wire)[15], corrosion rate falls dramatically. In fact, the inhibitor concentration can then be reduced considerably with no adverse effect upon the protected metal[16]. Chromate, like many other anodic inhibitors, is classed as "dangerous". If insufficient inhibitor concentration is employed, then small anodic areas will be left. These, when present amongst large cathodic sites, lead to localised pitting corrosion. Therefore, overdosing with excess anodic inhibitor at the start of treatment is a standard precaution.

### 3.2.2 NITRITES

Nitrite is a good corrosion inhibitor in systems where the pH is maintained above 6. Protection is believed to occur from the oxidation of the corrosion products to less soluble states of higher valency. In the absence of oxygen, the nitrite itself acts as a cathode reactant and increases the mixed corrosion potential. This should result in the liberation of ammonia. However, in practice ammonia is undetected, indicating the involvement of an intermediate step. The adsorption of the inhibitor as an intermediate step has been proposed. This is based on the nitrite ion geometry in relation to the iron-iron metallic bond length[17], when an iron oxide film is formed at anodic sites. In practice nitrite has to be used at high concentrations (500ppm - 1000ppm) to be fully effective. In open systems it is particularly susceptible to bacterial decomposition to nitrate and often leads to microbiological fouling. For these reasons nitrite is rarely used alone, but often in inhibitor mixes where a biocide is present.

### 3.2.3 PHOSPHATES

Phosphates are widely used as corrosion inhibitors due to their low toxicity. For this reason they are suitable for use in potable waters and once-through systems. The protective properties of phosphates are dependent on the pH they create, generally the higher the pH the better the inhibitor. Phosphates used as inhibitors are either ortho-phosphate or poly-phosphate.

Ortho-phosphates of the type $M_3PO_4$, where M is a monovalent cation, show inhibitive properties. The inhibitive strengths correlate with pH in solution i.e. in the series $Na_3PO_4 > Na_2HPO_4 > NaH_2PO_4$. The poor protective properties of monosubstituted phosphates arise from acidification of the medium as a result of its hydrolysis. The pH effect on phosphate addition is not the exclusive criteria for inhibition as the phosphate anion itself greatly assists in the protection process. The surface film formed with both $Na_2HPO_4$ and $Na_3PO_4$ has been analysed by electron-diffraction and found to consist of $\gamma$-$Fe_2O_3$ and $FePO_4.2H_2O$[18]. The amount of phosphate present decreases with increasing pH. Oxygen is necessary for effective protection, so a film repair mechanism is envisaged[11]. Ferric phosphate is deposited at areas of iron dissolution (i.e. in the protective film) and plugs any gaps in the ferric oxide surface film.

Polyphosphates are difficult to define precisely as they often have variable chain lengths. Classification is usually from the molar ratio of $Na_2O$ to $P_2O_5$, with these ratios varying from 1.1 to 1.5. Dosage varies between 2ppm and 100ppm as $PO_4$, depending on conditions, with more effective inhibition arising in circulatory systems. Film formation and protection are achieved between 4 and 99°C and down to pH5[19], making it a versatile inhibitor. Above 99°C polyphosphates are readily converted into the orthophosphate, which then contributes to any carbonate deposits. The rate of film formation depends upon the diffusion of phosphate to the metal, a steady flow and high initial dose being important. Once protection has occurred, polyphosphate can maintain this state for as long as 14

days in the absence of further inhibitor[20], which is an advantage should the inhibitor supply stop.

Polyphosphate requires oxygen and calcium or magnesium to function satisfactorily. The more calcium, the lower the oxygen concentration required for inhibition[21]. The mechanistic action is complex, since polyphosphates fulfil a dual role, protecting the metal against corrosion and preventing the deposition of a film at the cathode[22]. The detection of iron in the protective film[23] does, however, suggest an effect upon the anodic dissolution.

### 3.2.4 BENZOATES

Anions of many organic acids have some inhibitive action. Benzoic acid, in the form of sodium benzoate ($C_6H_5COONa$) has proven to be the most suitable. Sodium benzoate is not a strong oxidising agent and according to Gatos[24] does not form insoluble iron salts (as do inorganic inhibitors). Therefore, it is not considered dangerous since very low concentrations do not lead to localised attack. Benzoate only operates in the presence of oxygen and is vulnerable to aggressive ions (chloride, sulphate and nitrate)[25].
The inhibitor mechanism is believed to be a combined effect, the benzoic acid anion $C_6H_5COO^-$ forming a strong chemical bond to the iron via the carboxyl group, with any remaining active sites being passivated by the oxygen present in solution. Benzoate is found to have no effect on the cathodic reaction.

### 3.2.5 MOLYBDATES AND TUNGSTATES

Molybdates and tungstates are chemically homologous to chromates, but possess considerably less oxidising power. Therefore, they require the presence of dissolved oxygen to inhibit corrosion effectively. A similar adsorption mechanism to that of chromate[26] is envisaged, although effective inhibitor concentration is higher. Stricter legislation and control over the use of toxic chemicals has caused an increased interest in molybdate as a replacement for chromate. Robitaille et al[27] found molybdate to be up to 3000 times

less toxic than chromate. Hence formulations based on molybdate are becoming common place.

### 3.2.6 SILICATES

Silicates are mainly used in cooling water systems and potable waters where low toxicity is essential. Low doses can be employed particularly in potable waters[28] where 4-10ppm is sufficient. In aqueous solutions, the chemistry of silicates is rather complex, various ionic, molecular and complex forms existing. Silicates have the variable composition $nNa_2O.mSiO_2$, their inhibitive efficiency depending upon the ratio m/n. For mild steel a m/n ratio of 2-4 has been suggested for effective inhibition[29]. Doses below a critical level accelerate corrosion[29] and since initial film formation is slow compared with other inhibitors, overdosing is commonly employed. A maintenance dose is then used to sustain protection.

The mechanism of inhibition induced by silicates is not clearly established. One school of thought believes inhibition to occur from the increase in pH caused by the silicate, but this has been disproved[30]. A widely accepted theory involves film formation when colloidal silicates deposit on the metal surface. A surface layer of iron oxide is beneficial for protection with silicates[31] and, despite being classed as an anodic inhibitor[32] it appears that a gel forms over the whole metal surface.

### 3.2.7 BORATES

Borates are usually employed as additives in inhibitor mixes. Their effectiveness is largely due to their capacity to maintain an alkaline pH. However, at high concentrations (>0.1M $cm^{-3}$) it has been suggested that borate acts as an anodic inhibitor[29].

## 3.3 CATHODIC INHIBITORS

Cathodic inhibitors have the advantage over anodic inhibitors since they are incapable of partial passivation. Therefore, localised attack after under-dosing is not a problem. Cathodic inhibitors act by retarding one or more steps in the cathodic reaction. As a rule, cations (which migrate towards cathode surfaces) that are precipitated chemically or electrochemically and block the surfaces, are good cathodic inhibitors.

The best known, and most commonly encountered cathodic inhibitor is calcium carbonate commonly known as "scale". It has long been known that hard waters are less corrosive than soft, and that soft waters can be made less aggressive with the addition of slaked lime. The calcium present in the water migrates to the cathodic sites upon the metal surface and is precipitated as carbonate. This forms a highly protective crystalline film that adheres firmly to the underlying metal surface. The primary mechanism leading to the formation of such scale in cooling water systems, involves the conversion of soluble bicarbonate salts into the much less soluble carbonate under the influence of heat:

$$Ca(HCO_3)_2 + HEAT \text{ --------> } CaCO_3\downarrow + CO_2 + H_2O$$

Scaling may also be a result of magnesium salts, sulphates and chlorides of calcium. Although scaling gives acceptable protection against corrosion, it is extremely undesirable. Scaling causes the loss of heat transfer from heat exchangers, with the consequent reduction in operating efficiency. It also blocks pipes and causes increased pumping costs and reduced water flow rates. Zinc is a more acceptable cation for use in cathodic inhibitors. Usually employed in mixed inhibitor formulations, zinc gives good protection, by forming sparingly soluble zinc hydroxide, with the hydroxyl ions produced at the cathodic sites upon oxygen reduction. Other cations that show inhibitive properties include $As^{3+}$, $Sb^{3+}$ and $Ni^{2+}$.

Organic inhibitors which carry positive charges or contain a lone pair of electrons, have been shown to have both cathodic and anodic properties. Nitrogen containing compounds such as amines, pyridines and quaternary salts of pyridine bases and sulphur containing compounds, show inhibitive properties in acid conditions. Organic phosphonates containing carboxyl groups have been found to be inhibitive in neutral electrolyte. Such compounds as H.P.A. and P.C.A. are commonly employed as cathodic inhibitors in many commercial formulations.

## 3.4 MIXTURES OF INHIBITORS

It is common-place for mixtures of inhibitors to be used for commercial formulations. These usually contain both an anodic and cathodic inhibitor component. The simultaneous addition of two inhibitors often results in a synergistic effect, giving better protection than predicted. An example of a mixture includes zinc sulphate (as the cathodic component) and sodium chromate (as the anodic component) which forms a protective film of zinc chromate. The addition of cationic polymers to inhibitor systems also induce a synergistic effect in relatively low concentrations.

# CHAPTER 4

# GENERAL ELECTROCHEMICAL THEORY

## 4.1 ELECTRODE-ELECTROLYTE INTERFACE

When an electrode is placed in an electrolyte solution, electrical neutrality is destroyed and two layers of opposite charge form. These two opposing layers are only a few tenths of a nanometre apart, and a potential difference is produced between the two. This interphase is so named because it is the region between the two phases where the properties have not been attained of either bulk phase. It is within this electrode-electrolyte interphase that electrochemical reactions occur and hence electrode kinetics are greatly influenced.

In the past, numerous attempts have been made to quantify the electrode-electrolyte interphase. The earliest model used to describe the conditions encountered within this region, was proposed by Helmoltz in 1879[33]. He simply regarded the interphase as two rigid slabs of equal but opposite charge. This representation has been modified by many workers to produce a more accurate and complex view.

Helmholtz's model was analogous to that of a parallel plate capacitor, and is shown in Figure 4.1. He suggested that solvated ions lined up along the surface of the electrode, being separated from it by a fixed distance, equal to the size of their hydration spheres.
The model however, required a number of assumptions. The separated charges were assumed to be in electrostatic equilibrium, whilst the charge near the interphase changed with potential. It was also assumed that changes in electrode potential did not cause charge transfer across the interphase. This implies that the double layer is purely capacitive, and is therefore only applicable to "ideally polarisable" electrodes. The model is further incorrect, as it proposes

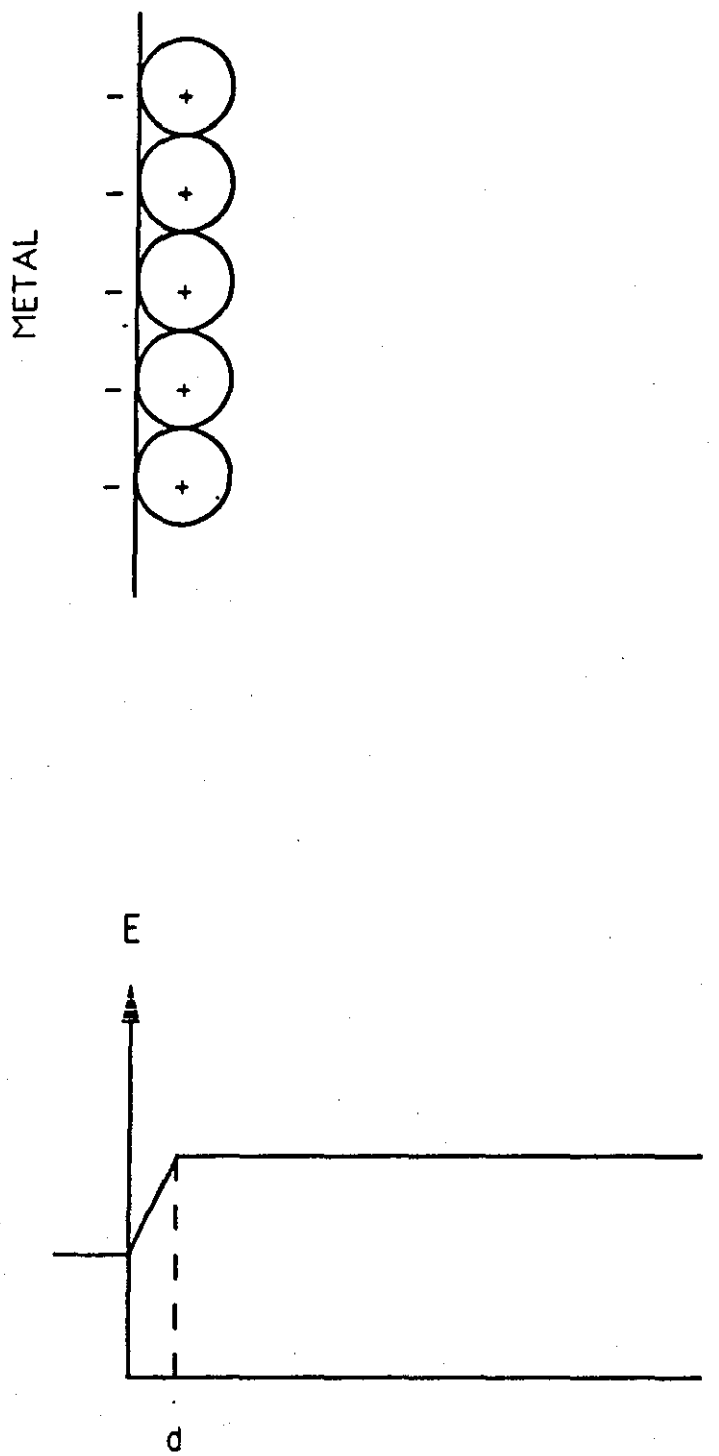


FIG. 4.1 - HELMHOLTZ MODEL OF DOUBLE LAYER

that the capacitance is independent of both potential and concentration.

Gouy[34] and Chapman[35] both independently proposed that the solution side of the double layer, has a diffuse structure due to random thermal motion and that there is a non-linear fall in potential, away from the electrode - see Figure 4.2. Although this model was a great improvement on the Helmholtz model, discrepancies were found to exist between the experimental and theoretically predicted values for the variation of double layer capacitance with concentration. The reason for this was that both Gouy and Chapman had assumed ions to be point charges which could approach to within infinitely small distances of the electrode surface.

Further improvement to the model was made by Stern, who in 1924[36] proposed a model considering the ions to have a finite size. He combined the concepts of Helmholtz with those of Gouy and Chapman to take into account the role that ionic adsorption could play at the electrode surface. In this model, Stern stated that the ions nearest the electrode are held in a fixed Helmholtz type plane (a monolayer thick), whilst beyond, the ions were diffuse into the bulk, as defined by Gouy and Chapman.

Grahame[37] then went on to subdivide the compact layer into a inner and outer Helmholtz plane. The inner plane passes through the centres of specifically adsorbed ions whilst the outer plane passes through the centres of hydrated ions at their nearest distance of approach - see Figure 4.3. Grahame showed that the total double layer capacitance was equal to that of two capacitors in series:

$$\frac{1}{C_{dl}} = \frac{1}{C_{compact}} + \frac{1}{C_{diffuse}}$$

Hence at potentials close to the point of zero charge (p.z.c), and in dilute solution, the double layer capacitance is essentially that of the

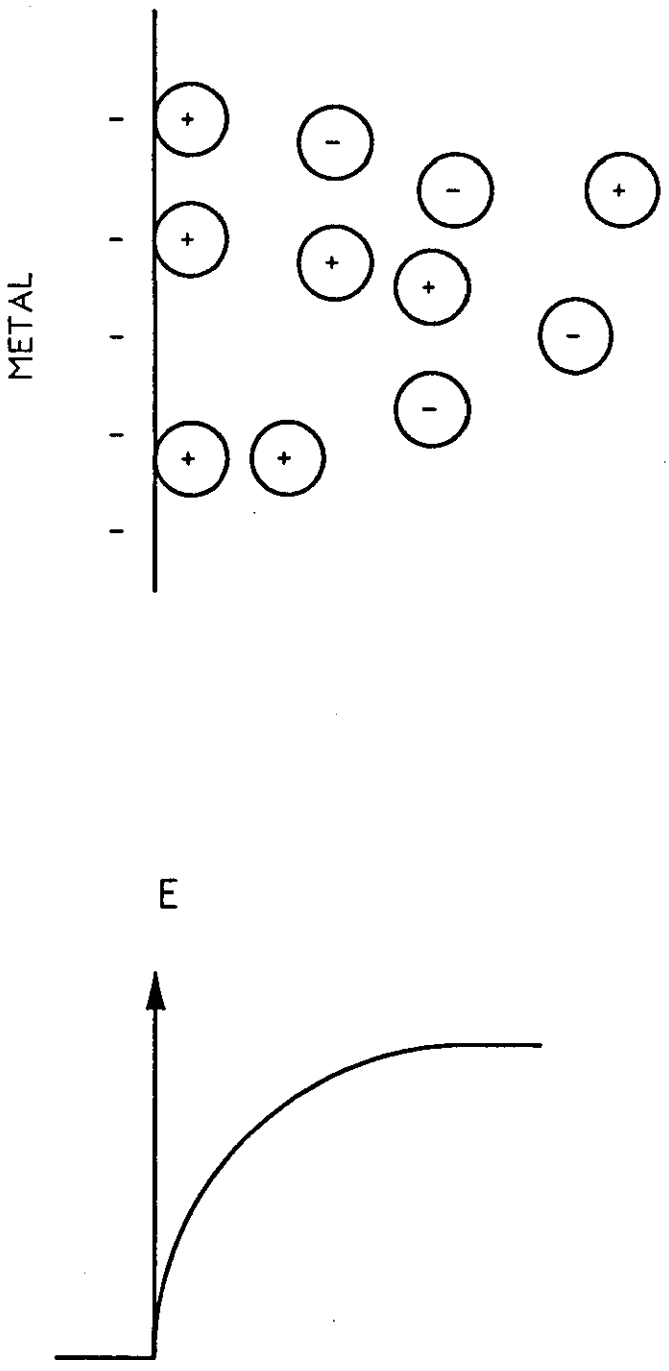


FIG. 4.2 - GOUY-CHAPMAN MODEL OF DOUBLE LAYER

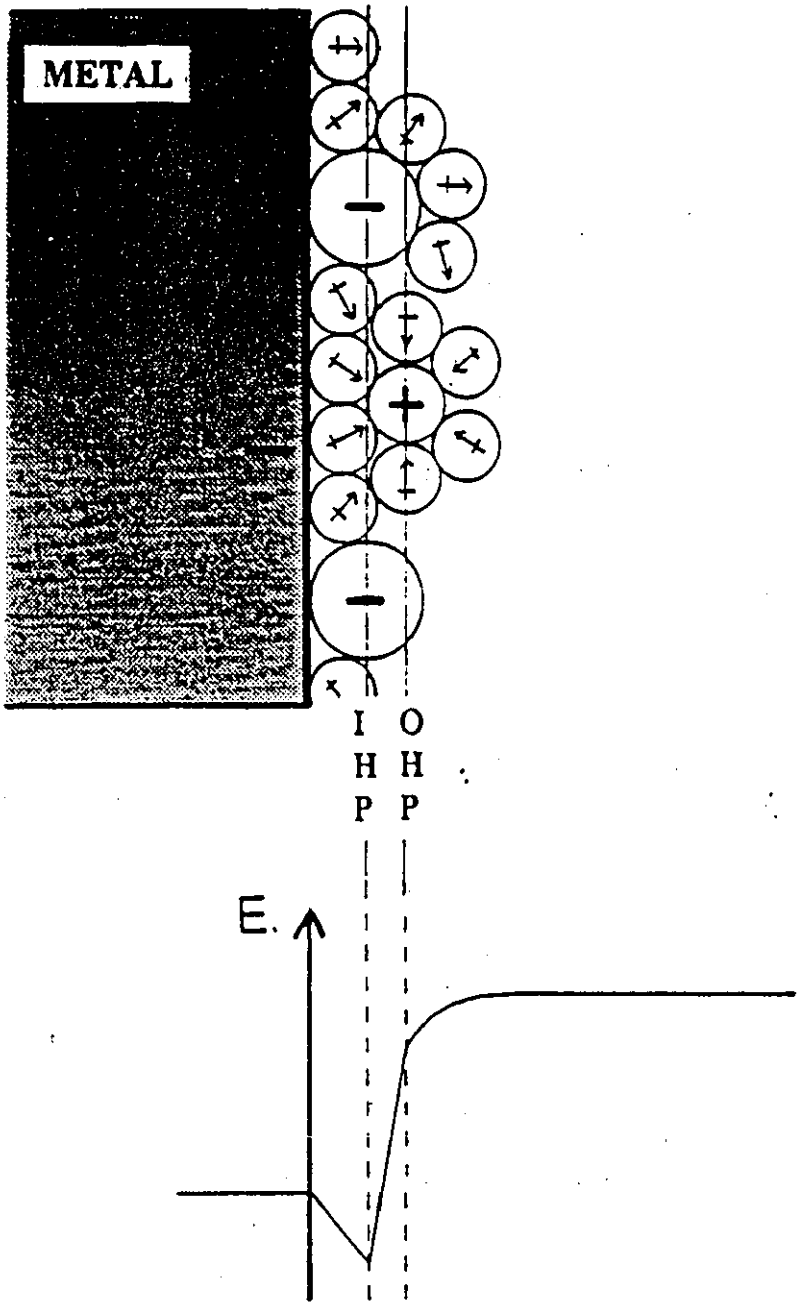


FIG. 4.3 - GRAHAME MODEL OF DOUBLE LAYER

diffuse layer. At higher concentrations the diffuse layer capacitance is large, and $C_{dl}$ equates to that of the compact layer.

The Stern model has been further developed more recently by Devanathan, Bockris and Muller[38]. They suggest that the electrode surface is covered with a layer of water molecules, with specifically adsorbed ions (non hydrated) being able to penetrate the sheath at certain sites. The next layer then consists of ions which retain their hydration shell - see Figure 4.4. Thus both inner and outer planes exist, the outer being further removed from the electrode surface, due to the presence of the primary hydration sheath.

## 4.2 ELECTRODE REACTIONS

Consider a simple electron transfer reaction in which two species O and R are interconverted at an inert surface :

$$O + ne^- \text{ --------> } R$$

Even in this simple case, the electrode reaction comprises of a sequence of more basic steps:

| | |
|---|---|
| O bulk----------> O electrode | MASS TRANSPORT |
| O electrode------> R electrode | ELECTRON TRANSFER |
| R electrode -----> R bulk | MASS TRANSPORT |

The rate of reduction is determined by the rate of the overall sequence, which in turn is dependent on the rate of the slowest step. Therefore, in order to understand the electrode reaction fully, both mass transport and electron transfer must be considered.

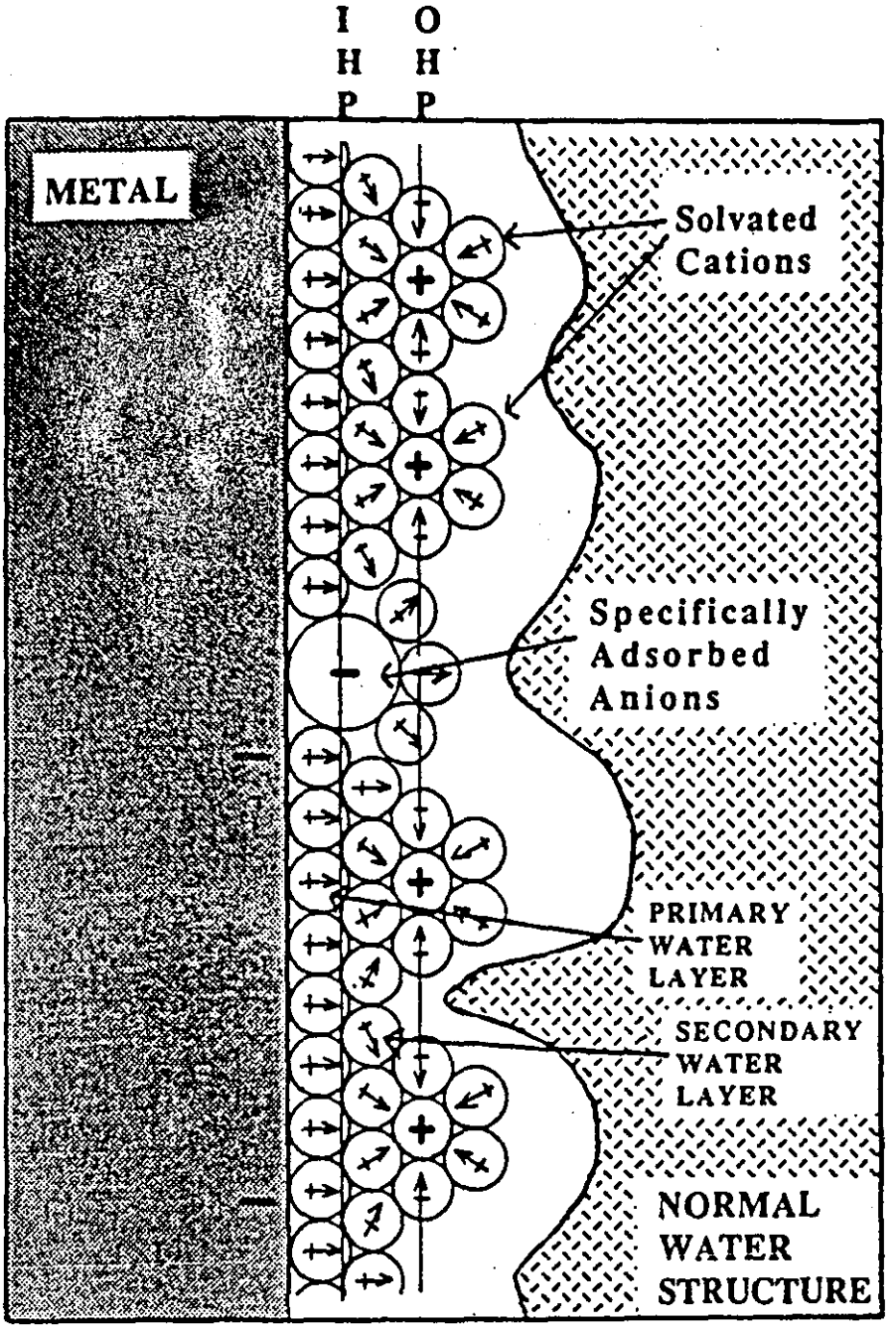


FIG. 4.4 - DEVANATHAN MODEL OF THE DOUBLE LAYER

### 4.2.1 CHARGE TRANSFER

Considering the general charge transfer reaction:

$$O + ne^- \underset{k_b}{\overset{k_f}{\rightleftharpoons}} R \qquad 4.1$$

where O is an oxidised and R a reduced species; $k_f$ the cathodic and $k_b$ the anodic rate constant; and n the number of electrons, e, transferred across the interphase in each charge transfer step. If no current has passed, both the bulk and surface concentrations will be equal, and the equilibrium is characterised by the Nernst Equation[39]:

$$Er = E^\theta + \frac{RT}{nF} \ln [ C_O^b / C_R^b ] \qquad 4.2$$

where Er is the reversible potential, $E^\theta$ the standard electrode potential and $C_O^b$, $C_R^b$ the bulk concentrations of the oxidised, O, and reduced, R, species respectively.

The Nernst Equation allows us to predict the effect of concentrations on potential.
NB. Activities should be used rather than concentrations, but providing this limitation is recognised concentration is acceptable.

The electrochemical rate constants $k_f$ and $k_b$ are known to depend upon potential. In order to understand the relationship the shape of the free energy profile must be considered - Figure 4.5.

Assigning some arbitary experimental scale to which we can refer, then when E=0, the forward and backward activation energies, at this potential, are $\Delta G^o{}_f{}^{\ddagger}$ and $\Delta G^o{}_b{}^{\ddagger}$ respectively. The energy barrier is due to the orientation, and ultimate removal of the hydration shell.

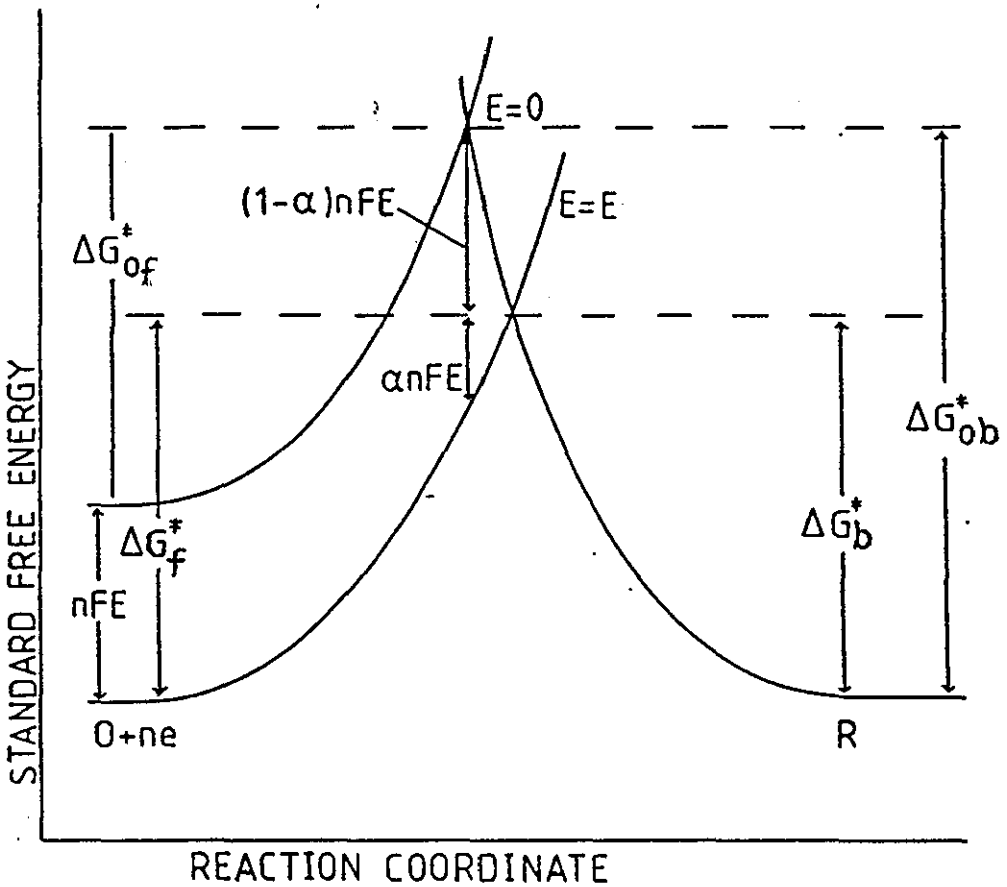


FIG. 4.5 – FREE ENERGY CHANGES FOR THE REDOX REACTION:
O + ne ----> R

On polarisation to a potential E, the relative energy of the electron on the electrode will change by -nFE. Figure 4.5 shows the effect of a positive shift in potential. It is apparent that now the energy for the forward process is greater than for the backward one. Thus a symmetry factor or charge transfer coefficient, $\alpha$, must be introduced to account for the variation in energies. The value of $\alpha$ is constant and characteristic of the reaction being studied. It is in the range $0 < \alpha < 1$, but it is often close to 0.5.

The Gibbs free energy change of activation for the forward reaction is given by:

$$\Delta G_f^{\ddagger} = \Delta G^{o}_f{}^{\ddagger} + \alpha nFE \qquad 4.3$$

and for the reverse reaction by:

$$\Delta G_b^{\ddagger} = \Delta G^{o}_b{}^{\ddagger} - (1-\alpha)nFE \qquad 4.4$$

Assuming $k_f$ and $k_b$ have an Arrenhuis form, both processes can now be expressed as:

$$k_f = A_f \exp^{-(\Delta G_f^{\ddagger}/RT)} \qquad 4.5$$

and

$$k_b = A_b \exp^{-(\Delta G_b^{\ddagger}/RT)} \qquad 4.6$$

Expansion of these rates in terms of activation energies gives:

$$k_f = A_f \exp^{-(\Delta G^{o}_f{}^{\ddagger}/RT)} \exp -(\alpha nFE/RT) \qquad 4.7$$

and

$$k_b = A_b \exp^{-(\Delta G^{o}{}_{b}^{\ddagger}/RT)} \exp\ ((1-\alpha)nFE/RT) \qquad 4.8$$

These expressions have both potential dependent and independent terms. When E=0 the first two factors in each of these expressions forms a product that is independent of potential and is equal to the rate constant, represented by $k^{o}{}_{f}$ and $k^{o}{}_{b}$. Hence:

$$k_f = k^{o}{}_{f}.\ \exp\ (-\alpha nF\,E\ /\ RT) \qquad 4.9$$

and

$$k_b = k^{o}{}_{b}\ .\ \exp\ \{\ (1-\alpha\ )\ nF\,E\ /RT\ \} \qquad 4.10$$

When the electrode is in equilibrium with a solution which has $C_O{}^{b} = C_R{}^{b}$, then $E = E^{\theta}$ and $k_f C_O{}^{b} = k_b C_R{}^{b}$. This implies $k_f = k_b$ and that:

$$k^{o}{}_{f}.\ \exp\ (-\alpha nF\,E^{\theta}/\ RT) \quad = \quad k^{o}{}_{b}\ .\ \exp\ \{\ (1-\alpha\ )\ nF\,E^{\theta}/RT\ \} \quad = \quad k^{\theta} \qquad 4.11$$

where $k^{\theta}$ is known as the standard or intrinsic rate constant and is the value of $k_f$ and $k_b$ at $E^{\theta}$. Substitution for this term allows the removal of the potential independent term thus:

$$k_f = k^{\theta}\ .\ \exp\ \{\ -\alpha\ nF(E\ -\ E^{\theta})/\ RT\ \} \qquad 4.12$$

and

$$k_b = k^{\theta}\ .\ \exp\ \{\ (1-\alpha)nF(E\ -\ E^{\theta}\ )/RT\ \} \qquad 4.13$$

It is often easier to consider currents than rate constants in electrochemistry:

The net current is measured, which is the difference between the forward and reverse reactions:

$$i = i_f - i_b \qquad 4.14$$

Since:

$$i = nFkC \qquad 4.15$$

Then:

$$i = nF(k_f C_o^s - k_b C_R^s) \qquad 4.16$$

where $C_o^s$ and $C_R^s$ are the concentrations of the oxidised and reduced species at the electrode surface. Hence

$$i = nFk^\theta [ C_o^s . \exp \{ -\alpha nF(E - E^\theta)/ RT \} - C_R^s .\exp \{ (1-\alpha) nF(E - E^\theta)/ RT \}] \qquad 4.17$$

This is known as the Butler-Volmer equation.

Under electrochemical equilibrium there is no net rate of reaction and the flow of current is zero. Therefore:

$$i_o = i_f = i_b \qquad 4.18$$

where $i_o$ is the exchange current density, and is a measure of the electrode reversibility (high $i_o$ = highly reversible). Since the charge transfer overpotential $\eta$ is given by:

$$\eta = E - Er \qquad 4.19$$

then substitution of all these factors simplifies the Butler-Volmer equation greatly, giving:

$$i = i_o[\exp\{ -\alpha nF\eta / RT \} - \exp\{ (1-\alpha)\ nF\eta / RT \}] \qquad 4.20$$

This is known as the ERDEY-GRUZ and VOLMER EQUATION[40] and applies when a solution is well stirred or when the currents are kept low, so that the surface concentrations do not differ appreciably from the bulk. The Erdey-Gruz and Volmer Equation is regarded as the fundamental equation of electrode kinetics.

There are 3 limiting forms of this equation. The first two apply at high overpotentials.

At high positive overpotentials, $[\ i_b\ ] \gg [\ i_f\ ]$ and the first term may be ignored. Hence 4.20 can be rearranged to give:

$$\eta = \frac{RT}{(1-\alpha)nF} \ln i_o + \frac{RT}{(1-\alpha)nF} \ln i \qquad 4.21$$

Conversely, at high negative overpotentials $[\ i_f\ ] \gg [\ i_b\ ]$ and:

$$\eta = \frac{RT}{\alpha nF} \ln i_o + \frac{RT}{-\alpha nF} \ln i \qquad 4.22$$

These two equations are the well known Tafel Relationships[41] and can be represented by the single equation:

$$\eta = a + b \ln i \qquad 4.23$$

from which a plot of $\eta$ versus ln i will be linear. The kinetic parameters, $\alpha$ and $i_o$, can easily be calculated from the slope and intercept respectively.

The third limiting form applies at very low overpotentials, where $\eta \ll (RT/\alpha nF)$ and $\eta \ll (RT/(1-\alpha)nF)$. Expansion of the exponentials, and ignoring quadratic and higher order terms leads to the simple equation:

$$i = i_o \frac{nF}{RT} \eta \qquad 4.24$$

Thus a plot of i versus $\eta$ is linear, passing through the origin. This is the basis for the Polarisation Resistance method described in Chapter 2.

### 4.2.2 MASS TRANSPORT

It is often the case that an electrochemical reaction is limited by the supply of reactant to, or removal of product from the electrode, rather than by kinetic factors. Therefore, mass transport processes must always be considered when studying electrode kinetics.
The flux of a species j to an electrode is given, in its most general form, by the Nernst-Planck equation:

$$J_j = -\underline{D}\nabla C_j - \frac{n_j F}{RT} . D_j C_j \nabla \emptyset + \underline{C}_j v \qquad 4.25$$

Diffusion Migration Convection

where J is the flux, D the diffusion coefficient and $\underline{v}$ the velocity profile. The operator is defined:

$$\nabla = \underline{i}\frac{d}{dx} + \underline{j}\frac{d}{dy} + \underline{k}\frac{d}{dz} \qquad 4.26$$

where $\underline{i}$, $\underline{j}$ and $\underline{k}$ are the unit vectors.
The 3 terms of 4.25 represent the 3 modes of mass transfer, i.e.. diffusion, migration and convection.

i) Migration.

The movement of ions due to the influence of a potential gradient is known as migration. The forces leading to migration are purely electrostatic and the majority of electrical current passing through the bulk of the solution does so by this process. If a large excess of inert electrolyte is used, this carries most of the charge and the contribution of migration to the flux of the electroactive species is minimised. Under these conditions, the second term in equation 4.25 can be neglected, simplifying the equation considerably.

ii) Diffusion.

Diffusion is the movement of species down a concentration gradient, and occurs when any chemical change takes place at a surface. This is simply expressed in Fick's First Law[42]:

$$\underline{J}_j = -D_j \nabla C_j \qquad 4.27$$

for the diffusional flux, $\underline{J}_j$. The time dependence of the concentration profile is given by Fick's Second Law[42];

$$\frac{dC_j}{dt} = D_j \nabla^2 C_j \qquad 4.28$$

where t is the time and $\nabla^2$ is the Laplacian operator defined by:

$$\nabla^2 = \frac{d^2}{dx^2} + \frac{d^2}{dy^2} + \frac{d^2}{dz^2} \qquad 4.29$$

The solution of Fick's Law depends on the choice of boundary and initial conditions. Consider diffusion to a plane electrode. Equation 4.25 reduces to:

$$J_j = -D_j \frac{dC_j}{dx} \qquad 4.30$$

In order to obtain a solution to this equation the relationship between $C_j$ and x must be established. This relationship has been the cause of some controversy.

According to Nernst[43], the concentration varies as a linear function of distance, within a stagnant layer of electrolyte of thickness $\delta$. The quantity $\delta$ is known as the Nernst diffusion layer thickness, and is an arbitrary quantity defined by 4.25.
Clearly:

$$\frac{dC_j}{dx} = (C_j^b - C_j^s)/\delta \qquad 4.31$$

where $C_j^b$ is the bulk concentration of species j. Hence:

$$J_j = -D_j (C_j^b - C_j^s)/\delta \qquad 4.32$$

Where the supply of reactant controls the reaction, the surface concentration of that reactant falls to zero. It is then possible to define the limiting current density, $i_L$ , as:

$$i_L = -n_j F . D_j C_j^b/\delta \qquad 4.33$$

Unfortunately, the Nernst diffusion layer thickness cannot be calculated. Indeed, for unstirred solutions $\delta$ has no steady state value, but the diffusion layer grows with time until disturbed by convective processes. The diffusion layer is, however, often assumed to be constant for experiments of short duration.

iii) Convection.

Convection is the movement of species due to mechanical forces. It is generally held to arise in two distinct ways, i.e. it may be natural (in

an unstirred solution) or forced. Natural convection occurs due to movement of a fluid under the influence of temperature or local density gradients. Therefore, it is impossible to formulate precisely and equally impossible to prevent. Its effects may, however, be minimised by the introduction of a forced convective regime which may be described exactly e.g. the Rotating Disc Electrode (section 4.3).

The process of forced convection is concerned with the transportation of solution by agitation or stirring, resulting in thorough mixing with an accompanying reduction in local density and temperature gradients. Where the hydrodynamics and cell geometry are well-defined it is often possible to obtain the velocity profile $\underline{v}$ (for an incompressible liquid) from the Navier-Stokes Equation[44] :

$$\frac{\rho\, d\underline{V}}{dt} = -\nabla p + \mu\nabla^2\underline{v} + \underline{f} \qquad 4.34$$

together with the continuity equation:

$$\nabla \cdot \underline{v} = \underline{0} \qquad 4.35$$

and the initial and boundary conditions pertaining to the system under consideration. In the above, $\mu$ is the viscosity, $\rho$ is density, p the pressure gradient and $\underline{f}$ the volume force exerted on an element of fluid. The term $\mu\nabla^2\underline{v}$ represents frictional forces.

Neglecting the effects of migration (i.e. experiments are normally undertaken with solutions containing a large excess of base electrolyte) and introducing the mass balance condition:

$$\nabla \cdot J_j = -\frac{dC_j}{dt} \qquad 4.36$$

then 4.25 becomes the general convective-diffusion equation:

$$\frac{dC_j}{dt} = D_j\nabla^2 C_j - \underline{v}.\nabla C_j \qquad 4.37$$

Clearly, when considering the steady state 4.37 reduces to:

$$D_j \nabla^2 C_j - \underline{v} . \nabla C_j = 0 \qquad 4.38$$

which is the familiar equation of convective diffusion. The exact solution of this equation is rarely possible. Indeed, the rotating disc electrode is one of the few systems for which the boundary conditions allow this.

The Nernst diffusion layer theory, is of little help in the solution of 4.38. A more realistic and quantitative theory is that of the hydrodynamics boundary layer, as developed by Levich[45]. In this theory, a fluid in motion relative to some surface, is divided into two regions. In the region adjacent to the surface the fluid velocity rises from zero at the surface, to the value attained by the bulk solution, with viscous forces present. Outside of this hydrodynamic layer, the fluid is essentially inviscid. Clearly, the viscous boundary layer or Prandtl layer is not stagnant as in the Nernst theory. The main change in concentration also occurs within this layer.

An appropriate relation exists for the thickness of the Prandtl layer, according to which:

$$\delta o = 5.2\sqrt{} \{\upsilon x / Uo\} \qquad 4.39$$

$\upsilon$ being the kinematic viscosity and Uo the fluid velocity. Consideration of 4.38 together with Navier-Stokes Equation leads to an expression for the thickness of the diffusion boundary layer in terms of $\delta o$. Hence:

$$\delta \sim \delta o \, Pr^{-1/3} \qquad 4.40$$

where Pr, the Prandtl Number, is a dimensionless quantity characterising the physical properties of the fluid. In fact:

$$Pr = \upsilon / D \qquad 4.41$$

Hence:

$$\delta \sim D^{1/3} \upsilon^{1/6} \sqrt{\{x / Uo\}} \qquad 4.42$$

A consequence of the form of 4.41 is that 4.42 admits a different boundary layer thickness for each species.

## 4.3 ROTATING DISC ELECTRODE

The rotating disc electrode (RDE) is a means of forced convection which allows careful control of the hydrodynamics of the electrode system and produces a well-defined diffusion layer. It is one of a few forced convective systems for which a complete solution of the hydrodynamic equations has been made. N.B. Others include the rotating cylinder electrode and the wall jet electrode.

The rotating disc electrode consists of a disc of the material under study, embedded in the centre of an insulating sheath. The disc is rotated at a strictly controlled angular velocity. Its action may be compared to a centrifugal pump. Fluid close to the surface rotates with the electrode and is flung outwards, to be replaced by fluid drawn up from the bulk of the solution. The flow patterns are shown schematically in Figure 4.6.

The hydrodynamics of the rotating disc electrode have been treated by Levich[45,46] (N.B. the review of Filinovsky and Pleskov[47] is noteworthy).

Levich[45] showed that for laminar flow, the boundary layer thickness, $\delta$, was dependent on the angular velocity of the electrode, $\omega$, such that:

$$\delta = 1.61\ D_o^{1/3} \upsilon^{1/6} \omega^{-1/2} \qquad 4.43$$

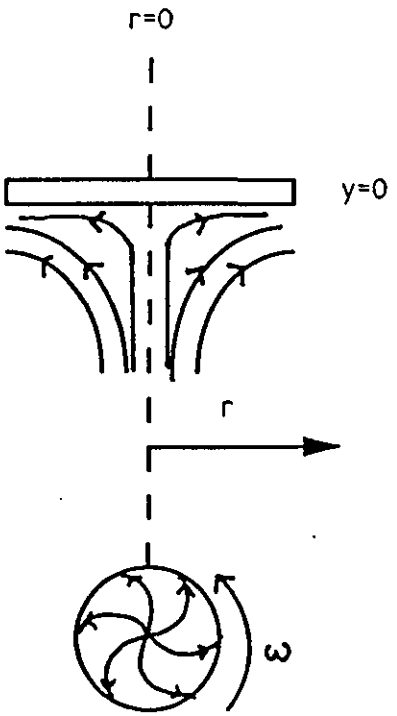


FIG. 4.6 - SCHEMATIC FLOW PATTERN AT R.D.E.

where $\omega$ = angular frequency, rad $s^{-1}$ ($\omega = 2\pi f$)

$D_0$ = Diffusion coefficent, $cm^2\ s^{-1}$

$\upsilon$ = Kinematic viscosity (viscosity/density), $cm^2\ s^{-1}$

Hence, as the angular velocity increases the boundary layer thickness decreases. The relationship holds between 100 - 10,000 r.p.m. At lower values of $\omega$ natural convection becomes significant, whilst at higher values turbulence becomes problematic.

The rotating disc is useful, as it is capable of distinguishing between mass transport and charge transfer control:

i) Mass Transport Control

At large overpotentials, where the concentration of the electroactive species is zero, mass transport is the controlling process and the current is dependent on the rotation speed. The limiting current density can be calculated from the Levich Equation[45]:

$$i = 0.621\ nFD_0^{2/3}\ \upsilon^{-1/6}\ C_0^{b}\ \omega^{1/2} \qquad 4.44$$

Thus a plot of i vs $\omega^{1/2}$ is linear and passes through the origin.

ii) Reversible Electrode Reaction

Considering the reversible reaction:

$$O + ne^- \underset{k_b}{\overset{k_f}{\dashrightarrow}} R$$

At high potentials, mass transport is the controlling process and the current density will be given by the Levich Equation[45]. In the mixed region where current is a strong function of potential, a plot of i vs $\omega^{1/2}$ is linear. Since the surface concentration does not equal zero, the slope will be less than that predicted by Levich.

iii) Irreversible Electrode Reaction

If we consider the irreversible electrode reaction:

$$O + ne^- \xrightarrow{k_f} R$$

the back reaction can be ignored.

The I-E curve will be S-shaped, and consist of 3 distinct regions:

a) In the mass transport controlled region, i will be proportional to $\omega^{1/2}$ .

b) In the intermediate zone, mixed control applies i.e. mass transport and electron transfer. i varies with $\omega^{1/2}$ but a plot of i vs. $\omega^{1/2}$ is non-linear.

c) At low current densities, the electron transfer alone becomes the rate determining step and:

$$i = nFk_f C_o^b = i_\infty \qquad 4.45$$

where $i_\infty$ = current at infinite rotation speed.

Therefore current is independent of rotation speed.

For cases when mixed control occurs, the current can be calculated from:

$$-\frac{1}{i} = \frac{1}{nFk_f C_o^b} + \frac{1.61\,\upsilon^{1/6}}{nFD_o^{2/3} C_o^b\,\omega^{1/2}} \qquad 4.46$$

A plot of $-i^{-1}$ vs $\omega^{-1/2}$ should be linear and the value of $k_f$ obtained from the intercept. $i_\infty$ can be used in the Tafel plot to determine io for the reaction.

In conclusion, the rotating disc electrode is a very useful electrochemical technique. It is capable of distinguishing between charge transfer and mass transport control, and allows characterisation of the electron transfer reaction along with the determination of electrochemical kinetics.

## 4.4 LINEAR SWEEP VOLTAMMETRY

Linear sweep voltammetry is a very useful investigative technique, which can be employed in both a qualitative and quantitative manner. Adams[48] has described some of the practical aspects of L.S.V., while Nicholson and Shain[49] have covered the theoretical side, of both single scan and cyclic methods for various systems. Whilst the experimental technique is fairly simple, the underlying theory is quite complex. Thus an indepth treatment of the theory will be avoided, and only the final equations and the conditions for which they apply will be stated[50].

Linear sweep voltammetry involves observation of the current response to a linear sweep in electrode potential from a initial value, $E_i$, (at which no electrochemical reaction occurs) at some rate $\upsilon$ to a final potential, $E_f$. After the initiation of a sweep, the potential of the electrode at time t is given by:

$$E_t = E_i + \upsilon t \qquad 4.47$$

Consider a simple reaction such as:

$$O + ne \text{ ----------> } R$$

and choose $E_i$ so that O is not reduced. If the potential is now moved cathodically from $E_i$ at a very low sweep rate, the species O is reduced and the rate of reduction accelerates, with increasing t. Mass transfer of O to the electrode surface eventually limits the rate of reaction and the process becomes diffusion controlled. The resulting i-t curve is that observed for the steady state. As the rate $\upsilon$ is increased, however, a peak on the i-t curve (see Figure 4.7) results due to a combination of high mass transfer rates in the non-steady state and progressive depletion of the concentration of O in the diffusion layer.

For a reversible reaction the peak current, $i_p$, may be written as:

$$i_p = 2.69 \times 10^5 \cdot n^{3/2} \cdot AD_O^{1/2} C_O \upsilon^{1/2} \qquad \text{at } 25^oC \qquad 4.48$$

The peak potential is independent of sweep rate and related to the half-wave potential by the following expression:

$$E_p = E_{p/2} - \frac{0.028}{n} \qquad \text{at } 25^oC \qquad 4.49$$

where $E_p$ is the potential at which $i_p$ occurs, and $E_{p/2}$ is the potential for which $i = i_{p/2}$.

If a reverse sweep is carried out, i.e. electrode potential varied from $E_i$ to $E_f$ and back to $E_i$ this is called cyclic voltammetry, and a peak of opposite sign, corresponding to the reverse reaction is observed on the return. In such a case, the separation $\Delta E_p$ of the two peaks is given by:

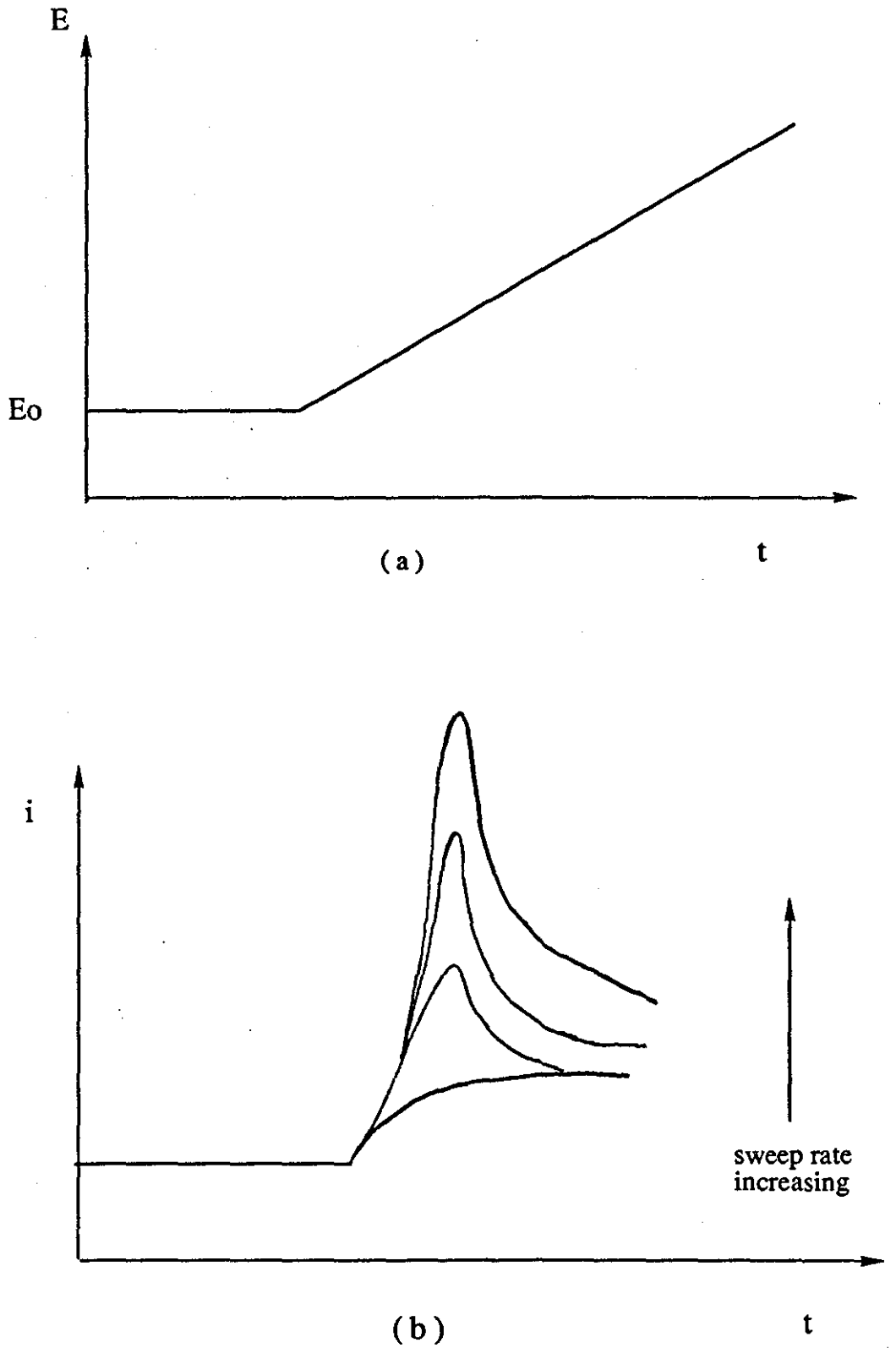


FIG. 4.7 - L.S.V. - a) POTENTIAL, E, VARYING LINEARLY WITH TIME, t.
b) EFFECT OF SWEEPRATE ON CURRENT RESPONSE WITH TIME

$$\Delta Ep = \frac{0.059}{n} V \qquad 4.50$$

for a reversible process.
For an irreversible reaction the peak characteristic is as:

$$ip = 2.99 \times 10^5 n (\alpha n_\alpha)^{1/2} . D_o^{1/2} C_o^b \upsilon^{1/2} \qquad 4.51$$

where n is the number of electrons transferred up to and including the rate determining step. The peak potential is a function of the sweep rate, $\upsilon$ and a plot of Ep versus $\upsilon^{-1/2}$ goes through the limiting value $\frac{0.059}{n}$ .

Therefore, L.S.V. indicates the number of electrons involved in the charge transfer reaction, the charge transfer coefficient, and the reversibility of a reaction. However it is usually only possible to obtain such information for simple systems. For more complex systems, LSV is normally employed as a qualitative tool.

# CHAPTER 5

# EXPERIMENTAL PROCEDURES AND CHEMICALS

## 5.1 ELECTROLYTE AND GLASSWARE

All solutions used were prepared with triply-distilled water and 0.1M sodium perchlorate, $NaClO_4$ (in some cases 1M sodium perchlorate was employed - see text). Sodium perchlorate was chosen because the perchlorate anion is not adsorbed under the experimental conditions[51], and there is no evidence to suggest that it either enhances or suppresses corrosion.

In order to achieve a neutral pH, appropriate amounts of perchloric acid ($HClO_4$) or sodium hydroxide (NaOH) were added. All chemicals used were Analar grade. The glassware employed in the experiments was thoroughly cleaned, first by soaking overnight in a 50/50 mixture of concentrated nitric acid and concentrated sulphuric acid, and second by repeated washings in triply-distilled water.
N.B. Particular care was taken to remove any acid from glass frits used in the electrochemical cell. The cells used are described in each chapter.
Temperature control was obtained using either a thermostated water-bath (Grant Instruments) or an adiabatic chamber.

## 5.2 ELECTRODES

Counter Electrode - the counter or secondary electrode was a rolled piece of platinum gauze of about $2cm^2$, affixed to a length of platinum wire.

Reference Electrode - the reference electrode, RE, employed was a saturated sodium chloride calomel electrode (E = 0.236V vs. S.H.E.). The ceramic junction was 1mm in diameter with a quoted electrolyte

leakage of 0.1ml per 24hrs (at 25 deg C) (Pye Unicam reference electrode). N.B. ALL POTENTIALS ARE REFERED TO THIS ELECTRODE UNLESS OTHERWISE STATED.

Working Electrode - the working electrode, WE, was dependent on the technique employed. Pure iron studs (99.999%) of 0.5cm diameter, supplied by Johnson-Matthey Chemicals Limited were used for rotating disc studies, whilst in the mechanically pumped techniques, iron sheet (99.9% pure) was used, supplied by Goodfellow Metals. The exact fabrication and cleaning method employed is given in each chapter.

## 5.3 ELECTRICAL EQUIPMENT

Potential control was induced using a Ministat Precision Potentiostat, and '16 Bit' Ramp Generator (where necessary) supplied by Thomson Electrochem. Ltd. The Rotating Disc Electrode apparatus was also supplied by Thomson Electrochem. Ltd. Current readings were obtained using a Hewlett Packhard "zero" resistance multimeter (Model 3478A) and potential readings using a Beckman digital voltmeter. All chart recorder traces and voltammograms were obtained from a Gould Series 60000 X-Y recorder.

## 5.4 CHEMICALS

All commercial inhibitor formulations were supplied by Grace Dearborn Chemicals Ltd. Any other compounds used were Analar grade with the exception of zinc perchlorate which was prepared from zinc powder and A.R grade perchloric acid.
The commercial inhibitor formulations are as follows:

| | | |
|---|---|---|
| POLYMATE 966 : | 100ppm contains : | 2.2ppm $Zn^{2+}$ |
| | | 8.8ppm phosphonate |

POLYMATE 945 : 100ppm contains : 2.2ppm $Zn^{2+}$
8.8ppm phosphonate
3.0ppm orthophosphate

HYDROXY-PHOSPHONO CARBOXYLIC ACID ( H.P.A.) :

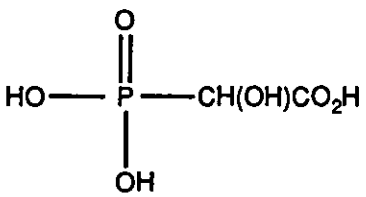


PHOSPHONO CARBOXYLIC ACID ( P.C.A.) :

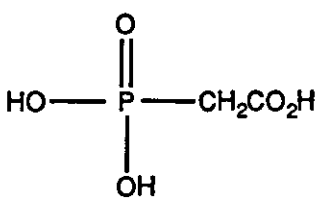

COMPOSITION OF LOUGHBOROUGH TAP WATER :

pH = 7.5

Methyl Orange alkalinity as $CaCO_3$ = 140ppm

Phenolphthalein alkalinity as $CaCO_3$ = 0ppm

Calcium hardness as $CaCO_3$ by EDTA = 200ppm

Total hardness as $CaCO_3$ by EDTA = 276ppm

Chloride as $Cl^-$ = 58ppm

# CHAPTER 6

# ROTATING DISC ELECTRODE STUDIES OF OXYGEN ON AN IRON SURFACE IN NEUTRAL ELECTROLYTE

## 6.1 LITERATURE REVIEW - OXYGEN REDUCTION ON IRON

In recent years, the increased interest in hydrogen-oxygen fuel cells[52-57] has lead to the electrochemistry of oxygen on precious metals receiving a great deal of attention. In comparison, the reduction of oxygen upon iron and mild steel has received minimal study. This is surprising, since oxygen reduction has a marked effect on the corrosion of iron, along with the anodic partial reaction (i.e. iron dissolution) which has been extensively studied[58-62]. Therefore, it is important that the mechanism of oxygen reduction on iron be fully appreciated when studying the action of cathodic inhibitors. When studies of the cathodic reaction on iron have been performed, acid[63] or alkaline[64] media has usually been employed. In acid media, oxygen reduction has no relevance and hydrogen evolution is the predominating cathodic process. Studies in alkaline solution were undertaken by Fabjan et al[64],who stated that the reduction of oxygen on iron, in alkaline solutions was similar to that for cobalt and nickel. Fabjan obtained Tafel slopes of -0.14 to -0.16 V per decade and a reaction order of 0.5 with respect to $O_2$ and -1 with respect to OH- ions. A reaction order of 0.5 is indicative of a disproportionation step in the reduction sequence. Schiffrin[65] discusses two reduction schemes, involving a disproportionation step:

1) $O_2 + e^- \text{-----> } O_2^-$

2) $O_2^- + H_2O \text{-----> } HO_2 + OH^-$

3) $HO_2 \text{-----> } OH + 1/2O_2$

4) $OH + e^- \text{-----> } OH^-$

SCHEME A

1) $O_2 + e^- \text{-----> } O_2^-$

2) $O_2^- + H_2O \text{-----> } HO_2 + OH^-$

3) $HO_2 + e^- \text{-----> } O_2H^-$

4) $O_2H^- \text{-----> } OH^- + 1/2O_2$

SCHEME B

Both schemes involve one electron reduction of molecular oxygen to the superoxide ion $O_2^-$. The rate determining step corresponds to the first electron-transfer step i.e. step 1). Both schemes also involve an overall two electron reduction mechanism, with the production of 1/2 mole of oxygen for further reduction. They differ in that scheme A involves the disproportionation of superoxide to give hydroxyl radicals (step 3), whilst scheme B involves the decomposition of peroxide.

A number of difficulties arise from the disproportionation step (3) in scheme A :

a) In alkaline media (i.e. 1M-KOH) step 3 should read:

$$O_2^- + O_2^- + 2H_2O \text{-----> } 2OH + 2OH^- + O_2 \qquad 3'$$

since the pK of the acid-base equilibrium:

$$HO_2 \quad <-------> \quad H^+ + O_2^-$$

is 4.69 [68] .

b) The free energy of the revised step 3' is +52.6 kJmol$^{-1}$ indicating that the homogeneous reaction is thermodynamically unfavorable. In contrast, the decay pathways for the superoxide radical observed from pulse radiolysis are well established[66]:

$$O_2^- + O_2^- + 2H_2O \quad <-------> \quad O_2 + H_2O_2 + 2OH^-$$

Thus, the generation of OH• radicals in reaction 3 of scheme A is unlikely, yet the possibility of this reaction occurring between adsorbed species must not be excluded.

The above is of great interest and importance, but has no direct relevance to cooling water systems, where a neutral medium is encountered. In fact, scant attention has been paid to oxygen reduction in neutral solutions[65,66]. Again, this is difficult to comprehend at first sight, since the use of neutral media is of great practical importance in the study of metallic corrosion. An explanation for the lack of studies in neutral media, maybe due to the difficulties arising from the increase in pH at the electrode surface, upon oxygen reduction. When oxygen is reduced upon the iron surface, hydroxide ion is generated, leading to an increases in pH in the vicinity of the double layer. This in turn, causes a change in the potential, at the electrode surface.

The few papers that have been devoted to studying oxygen reduction on iron in neutral solution, have only briefly discussed mechanistic details. Foroulis[67] studied the effect of dissolved oxygen concentration and rotation speed (i.e using a rotating disc electrode) on the initial corrosion of iron in 'pure' water. Delahay[68] conducted studies in near neutral solutions, and since he detected little $H_2O_2$ , concluded that oxygen reduction involved a four electron

mechanism. Sawyer[69] in contrast, disputes a four electron process, referencing the work of Wroblowa et al[70], and confirms that the superoxide ion is the reduction product generated in aqueous media[71-73]. Sawyer proposes two mechanistic schemes for the reduction of oxygen. The first applies to an inert electrode surface. Here, the initial step involves one electron reduction of oxygen to superoxide ion, followed by a chemical step. The second mechanism applies to a non-inert, pre-oxidised electrode surface and involves a chemical step preceding the electron transfer to molecular oxygen. Both mechanisms are discussed only briefly, and with reference to acid and alkaline solutions alone.

Jovancicevic and Bockris[74], studied the mechanism of oxygen reduction on both bare iron and passive iron in a borate buffer solution. A buffer was used to remove any pH effects at the electrode surface. Rotating ring disc electrodes were used, and Tafel slopes of -110mV/decade (passive iron) and -120mV/decade (bare iron) obtained. The mechanisms of oxygen reduction on passive iron and bare iron are discussed.

On a passive iron film, oxygen reduction was found to occur via a two electron transfer reaction with the formation of $H_2O_2$ at 0.11V (N.H.E.)[75]. The most probable pathways and rate determining steps are summarised. The experimental data obtained, i.e. Tafel slope of 2RT/F, reaction order with respect to oxygen of 1 and reaction order with respect to ($OH^-$) of -0.4, give rise to the pathways below:

$$O_2 \text{ -----> } O_{2ad}$$

$$O_{2ad} + H_2O + e^- \text{ -----> } O_2Had + OH^-$$

$$O_2Had + e^- \text{ -----> } O_2H^-$$

$$O_2H^- + H_2O \text{ -----> } H_2O_2 + OH^-$$

and

$$O_2 + H_2O \text{ -----> } O_2H^+ + OH^-$$

$$O_2H^+ + e^- \text{ -----> } O_2Had$$

$$O_2Had + e^- \text{ -----> } O_2H^-ad$$

$$O_2H^-ad + H_2O \text{ -----> } H_2O_2 + OH^-$$

Of the two, the second is unlikely, since oxygen reduction on the passive layer takes place between +0.05 to -0.2V (N.H.E.). This is believed to be 0.2V positive of the point of zero charge for $O_2H^+$ on the passive layer, (cf. the p.z.c. on the bare iron is about -0.64V vs. N.H.E. in neutral media)[76]. Therefore, the first mechanism is believed the more probable.

The chemical rate determining step involves the chemisorption of dioxygen on the surface active sites i.e.:

$$O_2 \text{ -----> } O_2ad \quad (\text{rds})$$

which is an important step in the oxygen reduction at catalytic surfaces. After the rate determining step, the following electron transfer steps occur:

$$O_2ad + H_2O + e^- \text{ <-----> } O_2Had + OH^-$$

$$O_2Had + e^- \text{ <-----> } O_2H^-$$

$$O_2H^- + H_2O \text{ <-----> } H_2O_2 + OH^-$$

Jovancicevic also showed that oxygen reduction on the passive oxide film (at pH = 7) is about 100 times higher than on bare iron. This is

in contrast to oxide covered metals such as Pt and Ni[77,78] where a decrease is observed.

On bare iron, Jovancicevic et al[74], found that 99% of the oxygen reduction current forms $OH^-$ and not $H_2O_2$, which contrasts to that on passive iron, where $H_2O_2$ is the reaction product. The reduction was found to be a four electron process, and a number of mechanisms are discussed. The first step of the reduction sequence involves the breaking of the O-O bond on adsorption of $O_2$ on the surface, in a side on configuration[79]. The reaction sequence can then proceed either through the electrocatalytic pathway, which involves bond breaking as the rate determining step, or, through the formation of superoxide or $O_2H_{ad}$. It is believed that the latter is more likely as water is less capable of bonding to O-O in a side on configuration. The most probable rate determining step involves:

$$O_2 + e^- \text{-----> } O_2^-$$

leading to either the chemical or electrochemical O-O bond breaking steps:

$$O_2 + e^- \text{-----> } O_2^-$$

$$O_2^- + H_2O \text{-----> } OH_{ad} + O_{ad} + OH^-$$

CHEMICAL

$$O_{ad} + H_2O + e^- \text{-----> } OH_{ad} + OH^-$$

$$OH_{ad} + e^- \text{-----> } OH^-$$

$O_2 + e^- \text{-----> } O_2^-$

$O_2^- + H_2O \text{-----> } HO_{2ad} + OH^-$

$HO_{2ad} + H_2O + e^- \text{-----> } H_2O_{2ad} + OH^-$ CHEMICAL

$H_2O_{2ad} \text{-----> } 2OH_{ad}$

$OH_{ad} + e^- \text{-----> } OH^-$

$O_2 + e^- \text{-----> } O_2^-$

$O_2^- + H_2O \text{-----> } HO_{2ad} + OH^-$

ELECTROCHEMICAL

$HO_{2ad} + H_2O + e^- \text{-----> } 2OH_{ad} + OH^-$

$OH_{ad} + e^- \text{-----> } OH^-$

Although the work of Jovancicevic gives good mechanistic detail for oxygen reduction in borate buffered solutions, it is inapplicable to cooling water systems. Borate buffer is used to maintain a constant pH and hence removes the difficulties associated with $OH^-$ production at the electrode surface. However, in a cooling water system the $OH^-$ concentration within the double layer vicinity increases. Further, many cathodic inhibitors require the presence of $OH^-$ ions at the metal surface to function effectively. Borate may also effect the inhibitor mechanism as it is adsorbed onto the iron surface. Therefore, to study the oxygen reduction mechanism in neutral media, and evaluate cathodic inhibitors, buffered solutions cannot be employed.

## 6.2 EXPERIMENTAL - INVESTIGATION OF THE OXYGEN REDUCTION PROCESS ON IRON

### 6.2.1 EXPERIMENTAL

In order to fully investigate the reduction of oxygen upon iron, and obtain kinetic data and mechanistic detail, a series of potentiostatically controlled experiments were undertaken. For all experiments, a conventional three limbed cell was employed, Figure 6.1, along with a rotating disc assembly. The rotating disc electrode consisted of a 0.5cm diameter Specpure iron stud (supplied by Johnson Matthey Chemicals), pressed and sealed into a P.T.F.E. shroud (Figure 6.2). This was threaded into a glass filled P.T.F.E. shaft fitted to the rotating disc. (N.B. Removal of the stud allowed ease of polishing and microscopic observation). Contact between the rotating disc's shaft and stud was made via a steel spring. The cell was sealed from the atmosphere using a P.T.F.E. cup and glass reservoir assembly filled with electrolyte (see Figure 6.3). Electrode preparation was identical for each experiment:

i) Polished on 600 grit wet "wet and dry" silicon carbide paper.
ii) Washed in tri-distilled water.
iii) Polished on 1200 grit wet "wet and dry" silicon carbide paper.
iv) Washed in tri-distilled water.
v) Polished with 0.5 μm alumina on a selvyt polishing cloth.
vi) Washed in tri-distilled water.
vii) Dried and placed immediately in a dessicator.

Using this regime a completely new surface was produced for each experiment.

The electrolyte used was 0.1M $NaClO_4$ adjusted to pH 7. This was saturated with oxygen for 30 minutes prior to each separate experiment.

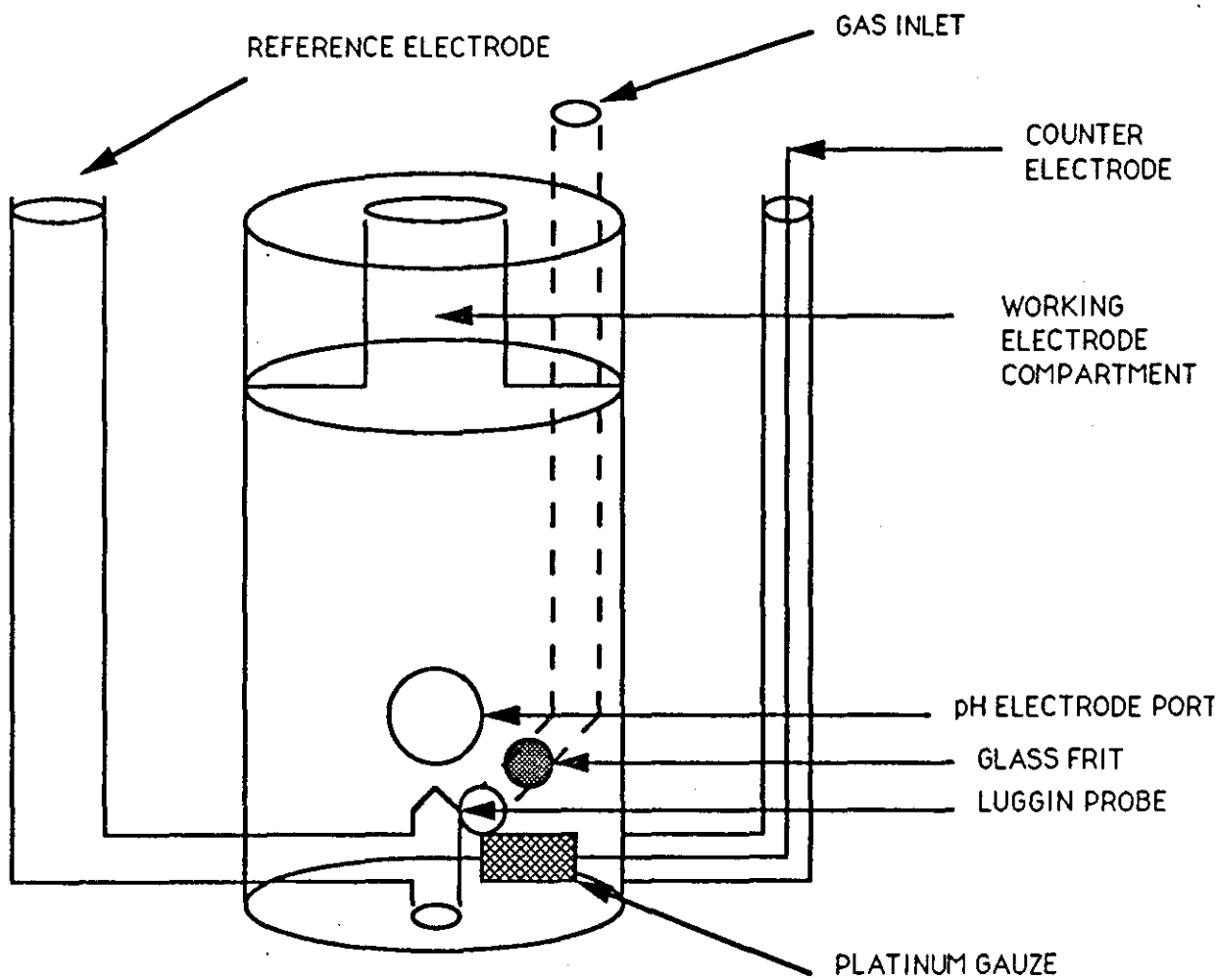


FIG. 6.1 GLASS CELL FOR L.S.V EXPERIMENTS

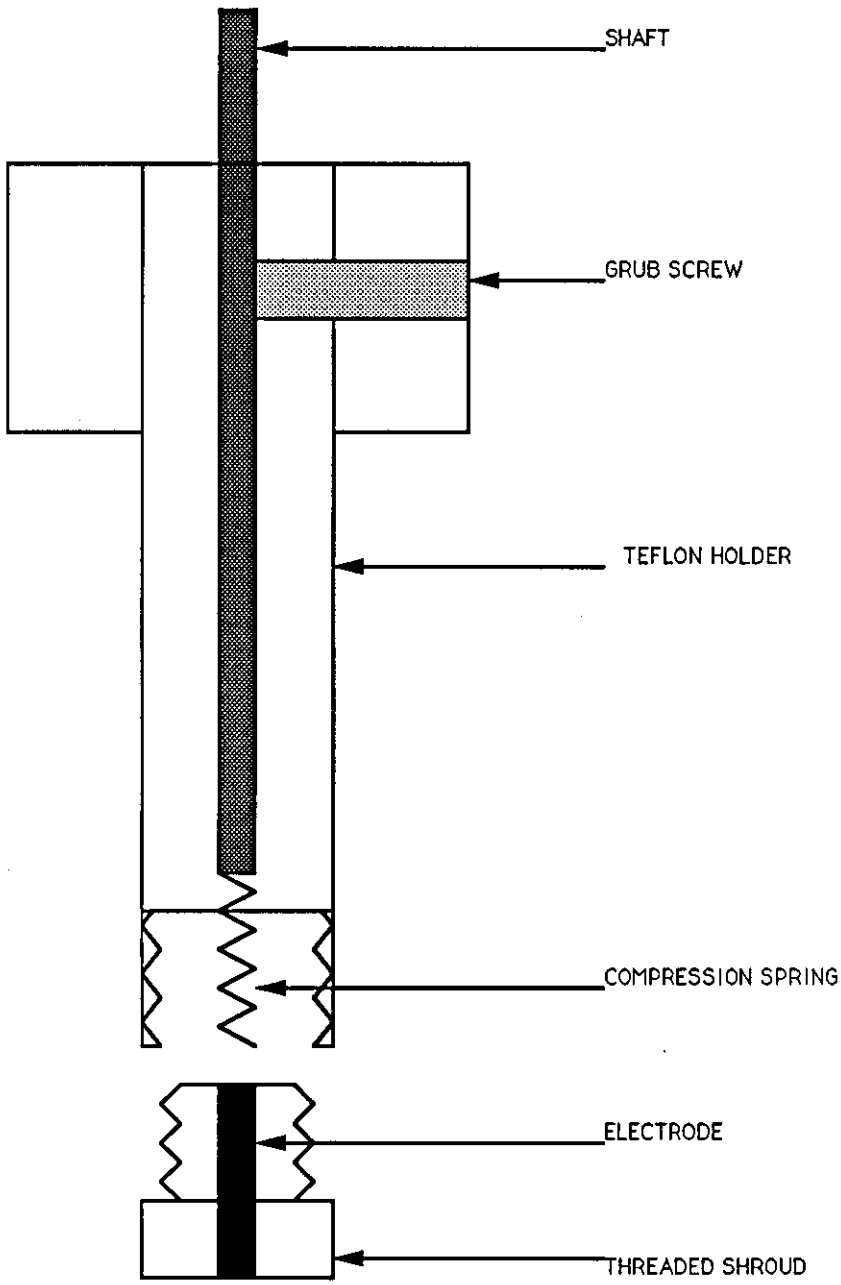


FIG. 6.2 - P.T.F.E. R.D.E. ASSEMBLY

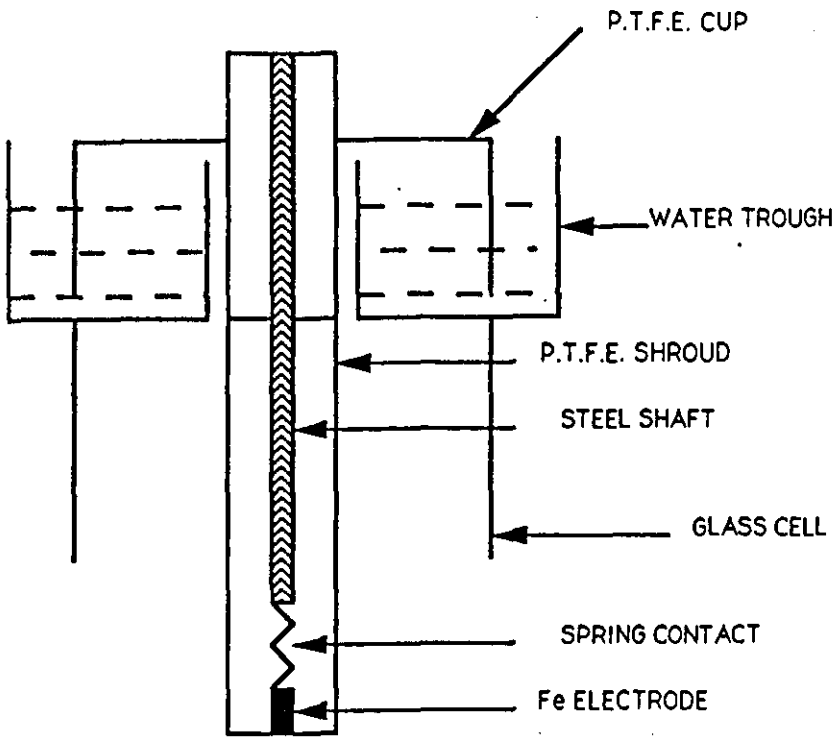


FIG. 6.3 - PTFE CUP AND WATER TROUGH ASSEMBLY

## 6.2.2 RESULTS AND DISCUSSION

Experiment 1

Initially, in order to obtain an overall picture of the cathodic processes occurring at a "clean" electrode, linear sweep voltammetry was employed (see Figure 6.4 for experimental assembly). The open circuit potential of iron in oxygenated 0.1M $NaClO_4$ was found to vary widely over the range -200mV ---> -280mV. Thus, in order to keep a "clean" corrosion free surface for mechanistic studies, the electrode was immersed negative of the open circuit potential i.e. at -300mV and at a rotation speed of 900rpm, to ensure a well defined flow pattern. The electrode was allowed to equilibrate for 10 minutes, until a relatively steady current value had been reached, before sweeping at 0.5mVs$^{-1}$ to -1500mV. Figure 6.5 shows a typical ' S ' shaped curve obtained on a consistent basis. The areas of the curve relate as follows:

| | |
|---|---|
| -300mV ----> -700mV | ELECTRON TRANSFER |
| -700mV ----> -850mV | MIXED CONTROL i.e. ELECTRON TRANSFER + MASS TRANSPORT CONTROL |
| -850mV ----> -1150mV | MASS TRANSPORT CONTROL |
| -1150mV ONWARDS | HYDROGEN EVOLUTION PREDOMINATES |

Experiment 2

Figure 6.6 shows the results obtained when various rotation speeds ranging from 373rpm to 1492rpm were employed and the electrode swept from -300mV to -1200mV at a sweeprate of 10mVs$^{-1}$. An increase in the plateau current (i.e. between -850mV and -1150mV) was observed with increasing rotation speed, whilst below -700mV the traces followed the same line. This proves that the current

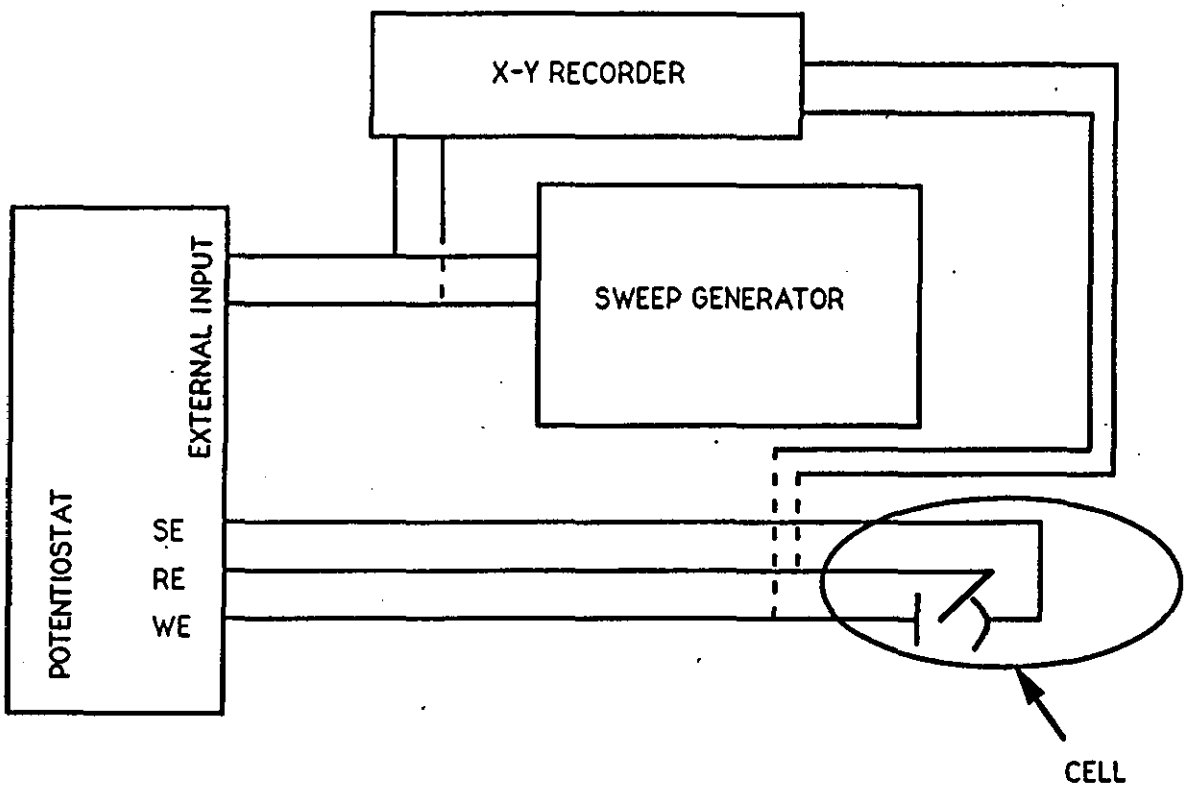


FIG. 6.4 - EXPERIMENTAL ASSEMBLY

FIG.6.5 - TYPICAL 'S' SHAPED CURVE FOR OXYGEN REDUCTION ON IRON

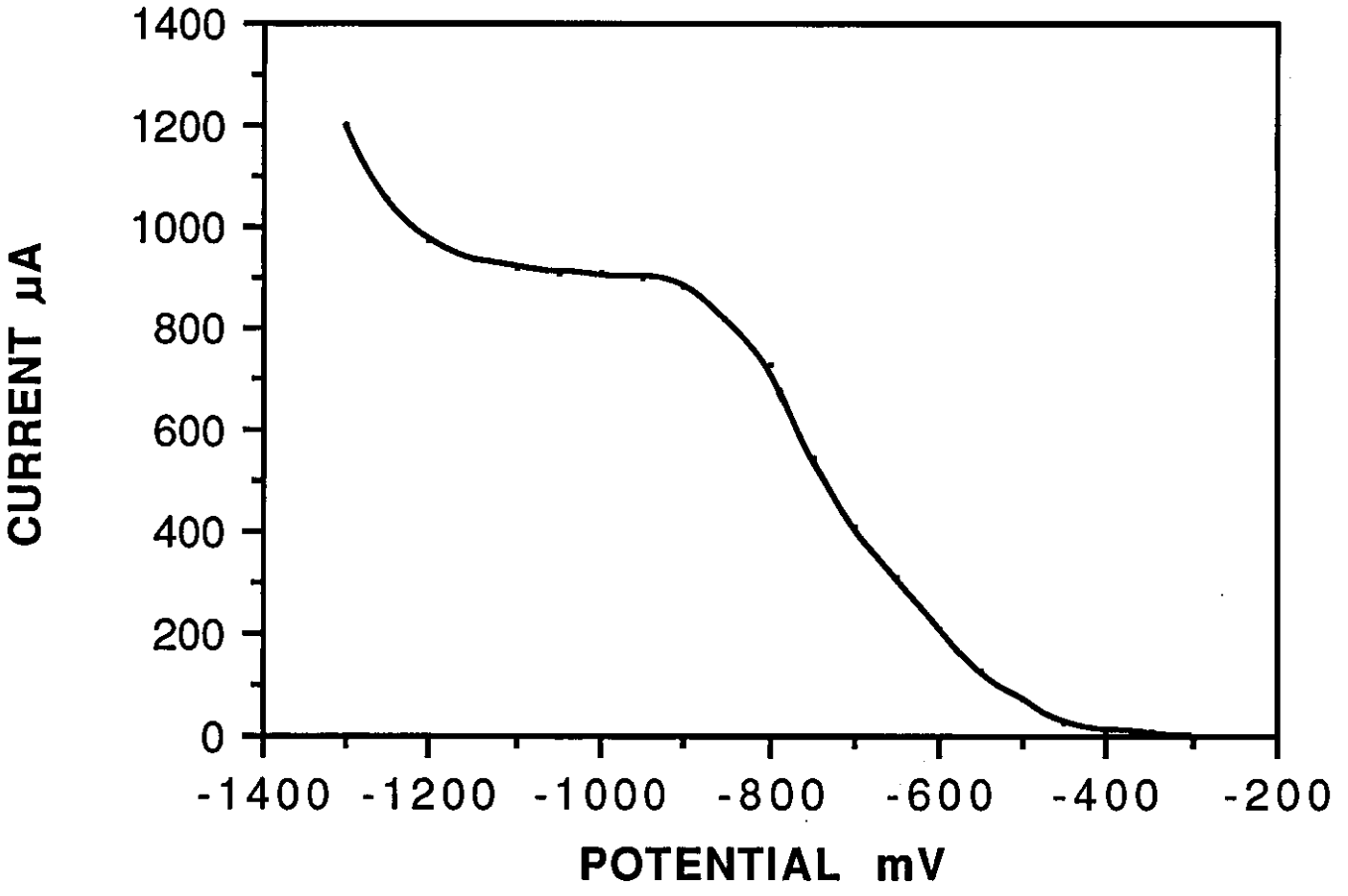

FIG. 6.6 - VARIATION OF CURRENT WITH ROTATION SPEED

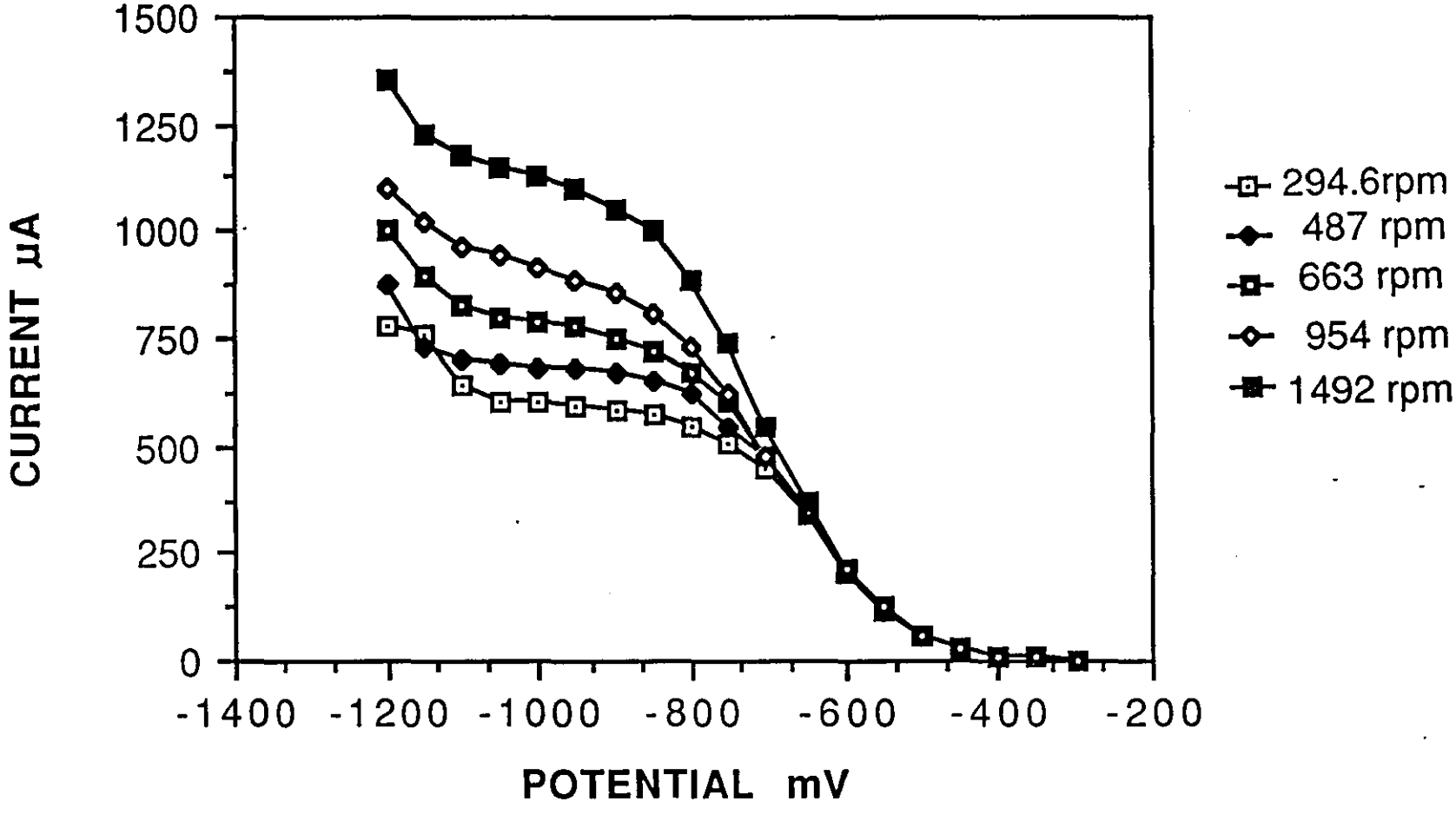

negative of -850mV is entirely mass transport controlled, and that above this potential the surface concentration of oxygen is zero. N.B. The increase in current with rotation speed, is a result of an increase in oxygen "pumped" to the electrode surface.

Experiment 3

The region of the 'S' shaped curve displaying total electron transfer control, i.e. between -300mV and -700mV, was used to obtain an I-E curve at a constant rotation speed of 900rpm. From the I-E curve, a Tafel plot was drawn and the number of electrons transferred during the rate determining step calculated from the slope. Figure 6.7 gives I-E curves typical of those obtained, whilst Figure 6.8 gives the Tafel plots for each. Slopes of 150mV/decade, 162.5mV/decade and 154mV/decade were obtained. This suggests that the rate determining step for the reduction of oxygen is a one electron transfer (i.e. ideally slope = 120mV/decade when $\alpha = 0.5$). Furthermore, values for the corrosion current densities were obtained for each experiment, these being $8.4 \times 10^{-6}$, $7.9 \times 10^{-6}$ and $9 \times 10^{-6}$ $Acm^{-2}$ respectively.

Experiment 4

Figure 6.9, shows the I-E curves for 0.1M $NaClO_4$ at pH values of 5 and 9. The resultant Tafel plots gave slopes of 180mV/decade and 150mV/decade respectively - Fig 6.10. Therefore, in the acidic solution, an increase in Tafel slope occurs. This can be explained as proton reduction (leading to hydrogen evolution) is occuring along with the oxygen reduction reaction.

From the results obtained in experiment 3, the changes in Tafel slopes and corrosion current densities on adding cathodic inhibitors to the electrolyte, should give a good indication of the relative inhibitor efficiencies.

FIG.6.7 - OXYGEN REDUCTION IN 0.1M NaClO4

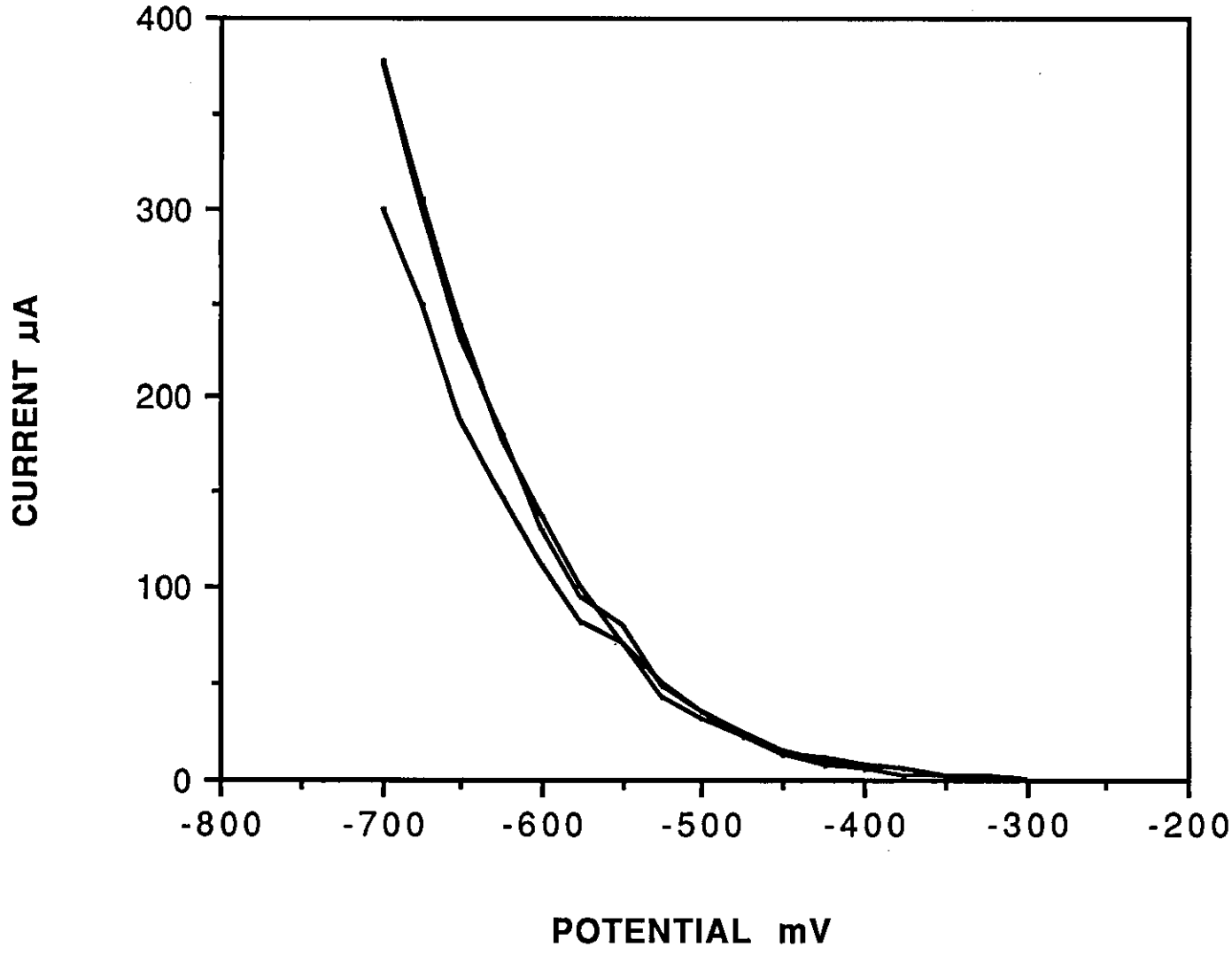

FIG. 6.8 - TAFEL PLOT FOR 0.1M NaClO4

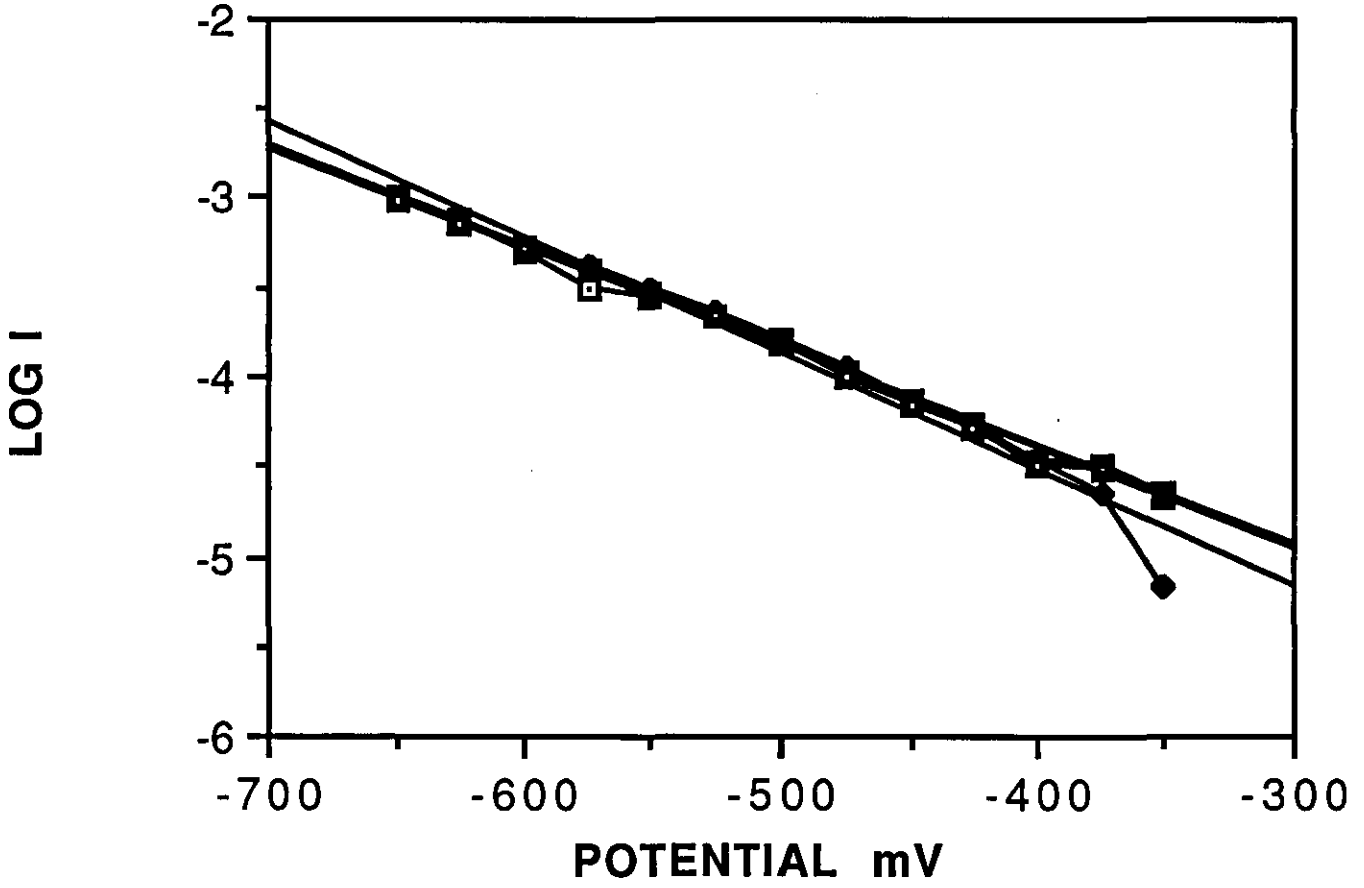

FIG. 6.9 - OXYGEN REDUCTION IN 0.1M NaClO4 (pH 5 AND 9)

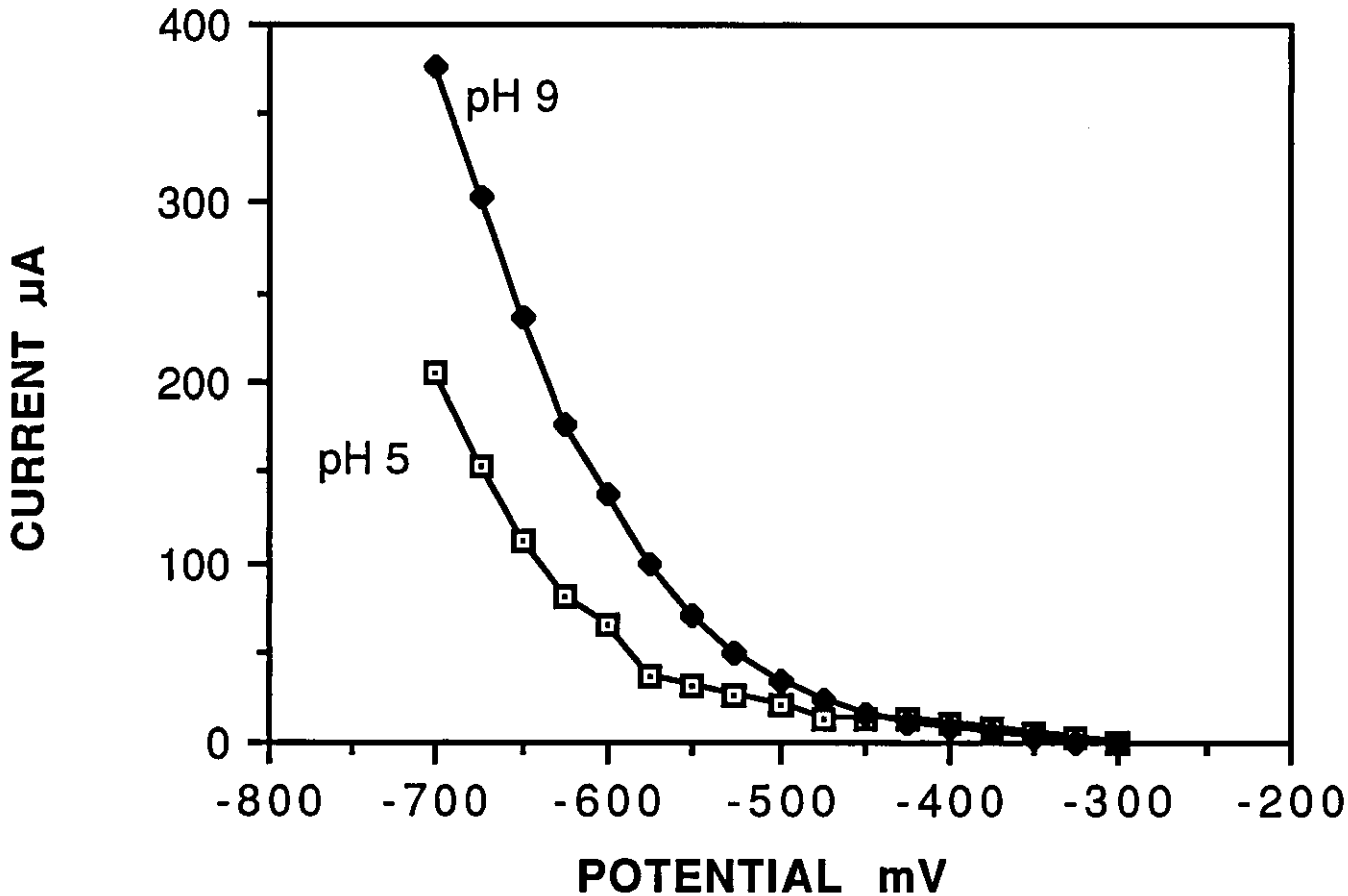

FIG. 6.10 - EFFECT OF pH ON TAFEL SLOPE

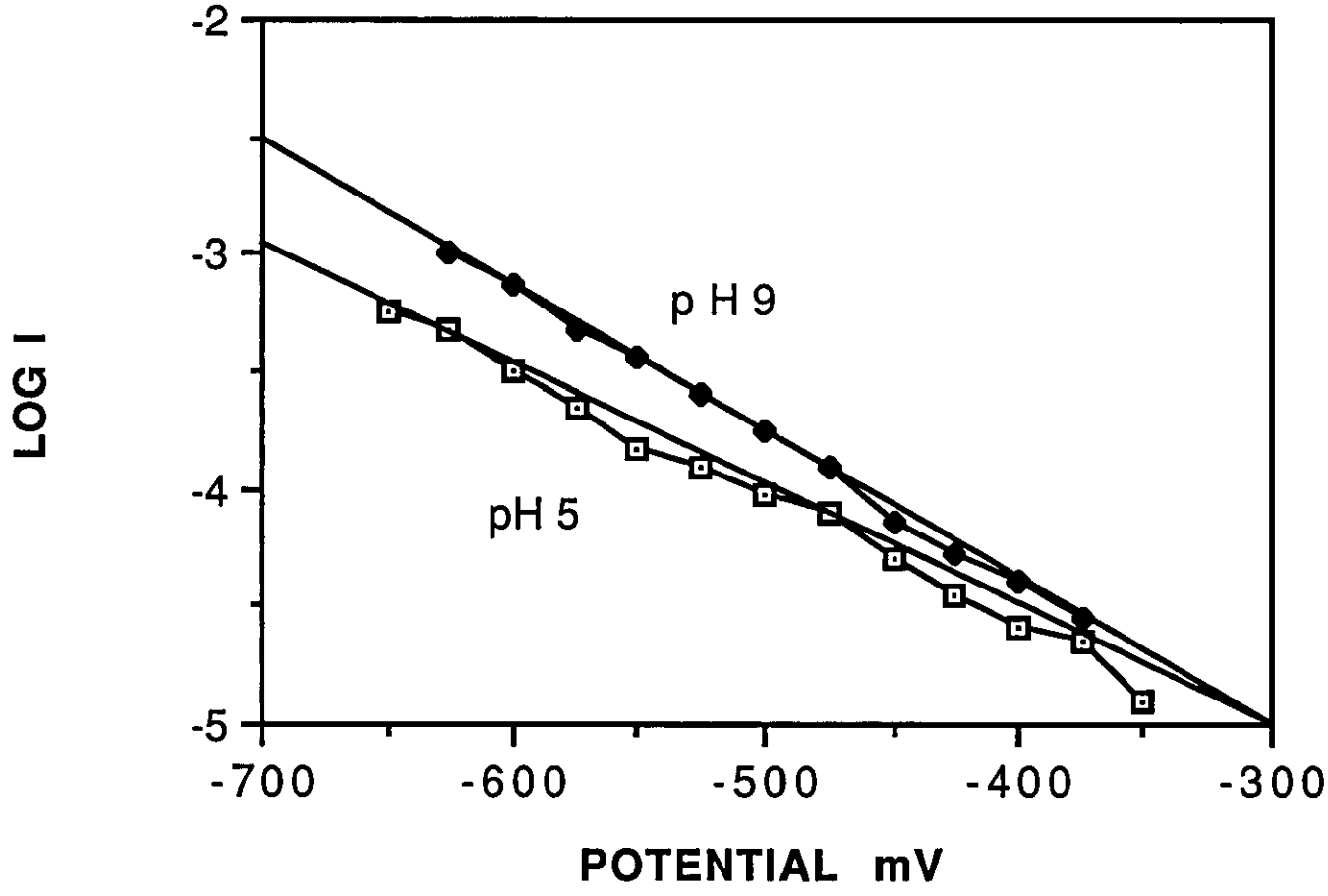

Experiment 5

Initial experiments to evaluate the effects of cationic species on the Tafel slope and corrosion current densities, involved the use of Loughborough tap water (see Chapter 5 for composition). This was used to simulate plant conditions in which a hard water would be encountered. Figure 6.11 gives the I-E curves obtained and Figure 6.12 the resultant Tafel plots. The recorded Tafel slopes were observed to change at a potential of -450mV, e.g.

122mV/decade ----> 275mV/decade

122mV/decade ----> 240mV/decade

On reproducing these experiments it was noted that the slope consistently increased, signifying a change in the mechanism of the rate determining step. Corrosion current densities for tap water also varied widely from 6.6 x $10^{-4}$ $Acm^{-2}$ to 8.5 x $10^{-6}$ $Acm^{-2}$. (N.B. These values are for the initial slopes i.e. below -450mV, as values above were even more varied). It is obvious that the tap water has an inhibiting effect on the oxygen reduction at the electrode surface. The change in slope is probably due to the formation of a surface film of scale upon the iron. Corrosion current densities are similar to those in 0.1M $NaClO_4$ .

Experiment 6

In an attempt to remove any irreproducibility that may be caused by inconsistency in the tap water composition, an electrolyte containing 200ppm $Ca^{2+}$ alone was prepared. Changes in Tafel slope (Figure 6.14) were observed from the I-E curves (Figure 6.13), giving reasonably reproducible values:

165mV/decade ----> 200mV/decade

170mV/decade ----> 200mV/decade

Corrosion current densities of 7.7 x $10^{-5}$ $Acm^{-2}$ and 3.39 x $10^{-6}$ $Acm^{-2}$ are representative of those calculated from the initial Tafel slopes. These infer an initial increase in oxygen reduction at the cathodic sites. However, these values must be taken lightly, since extrapolation of the second Tafel slope i.e. above -450mV to the original corrosion potential (taken as -300mV for

FIG. 6.11 - OXYGEN REDUCTION ON IRON IN TAP WATER

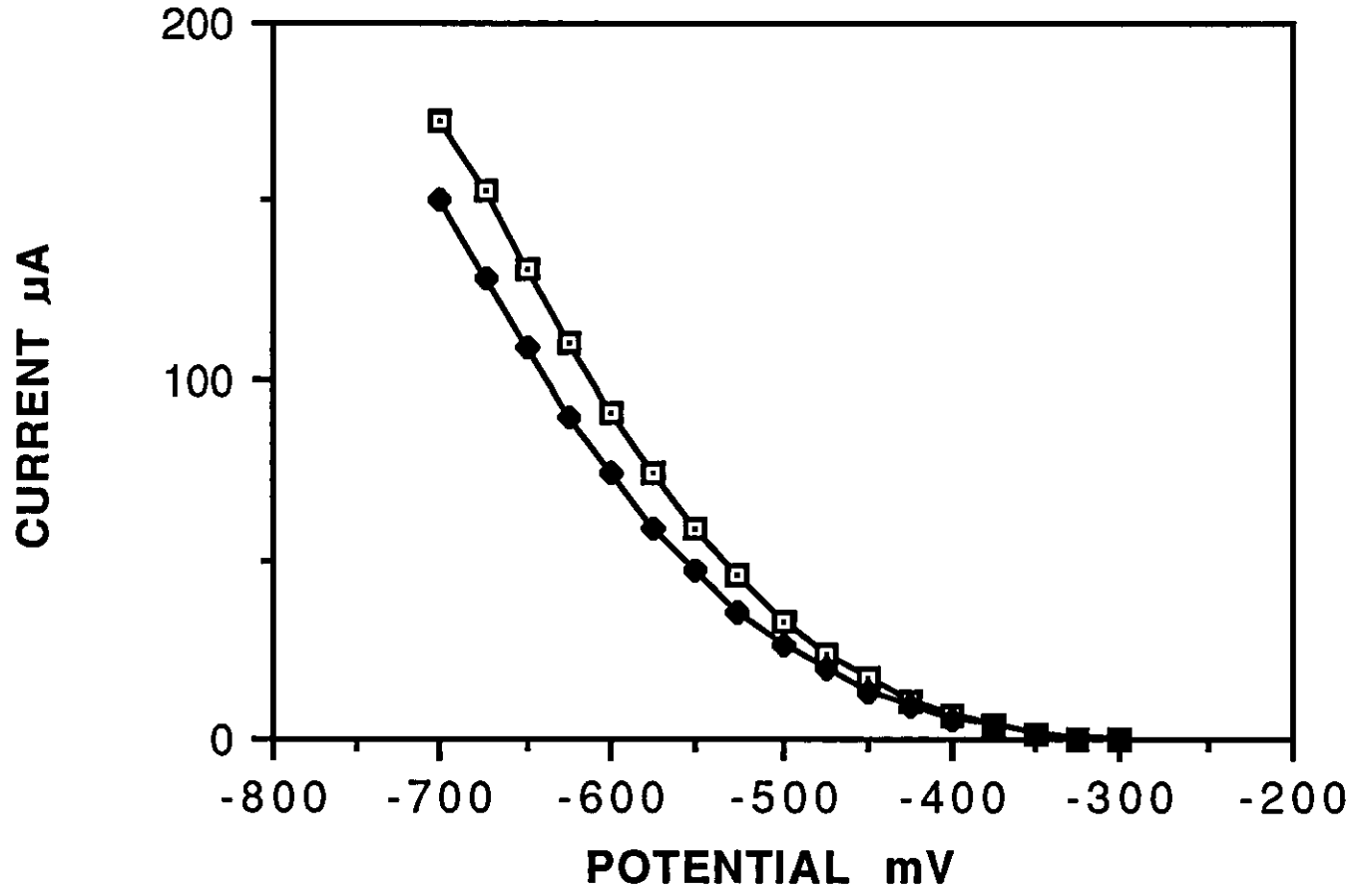

FIG. 6.12 - TAFEL PLOTS FOR TAP WATER

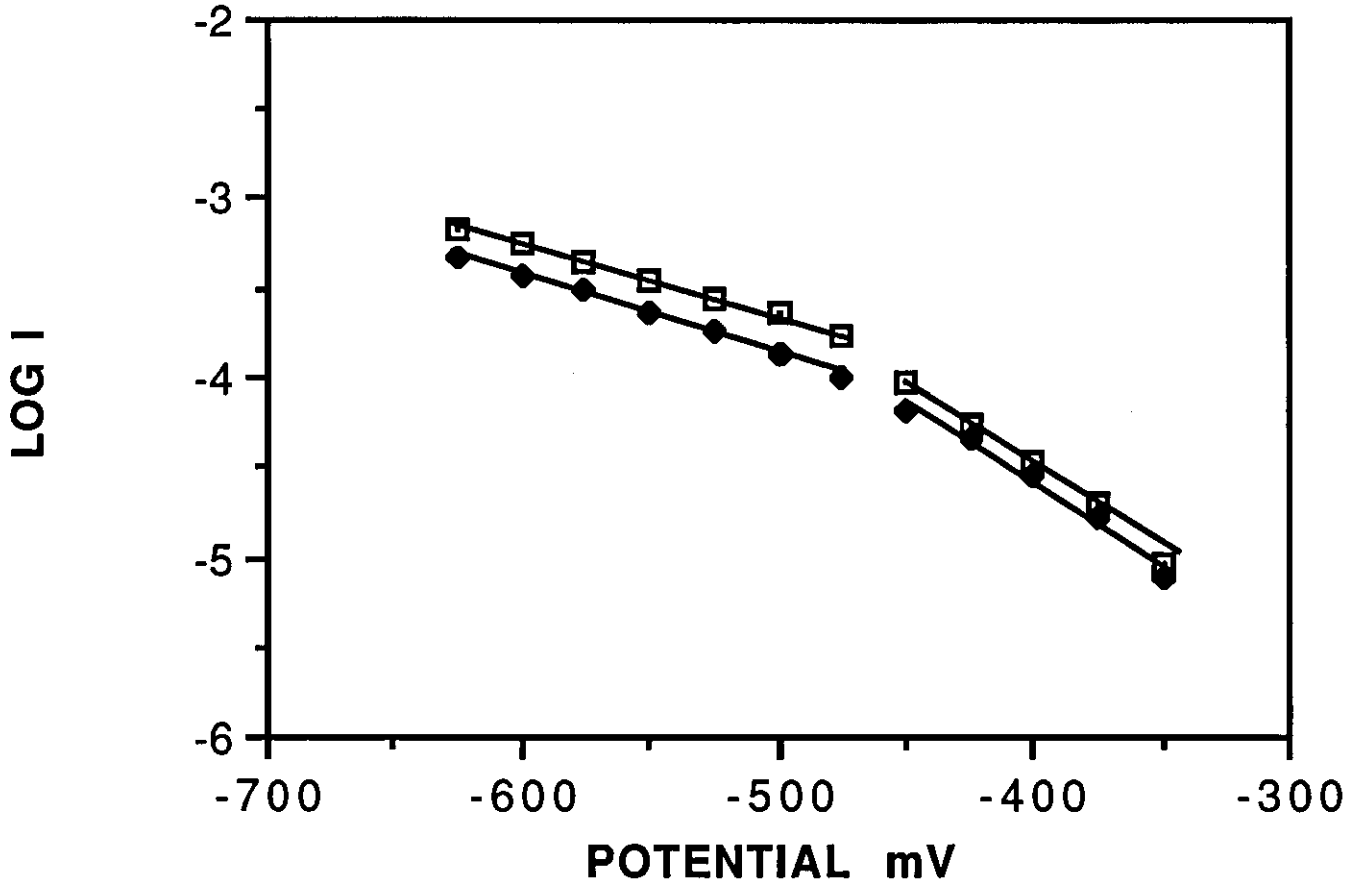

FIG. 6.13 - OXYGEN REDUCTION ON IRON WITH 200ppm CALCIUM

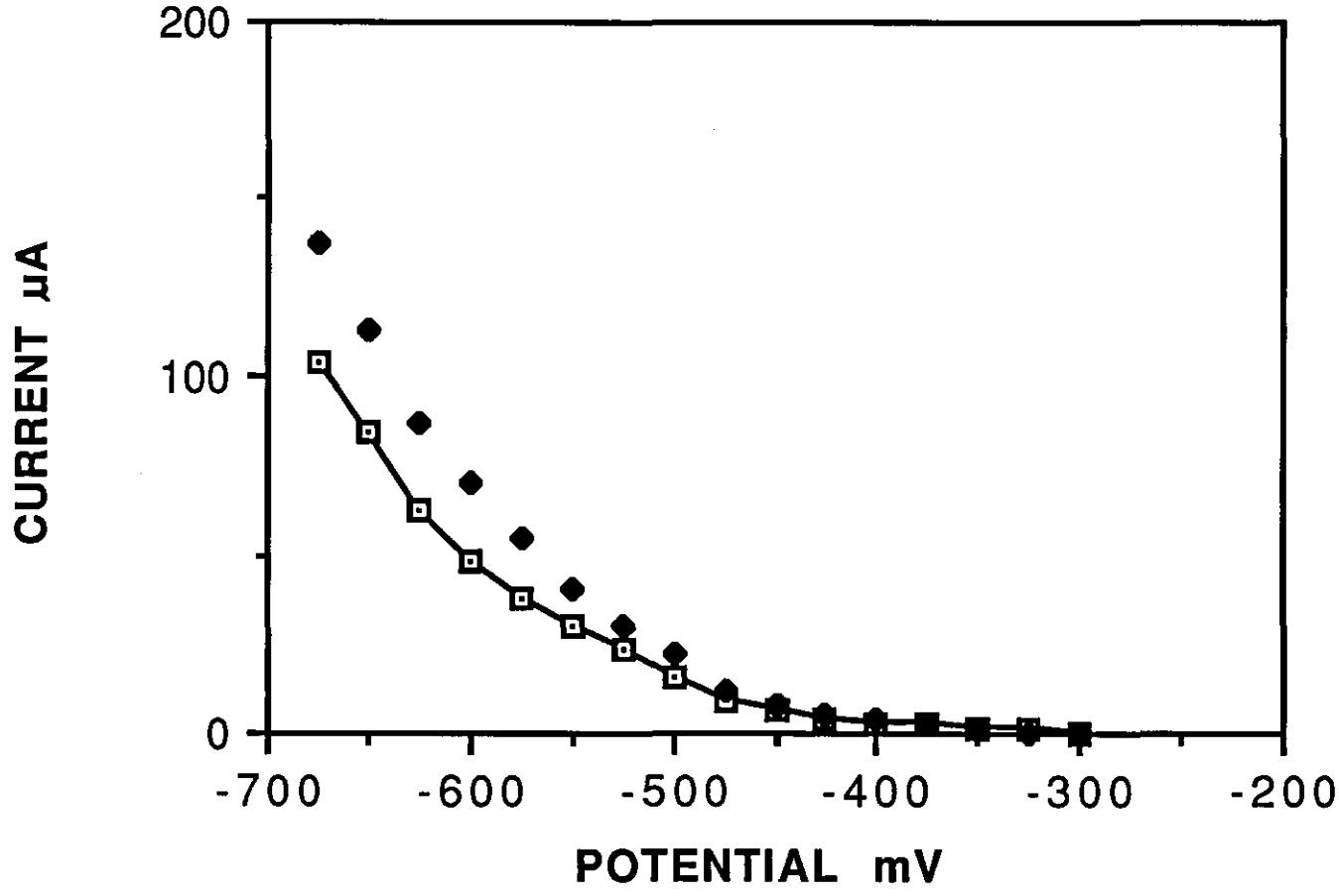

FIG. 6.14 - TAFEL PLOT FOR 200ppm CALCIUM

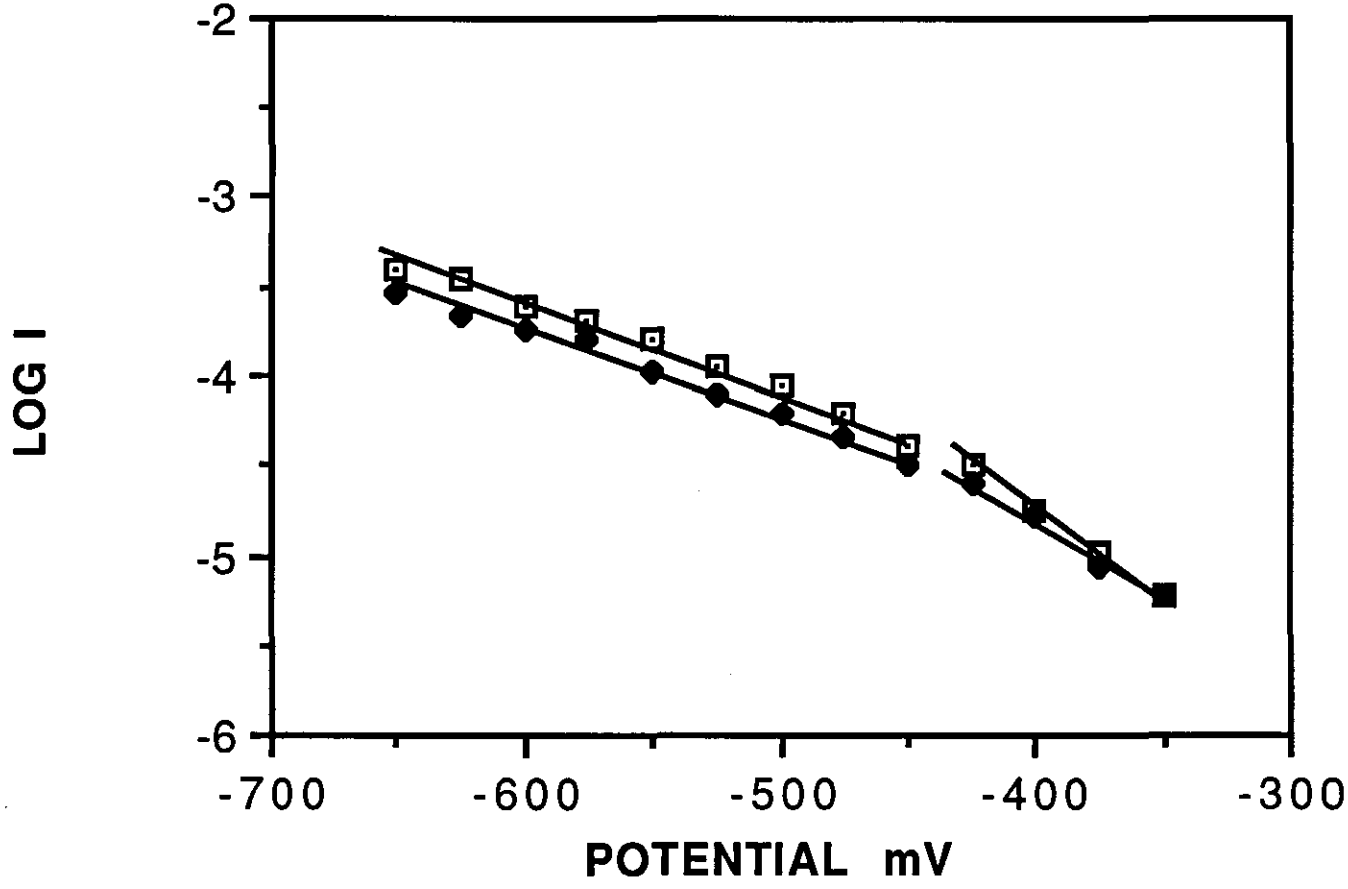

0.1M $NaClO_4$) indicates an increase in corrosion current. This is obviously a nonsense, as inhibition is definitely occuring above -450mV. It should be noted that a shift in the corrosion potential will occur on forming a protective surface film. Although cathodic processes are being studied, at these low negative overpotentials, both the cathodic and anodic Tafel lines will be effected by the film formation and a true corrosion current can only be obtained by extrapolation to this new corrosion potential. This is an extremely difficult potential to quantify and reproduce, and will be different for each experiment.

Experiment 7

Zinc was used to evaluate the effectiveness of the technique in testing a well known cathodic inhibitor, employed in numerous commercial formulations. No easily interpretable I-E data was obtained, Figure 6.15, and the Tafel plot showing a curved line - Figure 6.16.

From the data, it can be assumed that zinc film formation occurs via a continuous thickening process, in contrast to that of calcium which was immediately initiated at -450mV.

Conclusions (Experiments1-7)

Comparison of Tafel slopes and corrosion current densities, obtained from the electron transfer region of the I-E plots, gives an indication of how film formation occurs. However, it is very poor for inhibitor evaluation. The corrosion currents obtained on extrapolation to the original corrosion potential (i.e. that in 0.1M $NaClO_4$) are meaningless, since the corrosion potential shifts with inhibitor addition and subsequent film formation.

In an attempt to decrease any effects of the anodic dissolution process on the Tafel data for oxygen reduction, more negative potentials were employed. Levich data for a series of rotation speeds in the mixed region was obtained.

FIGURE 6.15 - I.E. CURVE FOR 50ppm ZINC

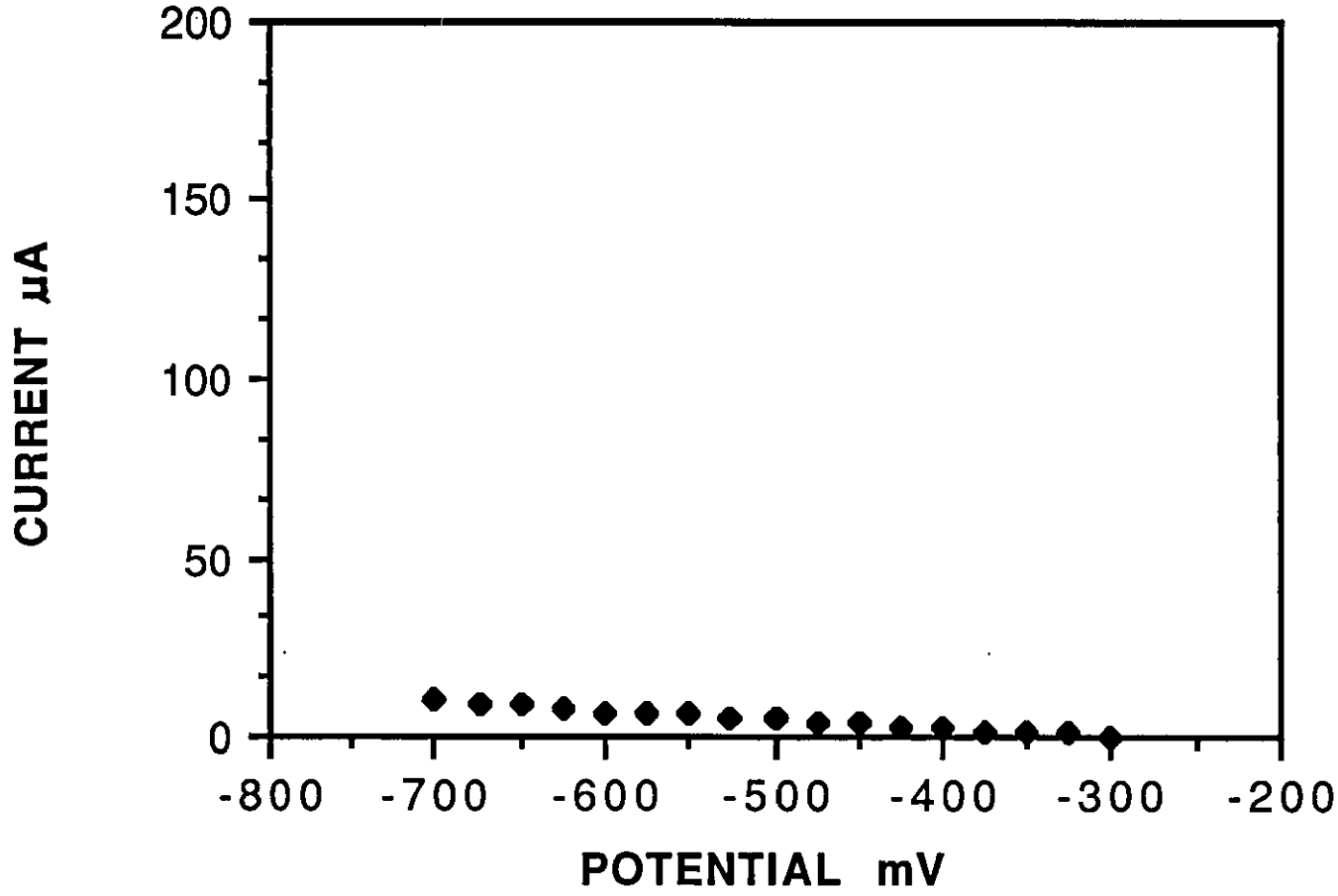

FIGURE 6.16 - TAFEL PLOT FOR 50ppm ZINC

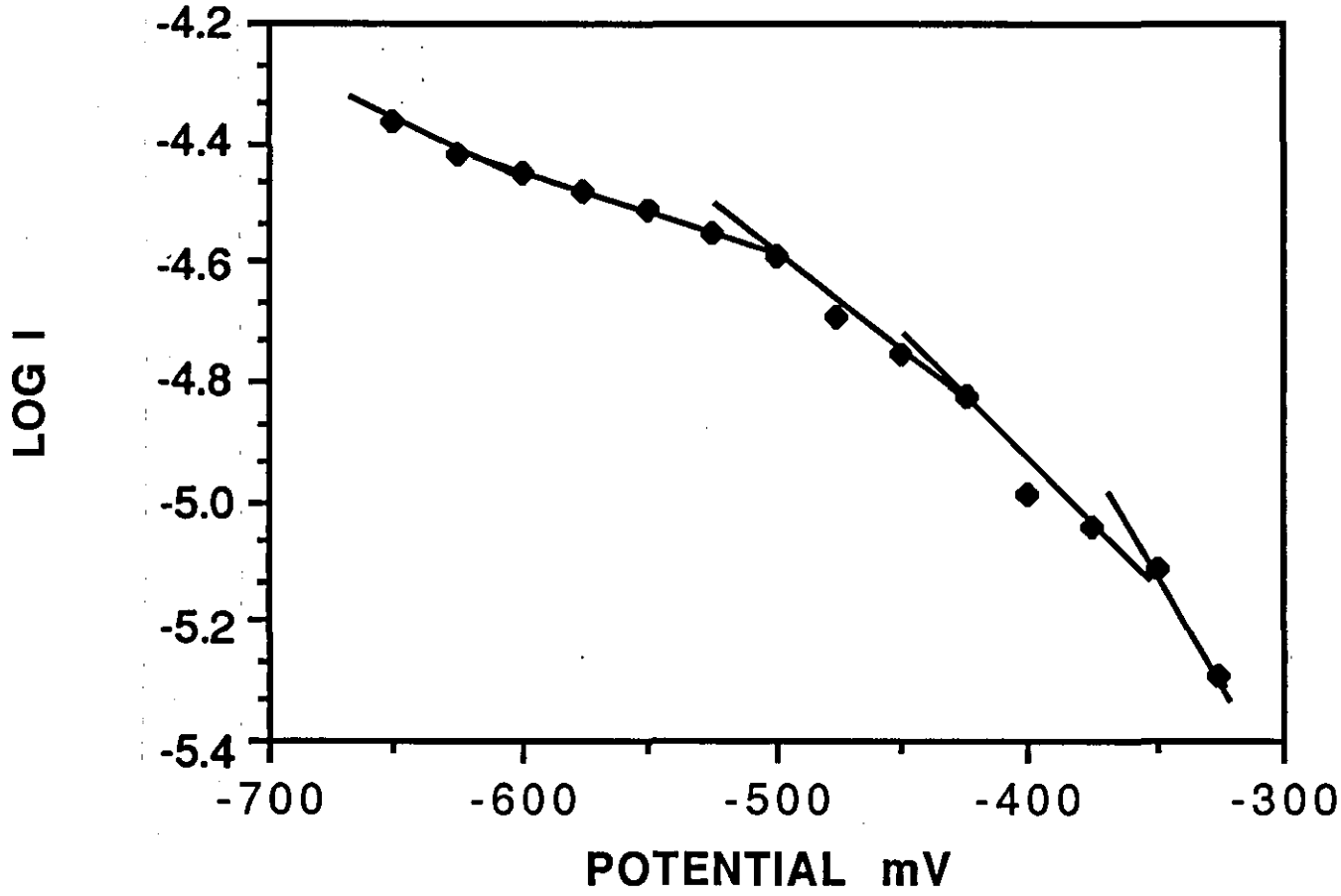

Experiment 8

Levich data was obtained between -600mV and -1000mV (at 100mV intervals) for oxygen reduction in 0.1M $NaClO_4$ alone. Figure 6.17 shows a typical Levich plot produced. A series of straight, parallel lines were obtained. The Tafel plot obtained - Figure 6.18 was again linear but with a slope of 225mV/decade. Slopes were found to range between 155mV/decade and 240mV/decade.

Experiment 9

In an attempt to reduce discrepancies in the Tafel slope, Levich data was obtained at higher potentials i.e. in mixed region, between -700mV and -850mV and at 25mV intervals. Figure 6.19 shows a typical Levich plot obtained, consisting of straight parallel sloping lines. The Tafel plot - Figure 6.20 was linear with slope of 260mV/decade.

It can be concluded, that a change in potential to more negative values does not remove the discrepancies and irreproducibility in the Tafel slopes. The most likely explanation for the discrepancies, is the large increase in pH at the electrode surface from oxygen reduction. The higher the negative potential, the faster the rate of oxygen reduction and hence the greater the pH change. The $OH^-$ concentration in the vicinity of the electrode surface therefore constantly changes, giving the resultant irreproducable behaviour.

Experiment 10

To investigate the effect of calcium ions on the Tafel slope, 200ppm calcium was added as the perchlorate salt. Levich data between -600mV and -1000mV was recorded. Figure 6.21 gives the Levich data obtained. A series of straight Levich lines were obtained similar to 0.1M $NaClO_4$. Figure 6.22 shows a typical Tafel slope of 175mV/decade. Tafel slopes were found to range between 170mV/decade and 200mV/decade. These results compare

FIG.6.17 - LEVICH PLOT FOR 0.1M NaClO4

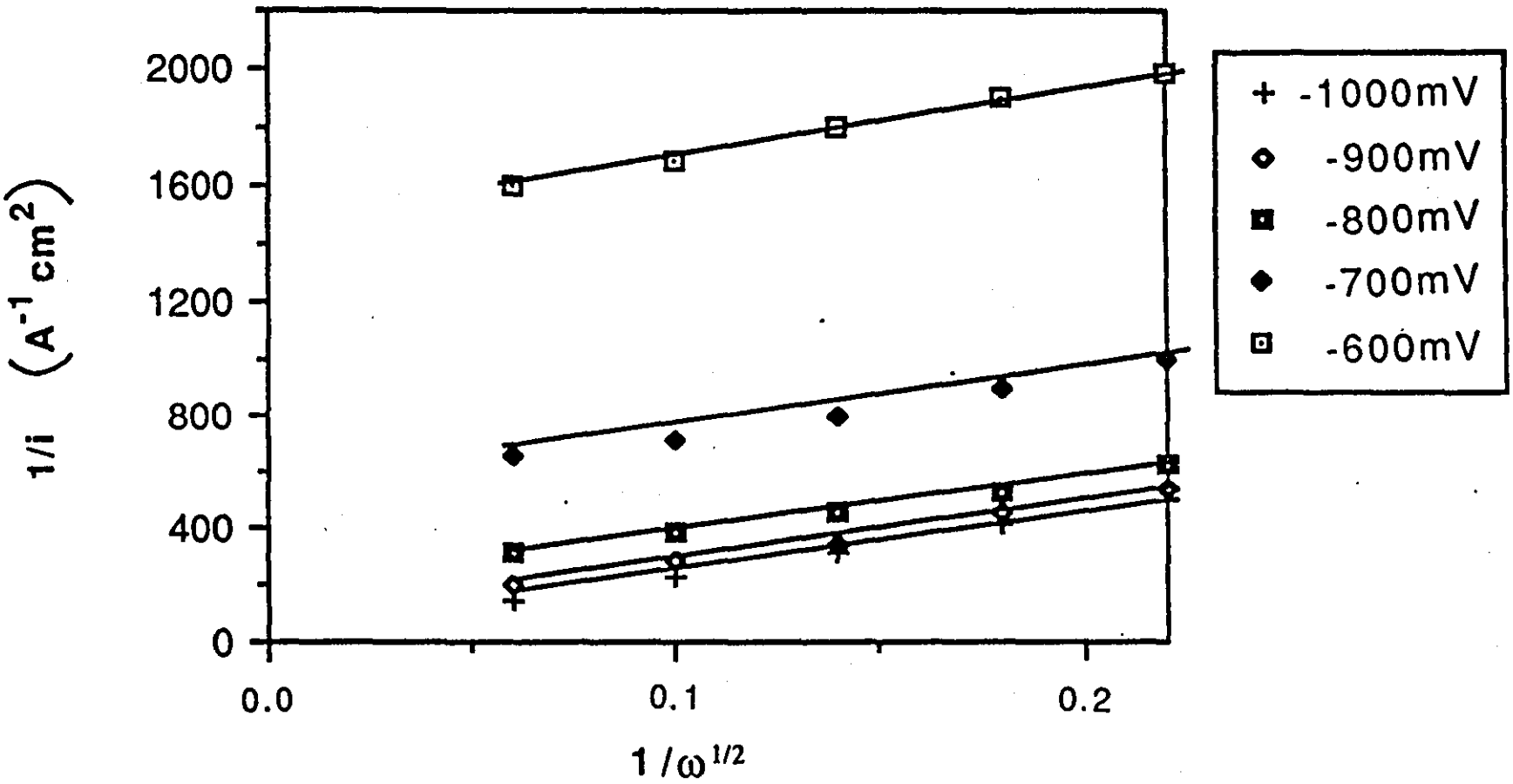

FIG. 6.18 - TAFEL PLOT FOR 0.1M NaClO4

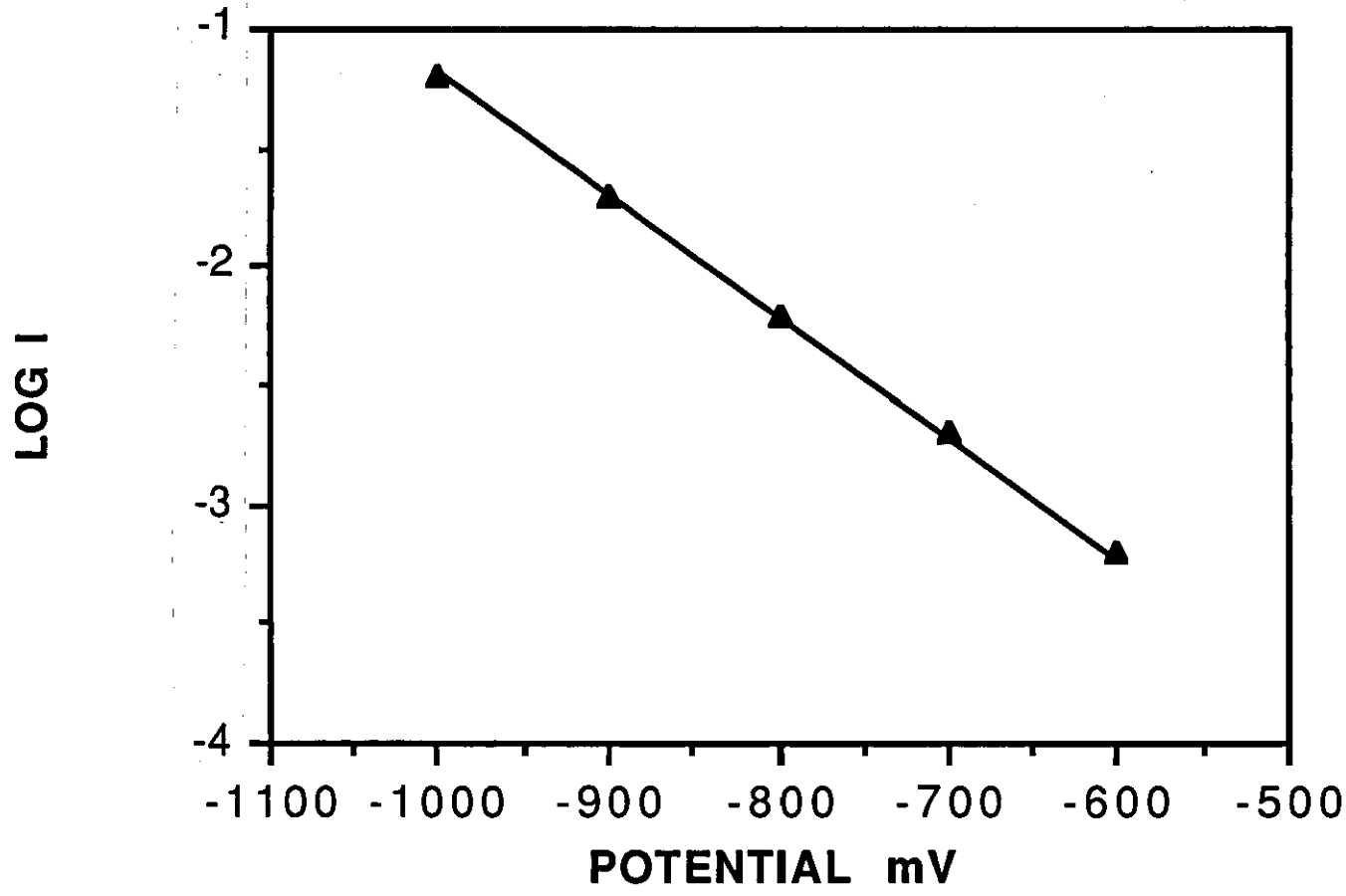

FIG. 6.19 - LEVICH PLOT FOR 0.1M NaClO4 (mixed region)

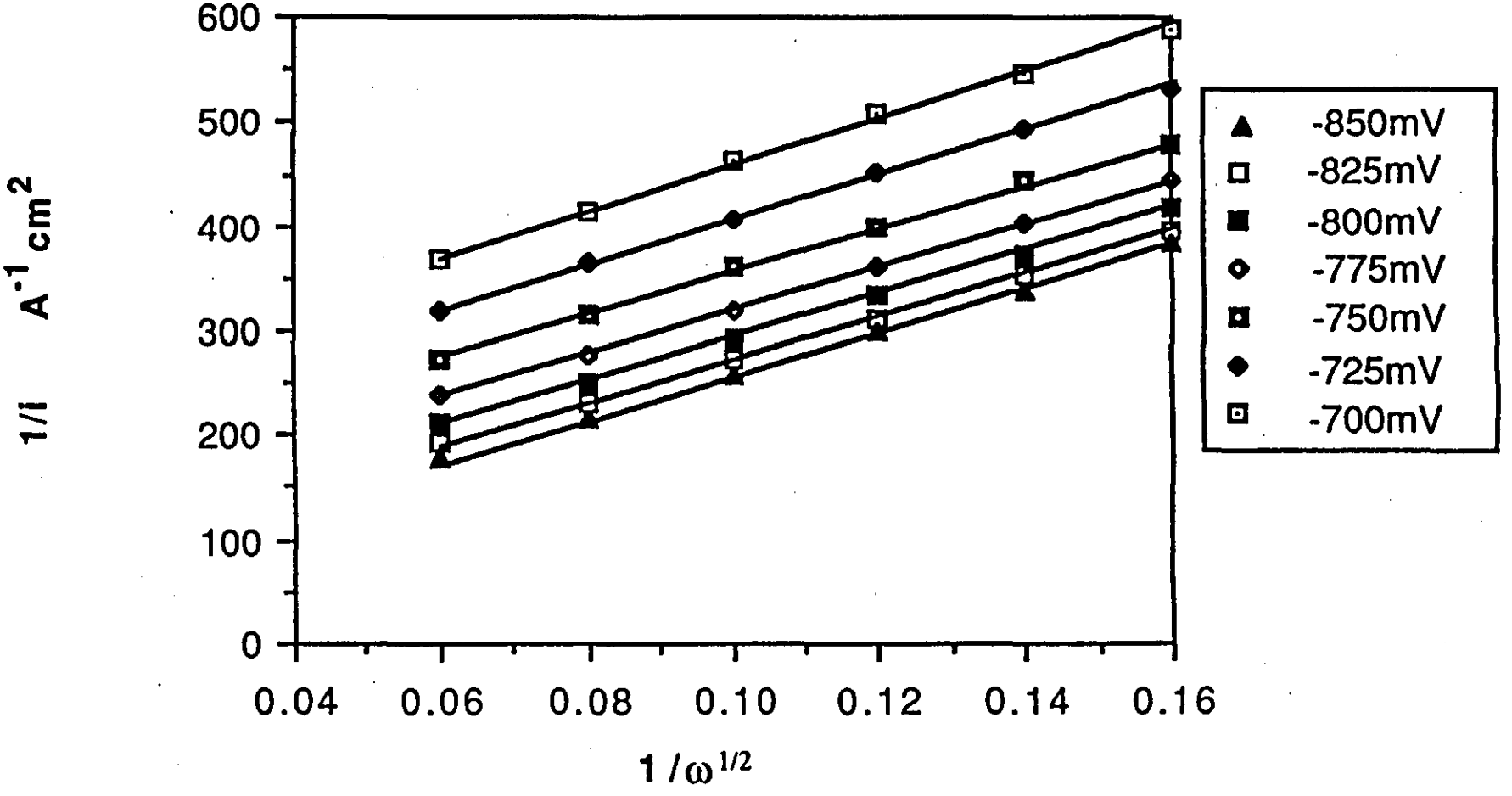

FIG. 6.20 - TAFEL PLOT FOR 0.1M NaClO4 (mixed region)

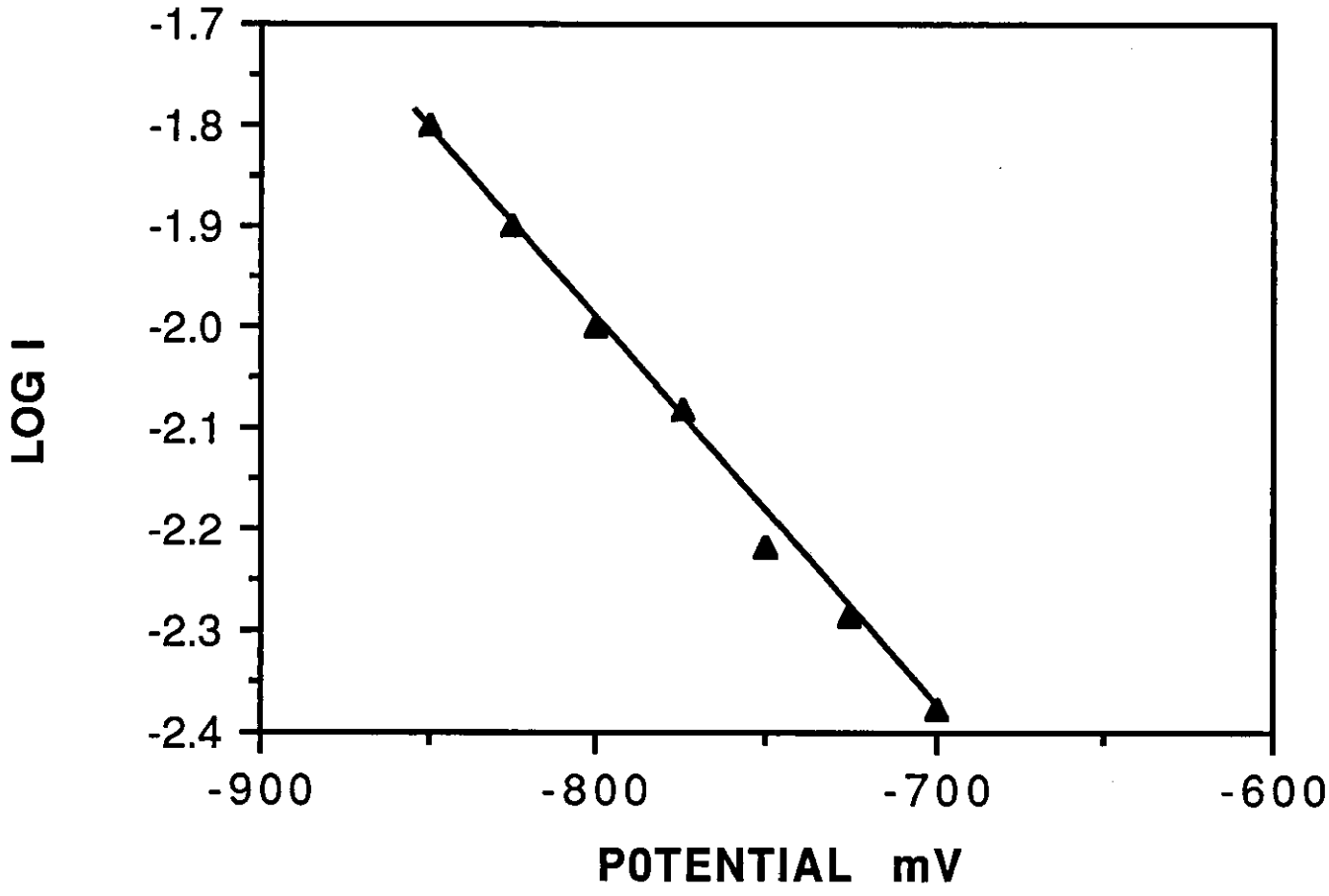

Fig. 6.21-LEVICH PLOT FOR 200ppm Ca

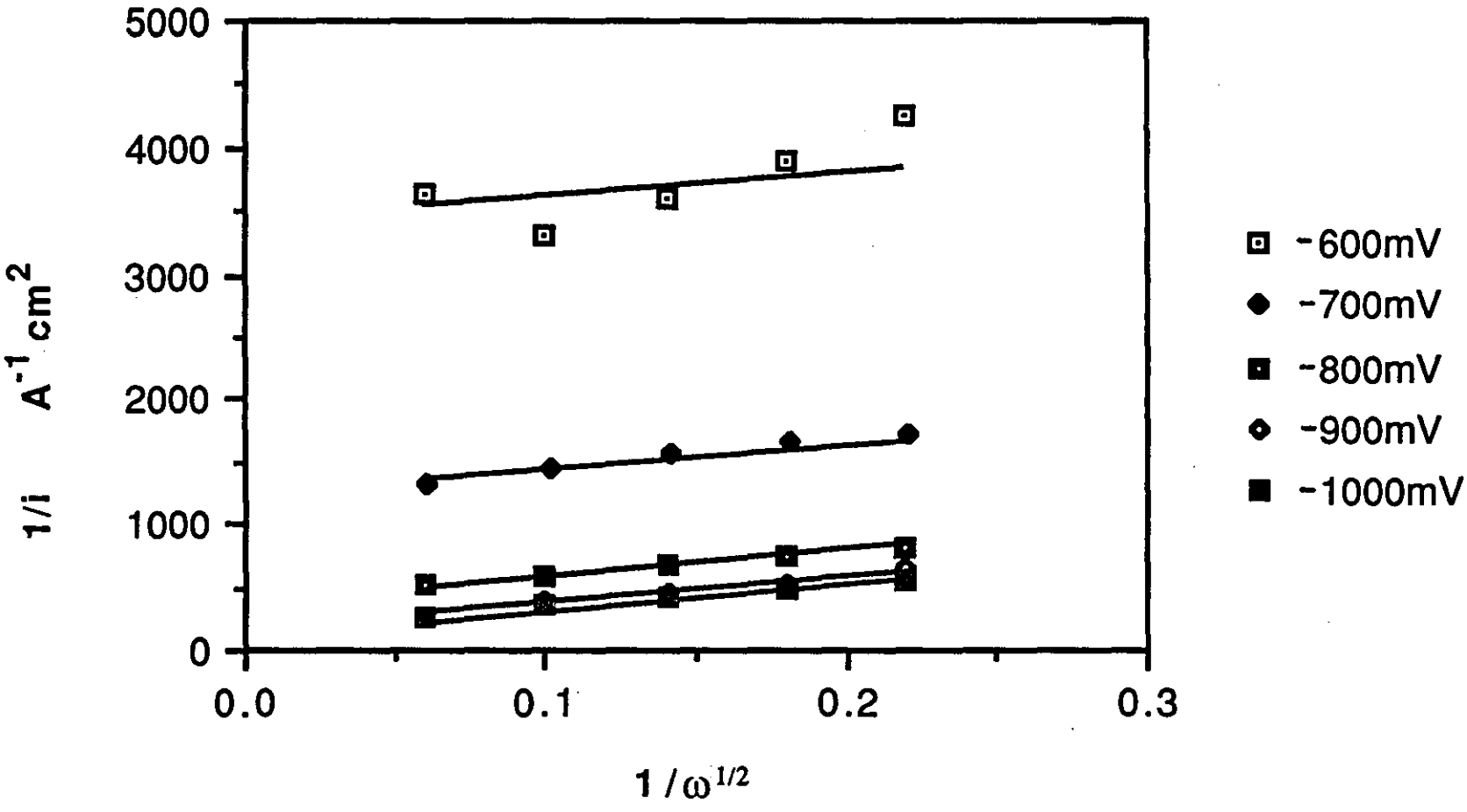

FIG. 6.22 - TAFEL PLOT FOR 200ppm CALCIUM

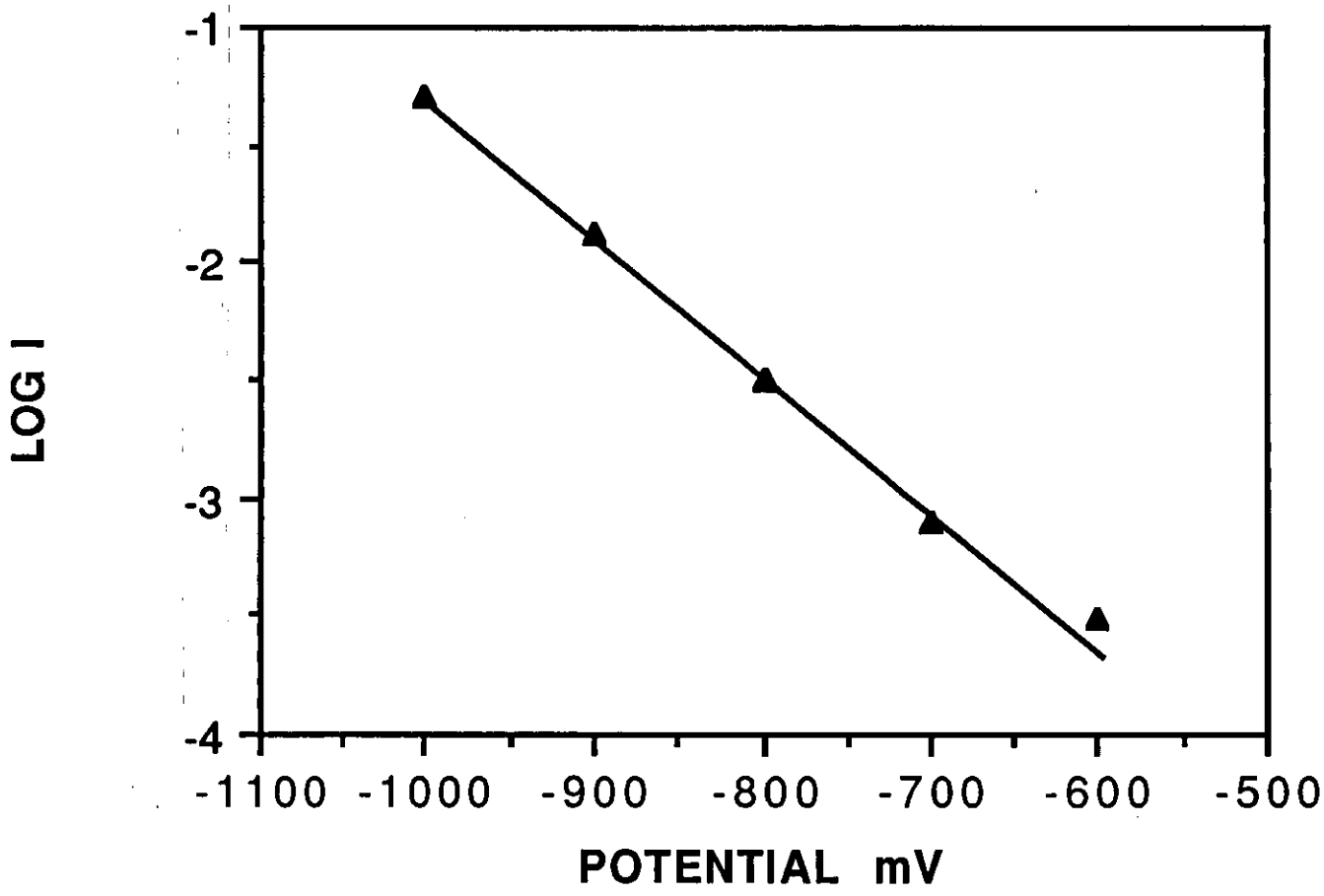

favourably with those obtained from I-E data. At -600mV a film of calcium should have already formed. Therefore no change in Tafel slope was observed between -600mV and -1000mV.

Experiment 11

Finally, 200ppm zinc was introduced. The Levich data recorded - Figure 6.23 showed linearity at low rotation speeds only. The resultant Tafel data - Figure 6.24 showed a change in slope at about -850mV, indicating possible zinc deposition and film formation. Further evidence for the formation of a surface layer of zinc was obtained from the corresponding voltammogram - Figure 6.25. A peak was observed on the reverse sweep (i.e. positive sweep) at -800mV, indicating the stripping of a deposited material from the surface.

### 6.2.3 CONCLUSIONS

It is apparent that no reproducible kinetic data could be obtained from either the I-E or Levich experiments. When 0.1M $NaClO_4$ was used alone, no stability was conferred through film formation and the data was particularly inconsistent. When inhibitors were introduced, a change in Tafel slope indicated film formation and hence a change in mechanism. Again, poor reproducibility occured, with the error margins in Tafel slopes, rendering them of little use.

Irreproducability could arise from a number of factors. At the lower negative overpotentials, iron dissolution still plays a part in the mechanistic behaviour. Therefore, surface preparation plays an important role. Any irreproducabilities in polishing will be magnified in the kinetic data. Similarly, changes in area due to electrode dissolution will contribute to the unreliability of this test method. At higher negative overpotentials, the effect of pH increase at the electrode surface, is very significant. Since this change is unquantifiable (depending upon so many variables, e.g. surface preparation, initial pH, iron dissolution etc.) then the resultant

FIG. 6.23 - LEVICH PLOT FOR 200ppm ZINC

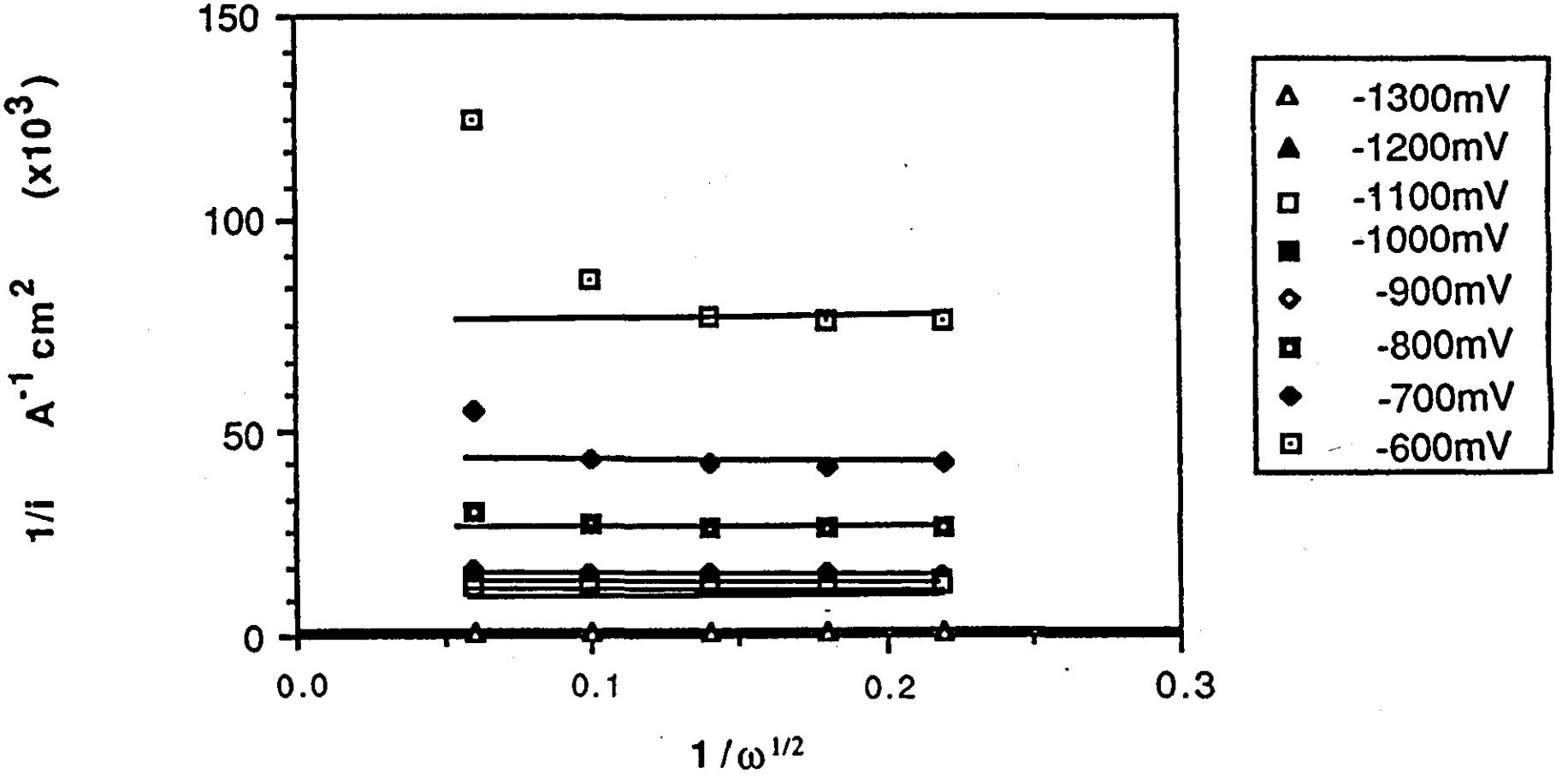

FIG. 6.24 - TAFEL PLOT FOR 200ppm ZINC

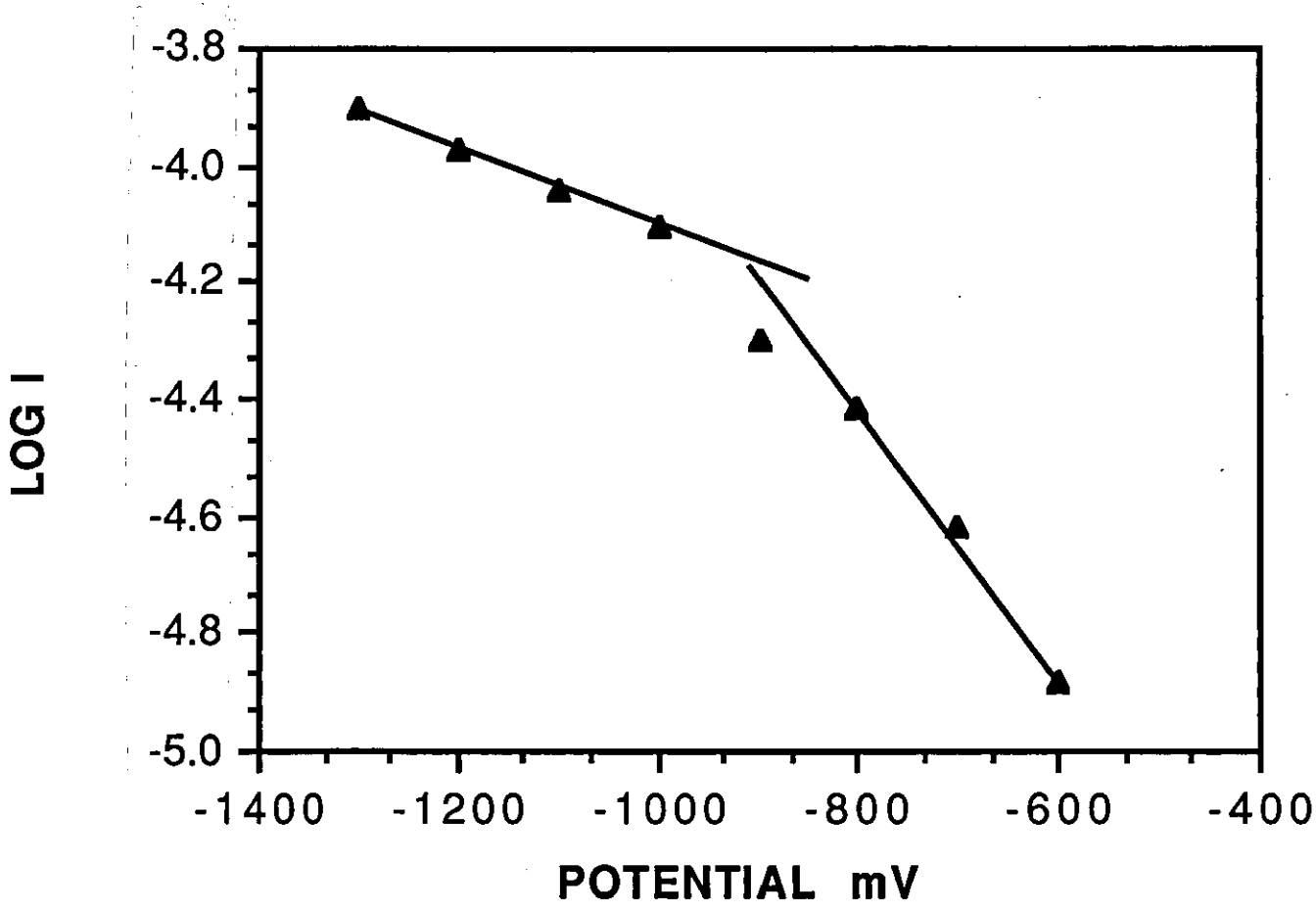

FIG.6.25 - VOLTAMMOGRAM FOR 200ppm ZINC

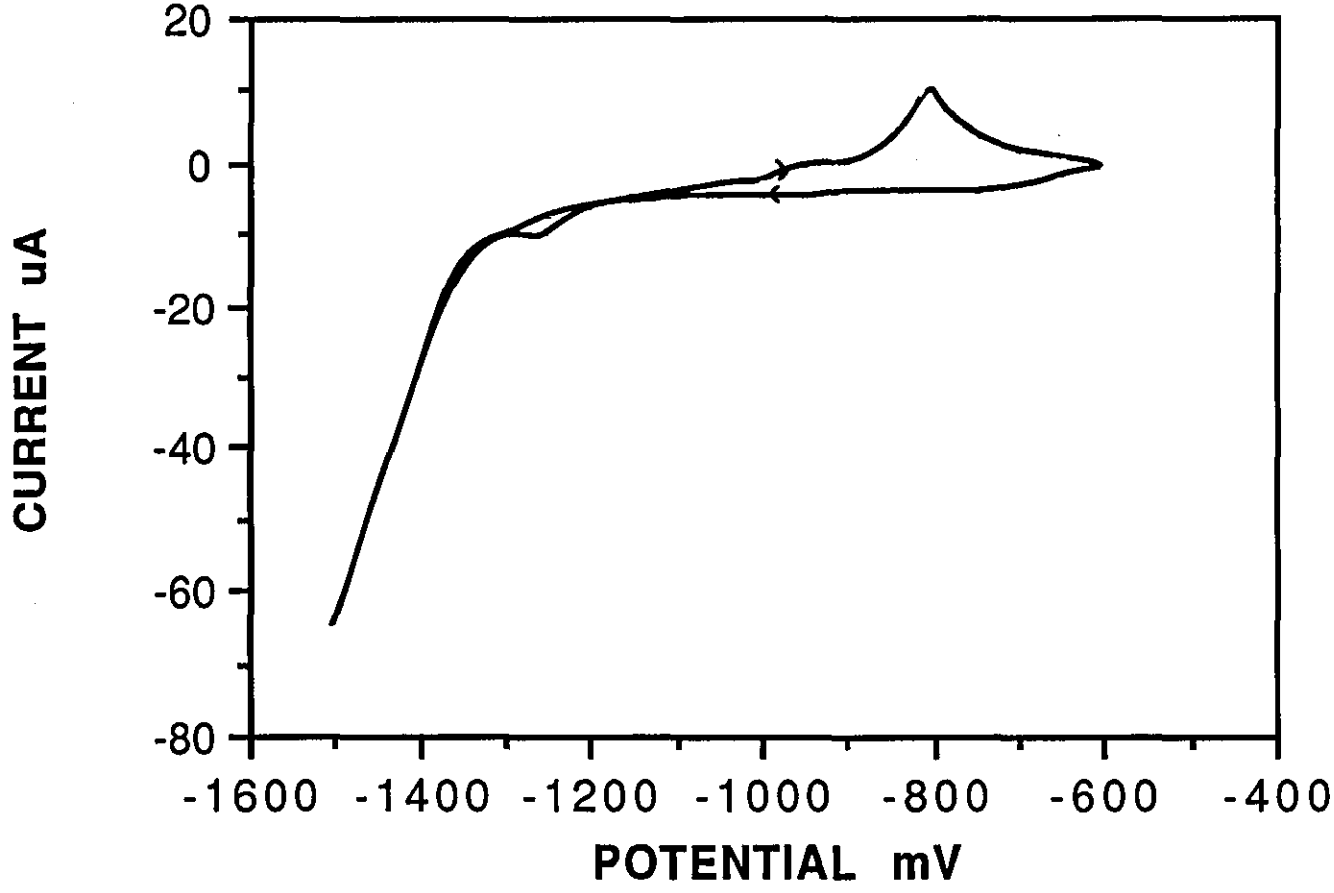

kinetic data will be unreliable. One possible method of removing the localised $OH^-$ concentration effects would be to buffer the system[71]. Borate buffers are generally used, but these move the pH to 8.3 and are themselves adsorbed onto the iron surface as shown in Figure 6.26, thus interfering with and distorting the inhibitor mechanism.

FIG. 6.26 - LSV FOR BORATE BUFFER

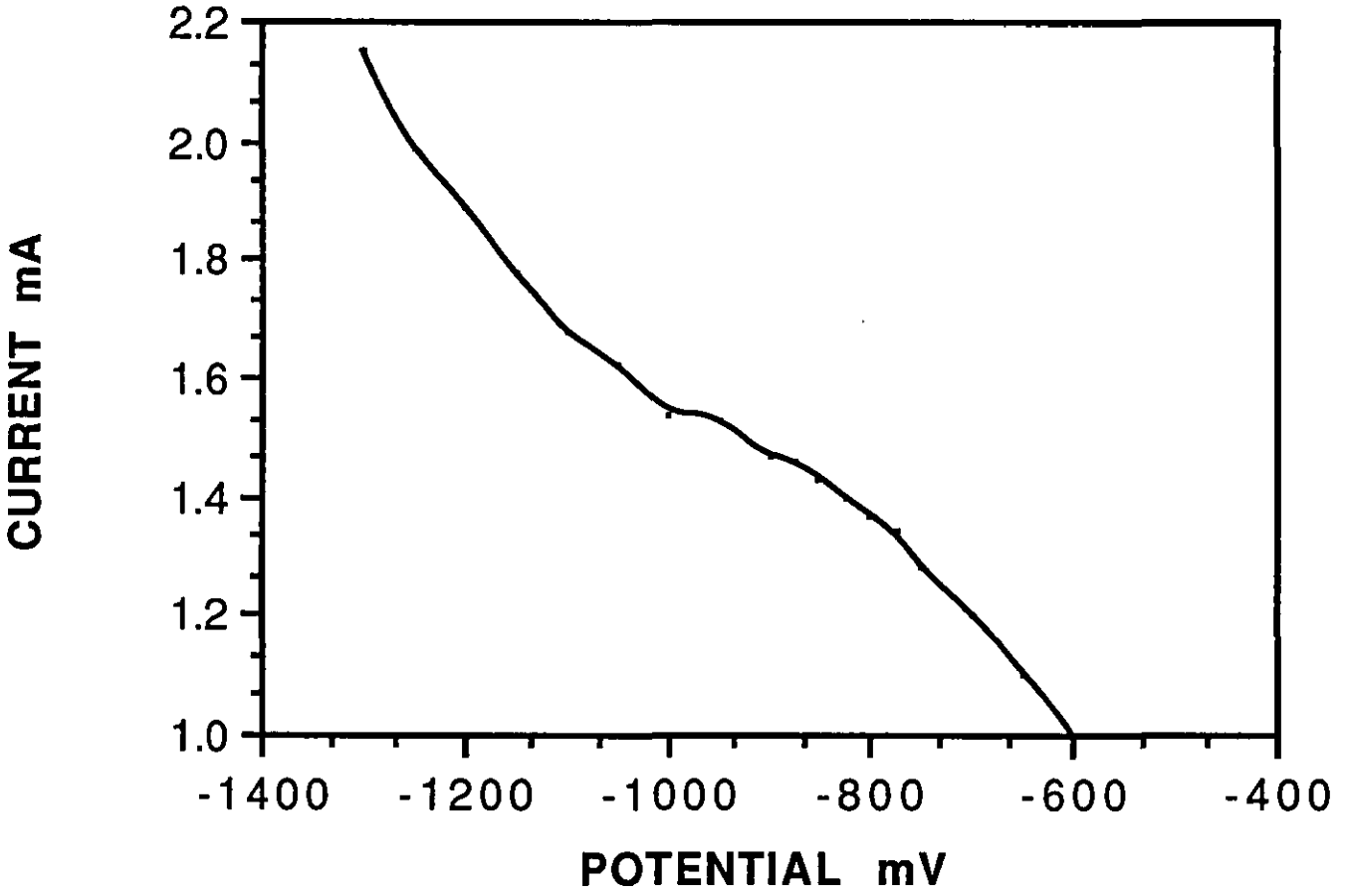

# CHAPTER 7

# A CONCENTRATION STEP METHOD FOR CATHODIC INHIBITOR EVALUATION

Due to the problems imposed by iron dissolution at low negative overpotentials, experiments were conducted at high overpotentials i.e. greater than -900mV versus S.S.C.E. to try to exploit the reproducibility corresponding to the oxygen diffusion limited plateau. At these potentials, any contribution to the overall reduction current by the anodic process, can be considered negligible.

The measurement of the plateau current and its subsequent response to inhibitor addition, was used to evaluate a variety of cathodic inhibitors. Both laboratory reagents and industrial formulations were used. Furthermore, experiments were conducted with a number of water compositions.

## 7.1 EXPERIMENTAL

The experimental procedure used in Chapter 6 was also adopted for this series of experiments. A constant rotation speed of 1500rpm was chosen for all experiments along with a sweep rate of 0.5 mV/s. The electrode was polarised between -1400mV and -900mV corresponding to the mass transport limited region for oxygen reduction. Consistent current density values of 4.59 $mAcm^{-2}$ were obtained and excellent reproducibility was observed within this potential window. The potential of -900mV corresponded to the edge of the limiting plateau. Irreproducibility was further minimised by establishing a pretreatment regime which would clean and condition the electrode surface. The best procedure involved polarising the electrode to -1400mV, for 20 minutes, under an atmosphere of nitrogen. This reduces any oxide film which may have been formed during the polishing operation, and the short period of time that the

surface was exposed to the atmosphere. The solution was then saturated with oxygen for a further 10 minutes until a steady current, due to hydrogen evolution and oxygen reduction was observed. The electrode was swept to -900mV, and the pH adjusted back to pH7 by the addition of perchloric acid.
N.B. An increase in the alkalinity of the electrolyte solution occurred from the production of hydroxide ions upon the reduction of oxygen, and the removal of protons from solution by hydrogen evolution.

A number of cationic species were tested, at a concentration of 50ppm. These were added at -900mV and the change in current observed after 10 minutes. The electrode was then swept back to -1400mV and the effect of the addition on the plateau current observed. A decrease in current signifies cathodic inhibitive properties. Sweeping back to -1400mV allows a check of whether the inhibitive action is a result of oxygen transport retardation alone, or is complicated by kinetic hindrance. Investigations into the effect of the various inhibitors, in 1M $NaClO_4$ alone and synthetic waters of 50/50 and 150/150 composition were undertaken. This allowed for correlation of the relative efficiencies in both soft and hard waters of varying alkalinity.
N.B. 50/50 refers to calcium hardness (as $CaCO_3$), ppm/ m-alkalinity (as $CaCO_3$),ppm.

## 7.2 RESULTS

Table 7.1 presents inhibitor efficiency as a percentage of an ideal cathodic inhibitor, i.e. one that gives zero current.

## 7.3 DISCUSSION

Zinc gives excellent inhibition at 50ppm concentration - Figure 7.1. Upon sweeping cathodically, there is some reduction in its inhibitive properties, reflected as spikes on the voltammogram. This is probably due to the partial disruption of the zinc film species (which exhibits an ohmic response), until the electric field gradient becomes so large as to cause breakdown. Some repair of this film is evident

TABLE 7.1

| INHIBITOR | 1M $NaClO_4$ | 50/50 WATER | 150/150 WATER |
|---|---|---|---|
| 50ppm Zn | 82% | 82% | 50% |
| 50ppm Mg | 56% | 54% | 69% |
| 50ppm 966 | 15% | 96% | 87% |
| 50ppm 945 | 13% | 96% | 93% |
| 50ppm P.C.A. | 21% | 85% | 83% |
| 50ppm H.P.A. | 21% | 91% | 94% |

FIG. 7.1- EFFECT OF 50ppm ZINC

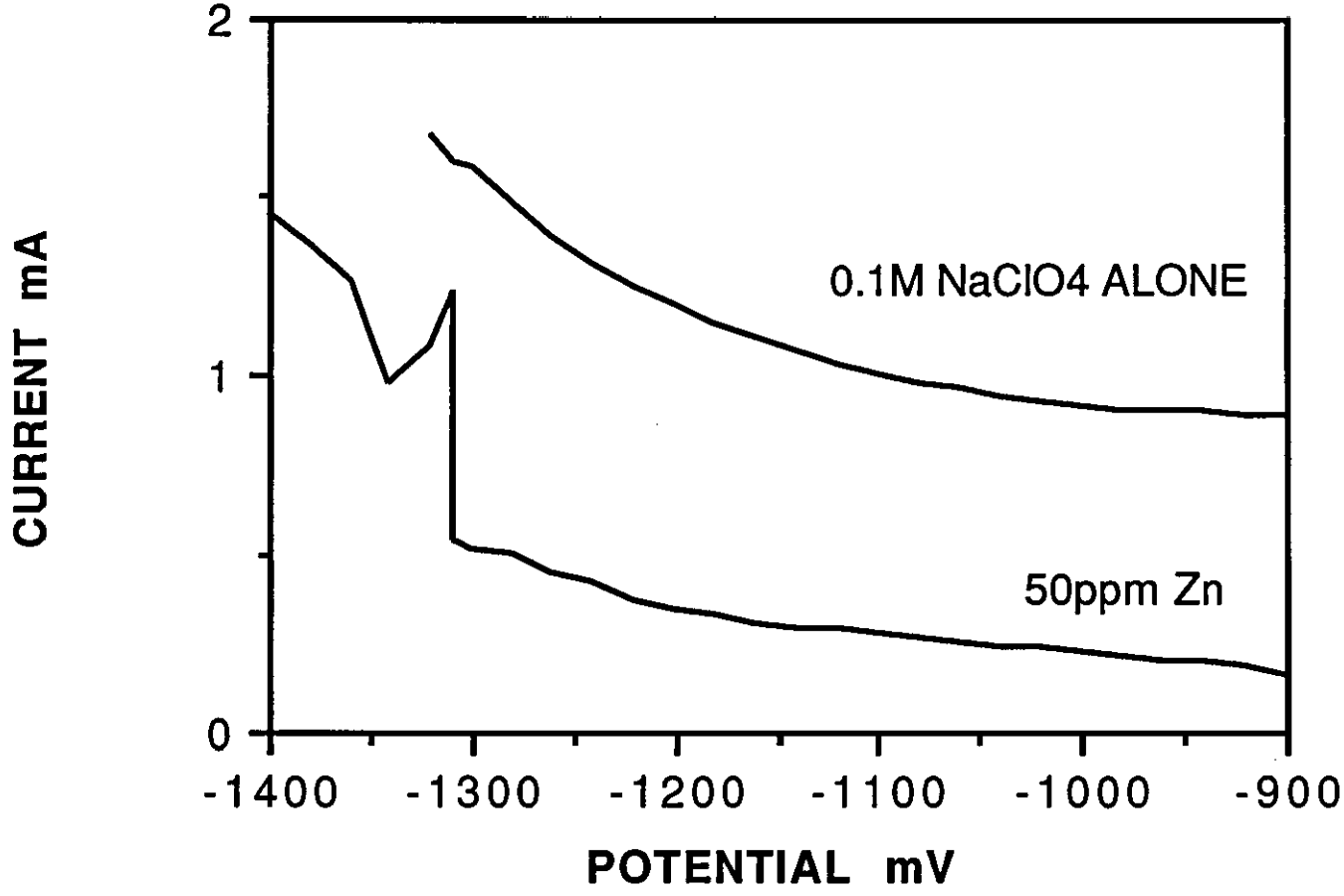

from the relaxation of the current spike. The film failure cannot be attributed to hydrogen evolution since in a synthetic water of 50/50 composition, breakdown is observed at much lower negative potentials - Figure 7.2. Self healing is again evident but the tenacity of the film formed in this case is not so great. One possible reason maybe due to aggravation of film reformation by the chloride ion in the electrolyte (from $CaCl_2$ used to add calcium hardness).

A 150/150 water gave only a 50% reduction in current upon addition of zinc - Figure 7.3. In such an highly alkaline environment precipitation of zinc hydroxide becomes an increasing problem. This decreases the availability of soluble zinc species resulting in only partial film formation at the electrode surface. The formation of a white suspension was observed, indicating precipitation. On sweeping cathodically, breakdown was apparent almost immediately, reinforcing the weak film formation argument.

Figure 7.4 shows that magnesium provides less protection than zinc at -900mV in perchlorate supported water. However an increase in inhibitive behaviour is observed on moving from 50/50 (Figure 7.5) to 150/150 water (Figure 7.6). A possible explanation for this behaviour is that the calcium carbonate formed, is of sufficient concentration, to affect incorporation into the magnesium hydroxide film, increasing its protective properties. It should also be noted that magnesium behaves in such a manner as to show a flatter diffusion limited current plateau. This contrasts with the linear sloping behaviour of the zinc film. In fact, the film formed in the presence of zinc shows very little current dependence on rotation speed, whereas that formed by magnesium has a pronounced hydrodynamic response. It should also be noted that in 150/150 water, magnesium provides better inhibition than zinc under the same conditions.

On refering to the respective Pourbaix diagrams[80] for magnesium and zinc (Figures 7.7a, 7.7b), magnesium remains in solution at a higher pH. Figures 7.8, 7.9(a,b) and 7.10(a,b) show optical micrographs of an iron surface alone, with zinc and with magnesium

FIG. 7.2 - EFFECT OF 50ppm ZINC IN 50/50 WATER

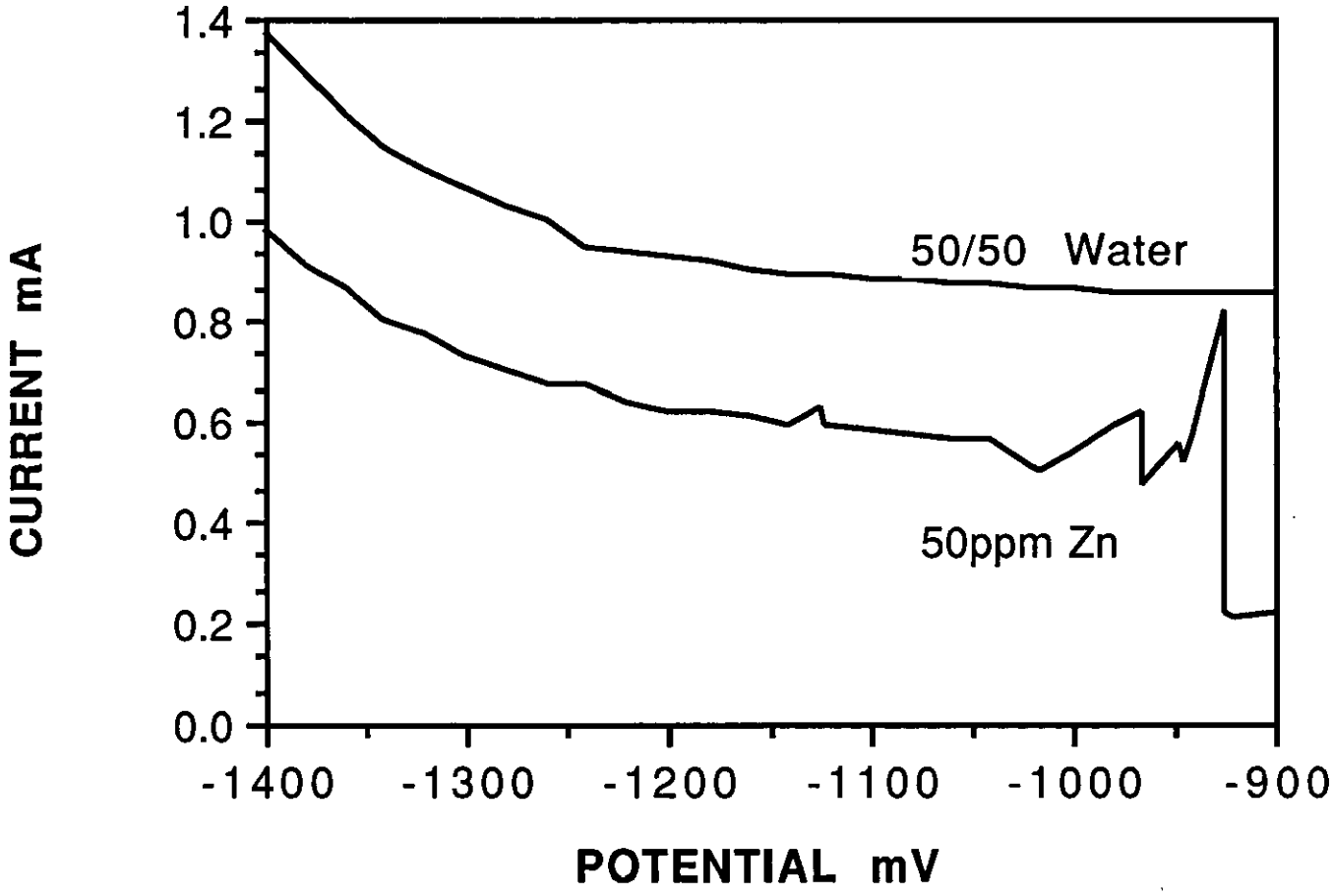

FIG. 7.3 - EFFECT OF 50ppm ZINC IN 150/150 WATER

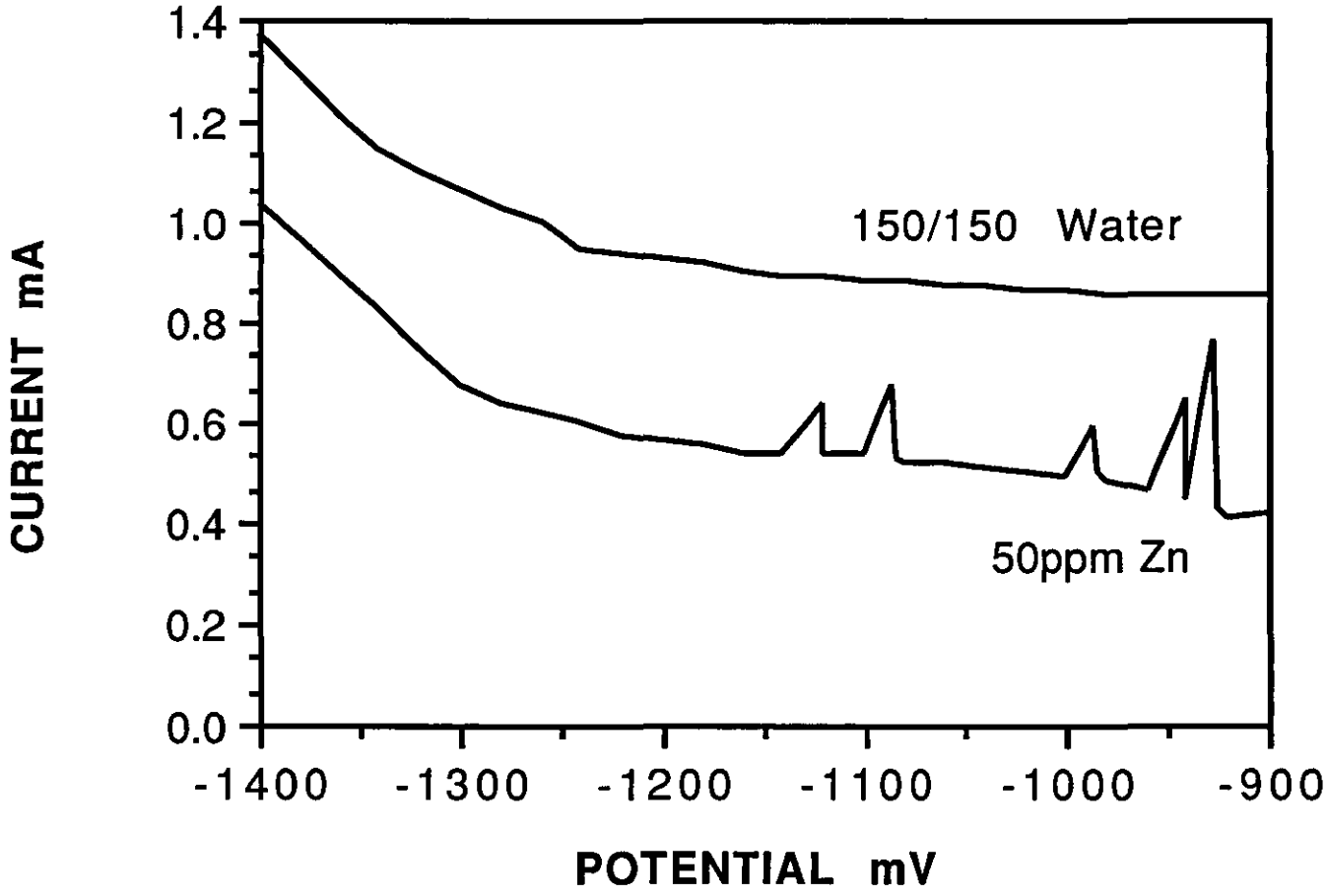

FIG. 7.4 - EFFECT OF 50ppm MAGNESIUM ON 0.1M NaClO4

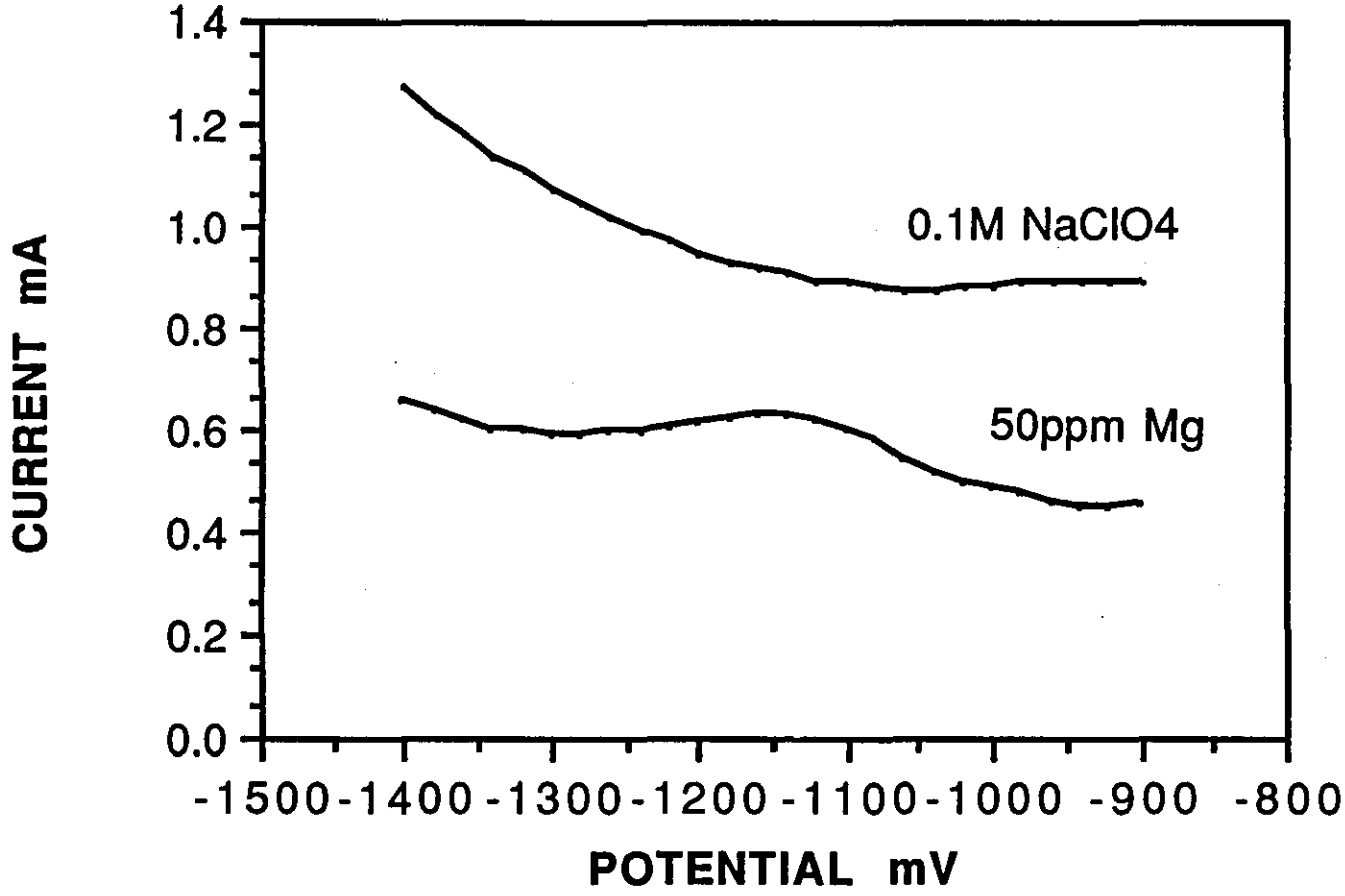

FIG.7.5 - EFFECT OF 50ppm MAGNESIUM IN 50/50 WATER

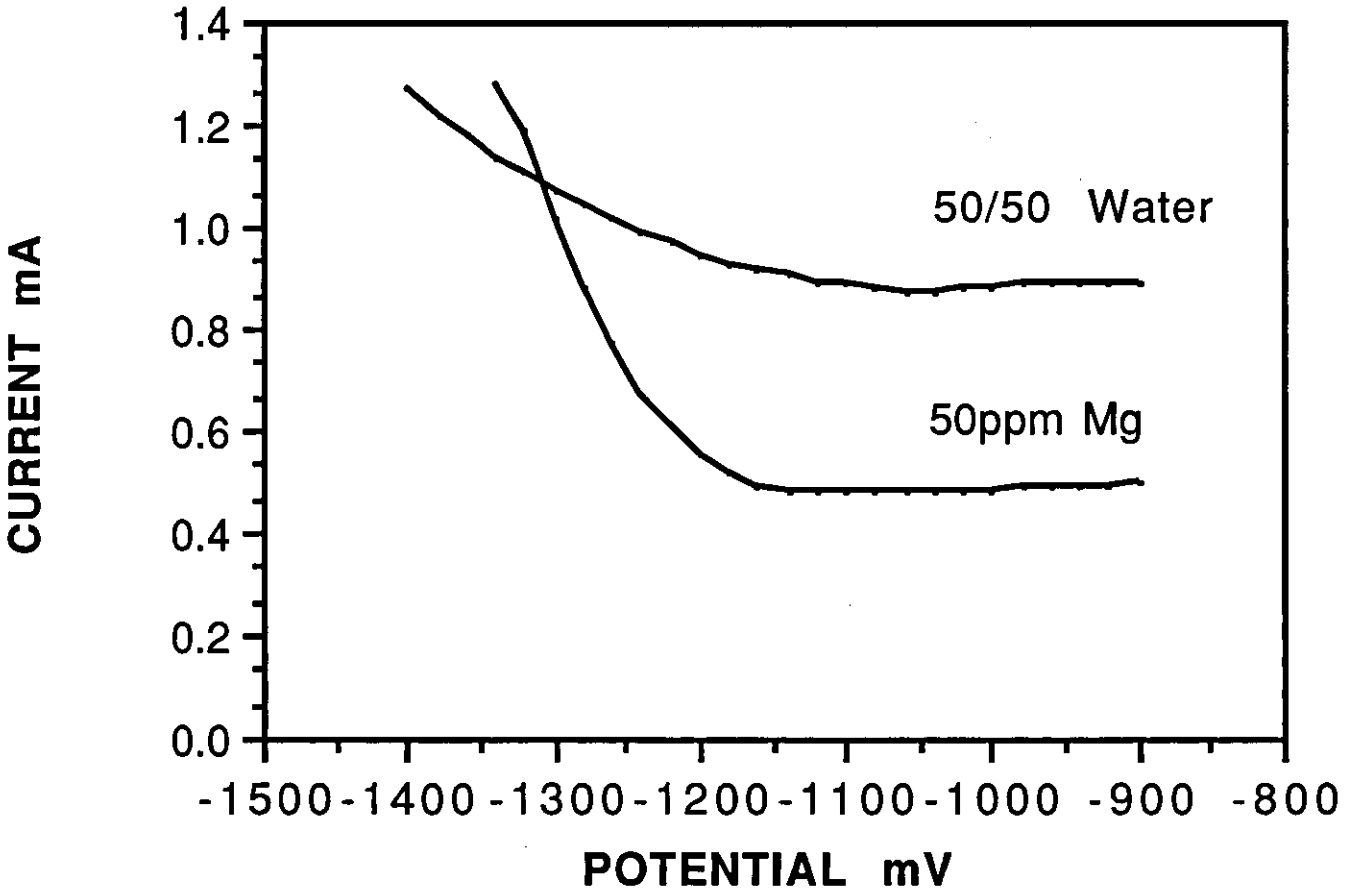

FIG.7.6 - EFFECT OF 50ppm MAGNESIUM IN 150/150 WATER

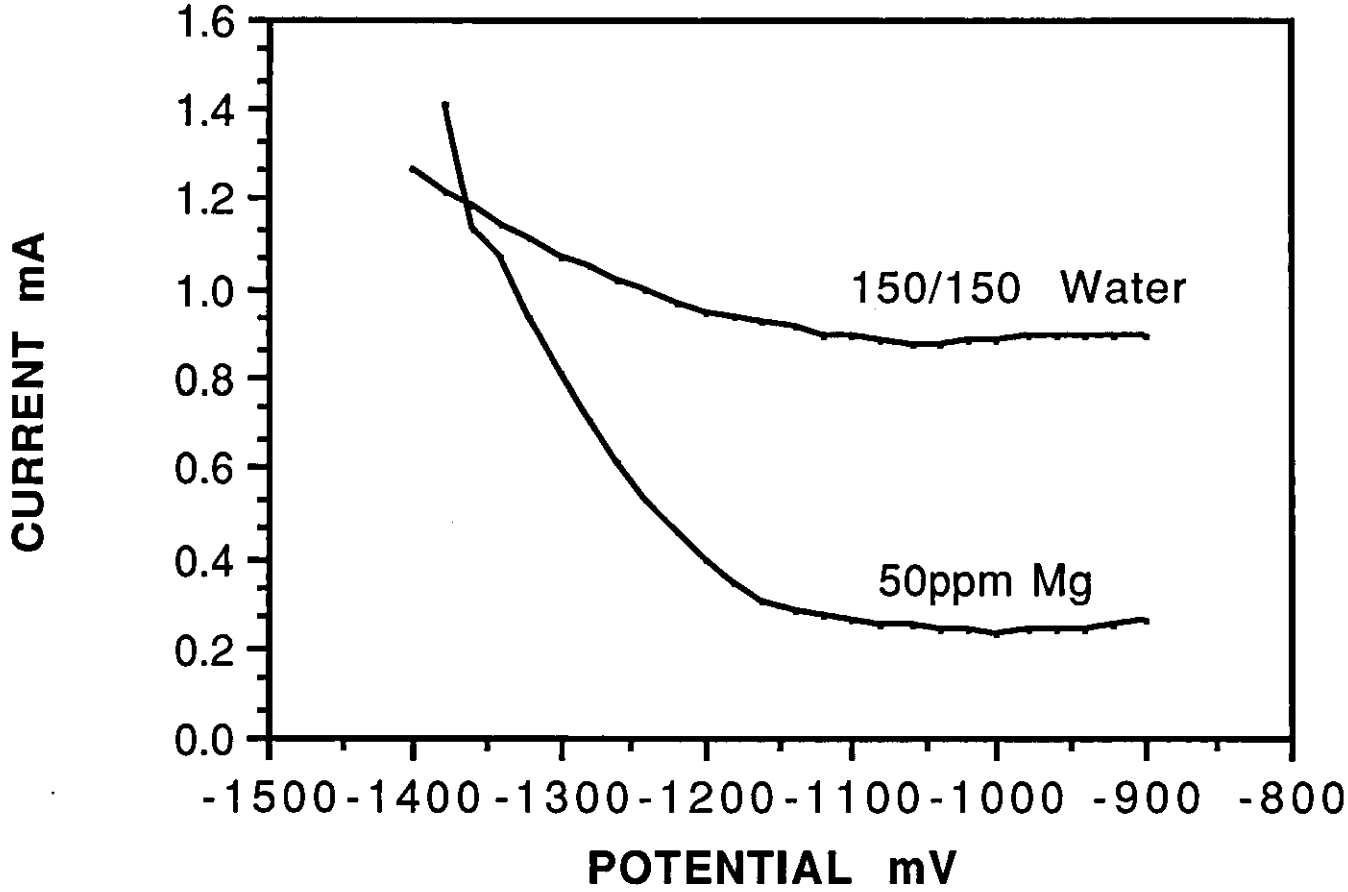

FIG. 7.7a - POTENTIAL-pH DIAGRAM FOR MAGNESIUM

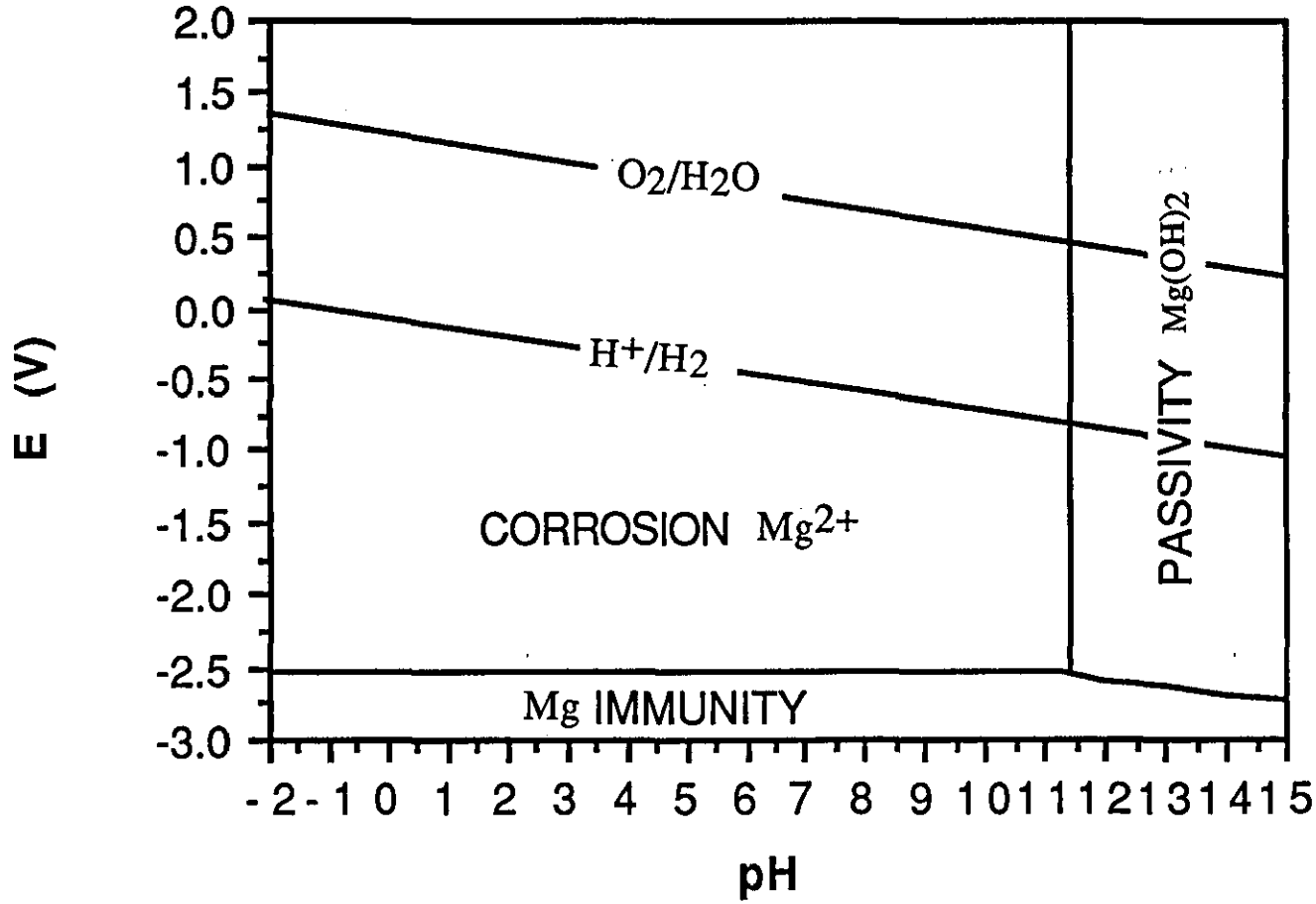

FIG. 7.7b - POTENTIAL-pH DIAGRAM FOR ZINC

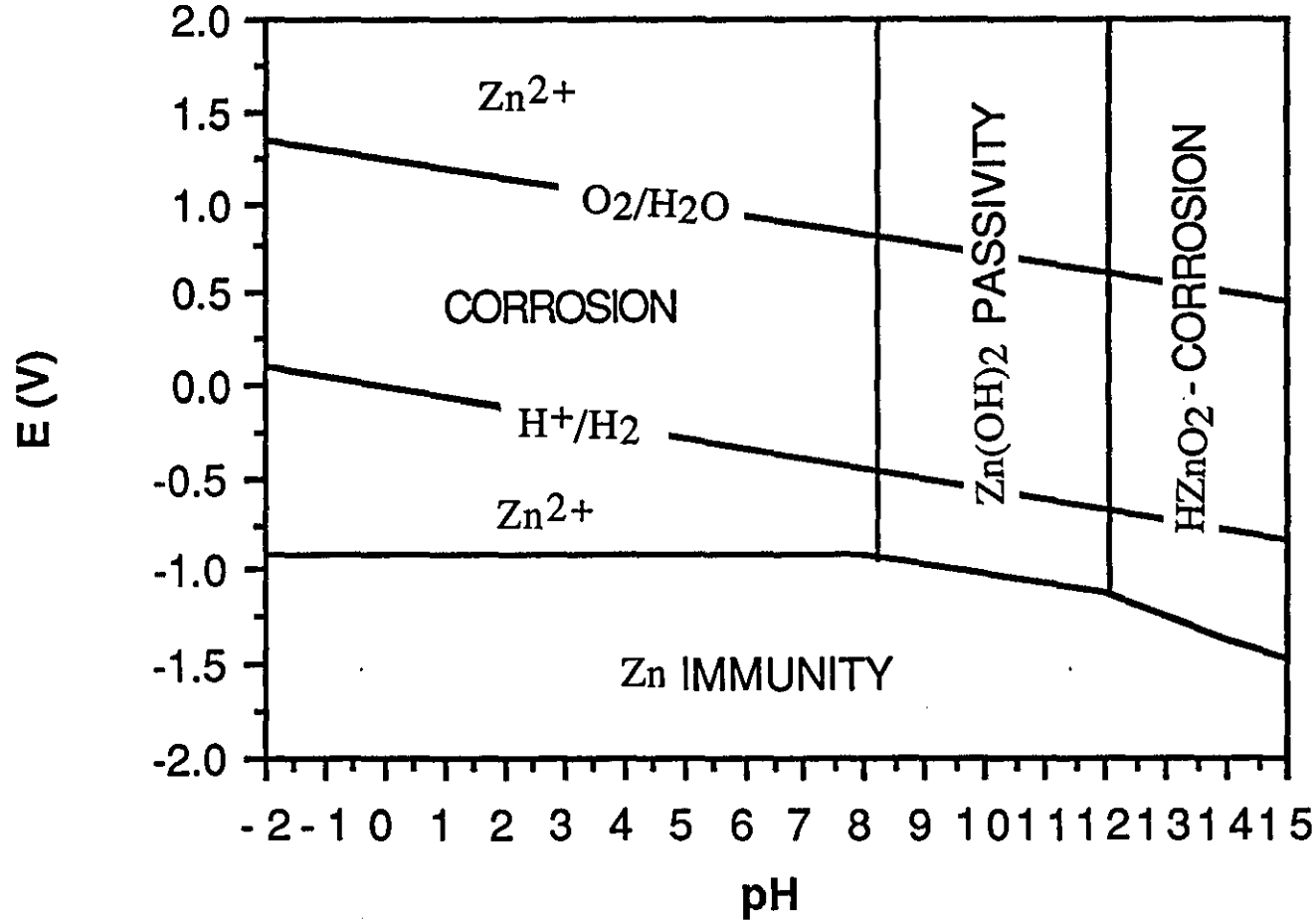

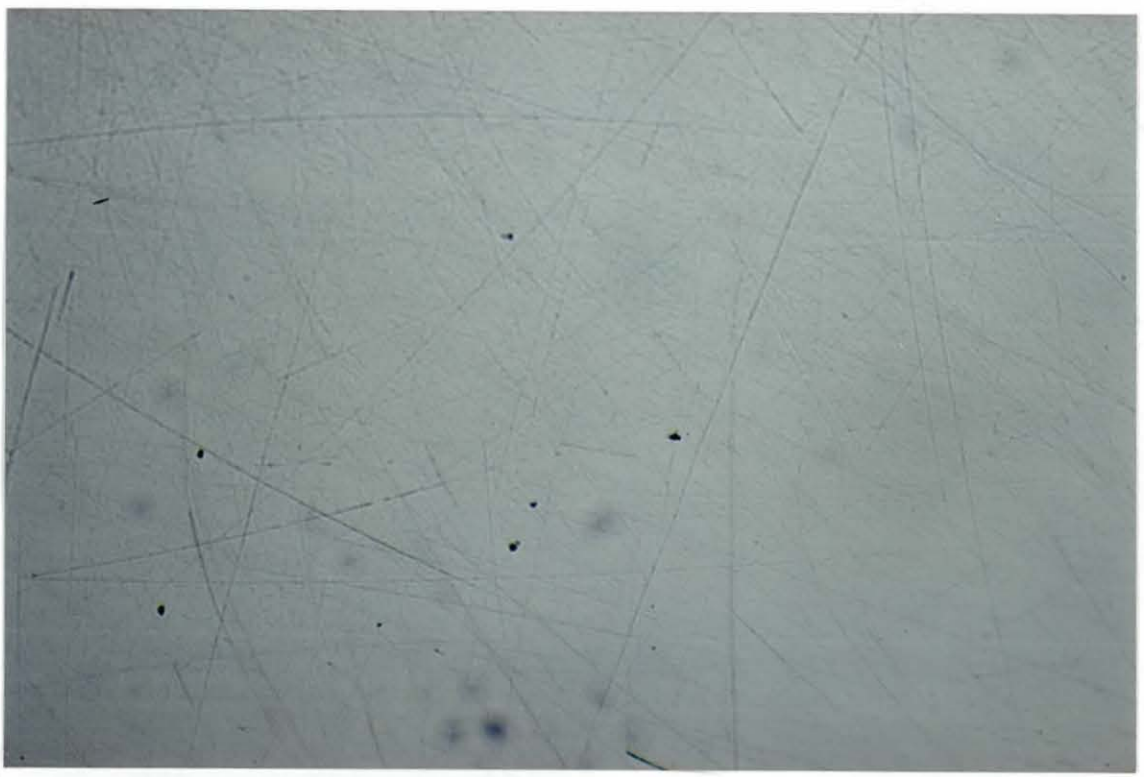

FIG. 7.8 - OPTICAL MICROGRAPH OF POLISHED IRON SURFACE

**200X Magnification**

FIG. 7.9a

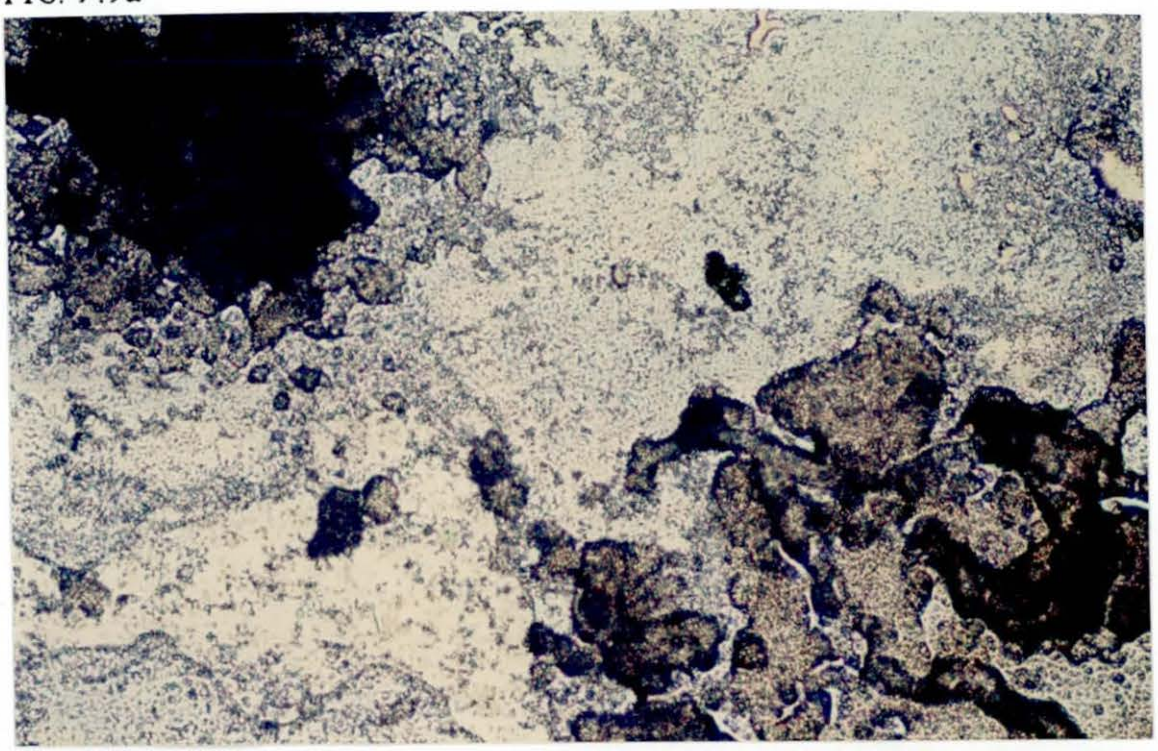

FIG. 7.9b

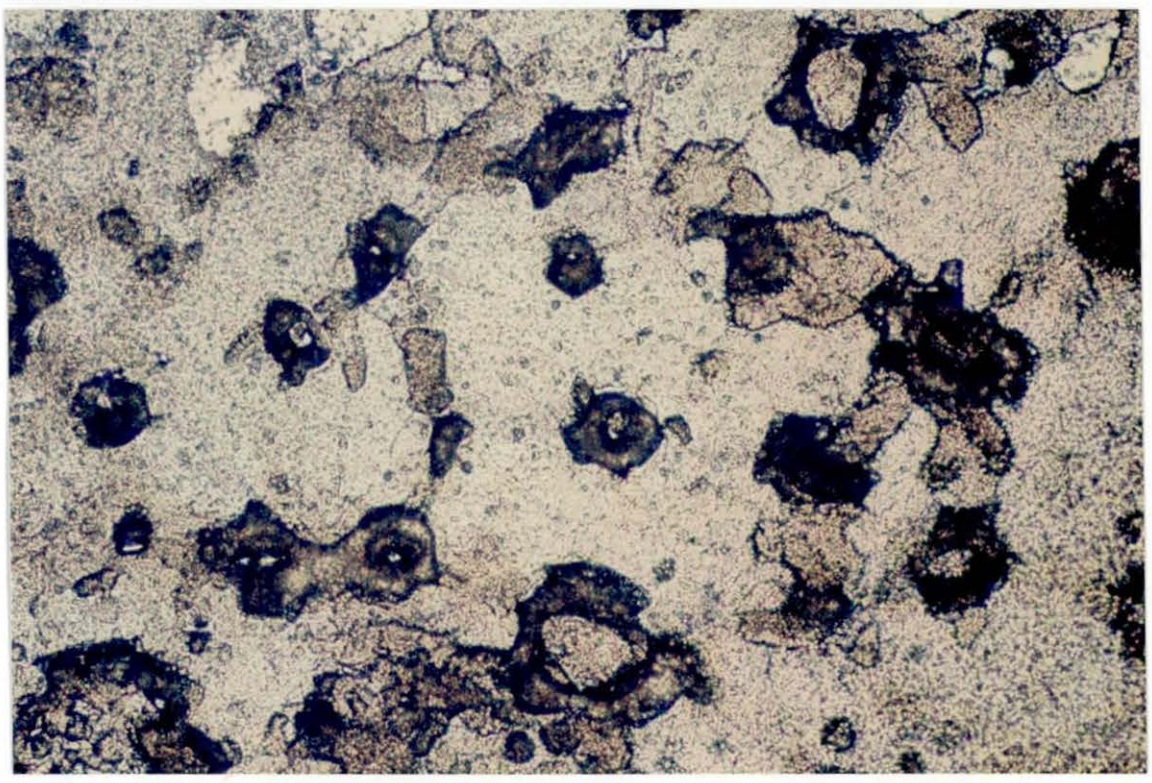

FIG. 7.9a,b - OPTICAL MICROGRAPHS OF IRON SURFACE WITH ZINC INHIBITION.

200X Magnification

FIG. 7.10a

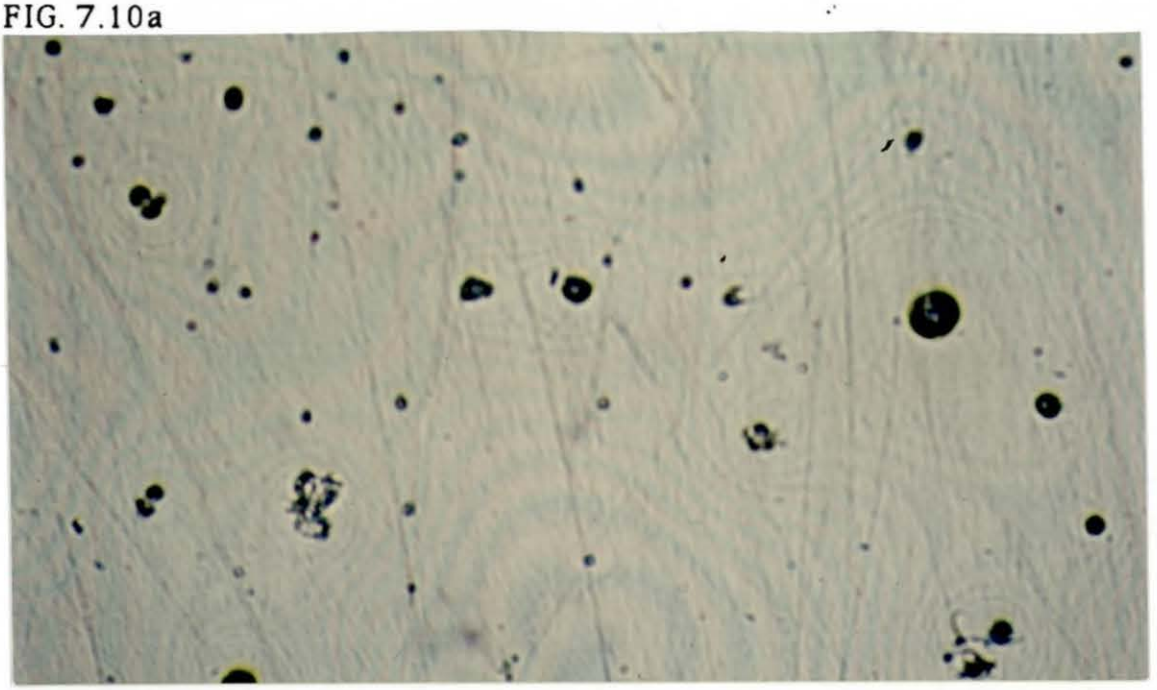

FIG. 7.10b

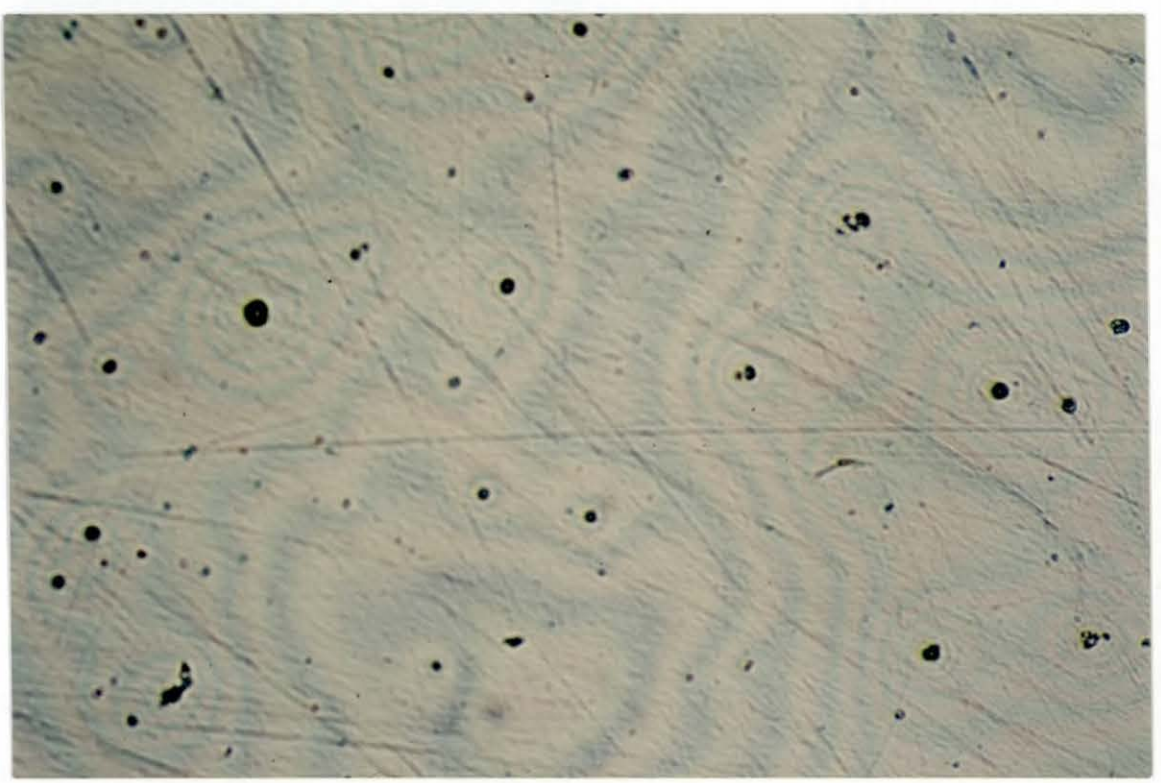

FIG. 7.10a,b - OPTICAL MICROGRAPHS OF IRON SURFACE WITH MAGNESIUM INHIBITION.

200X Magnification

inhibitors respectively. Figure 7.9a shows a marked change in surface morphology with respect to Figure 7.8. The zinc deposit is non-uniform and of varying thickness. The areas of least reflection indicate the thickest deposition. Figure 7.9b allows us to look at another photograph of the same surface. We can see that the heavier deposits are distributed at random. These are areas of maximum growth. A possible explanation for this behaviour is that the surface morphology determines the points where nucleation is more thermodynamically favoured. Alternatively, although the surface is presumably equipotential, these thicker areas may correspond to sites which were initially highly active for oxygen reduction. Similar discrete areas of deposition are noted with magnesium - Figures 7.10 a,b. These are surrounded by a thin film of reaction product which adheres strongly to the electrode. Unlike zinc, the metal surface can be seen through the deposit. Observing this thin film may reinforce the theory that magnesium inhibition is caused by reduced oxygen transport, whereas zinc inhibition is the result of electrical isolation.

As well as simple cations a number of commercial inhibitors were investigated. Polymate 945 and 966 are synergised zinc/organic phosphate inhibitors. Figures 7.11 and 7.12 show that hardness is required for inhibition. The performance in 50/50 water was excellent (see Figures 7.13 and 7.14). A slight drop in efficiency was observed in moving to a 150/150 solution (Figures 7.15 and 7.16) due to the increase in alkalinity and its affect on zinc solubility.

Finally, two common constituents of commercial formulations which do not contain zinc were tested. H.P.A. and P.C.A. (as organic phosphonates) were observed to operate extremely well in both 50/50 ( Figures 7.19 and 7.20 ) and 150/150 (Figures 7.21 and 7.22) waters whilst incurring little inhibition in 0.1M $NaClO_4$ alone (Figures 7.17 and 7.18). No apparent loss of effectiveness was observed on moving to the harder, more alkaline water. However, H.P.A. was observed to be the better cathodic inhibitor of the two, under these experimental conditions.

FIG.7.11- EFFECT OF 50ppm POLYMATE 945

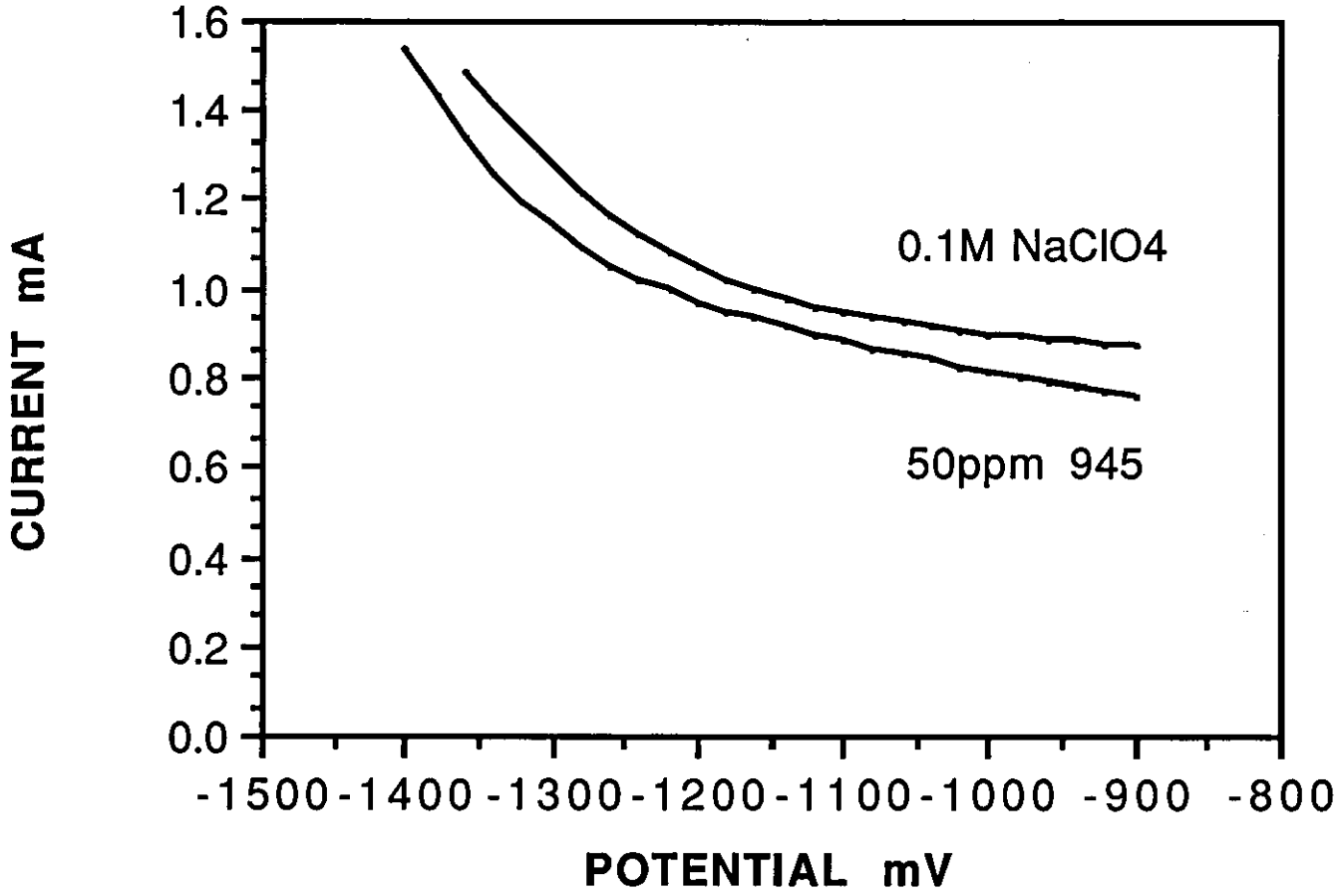

FIG.7.12 - EFFECT OF 50ppm POLYMATE 966 IN 0.1M NaClO4

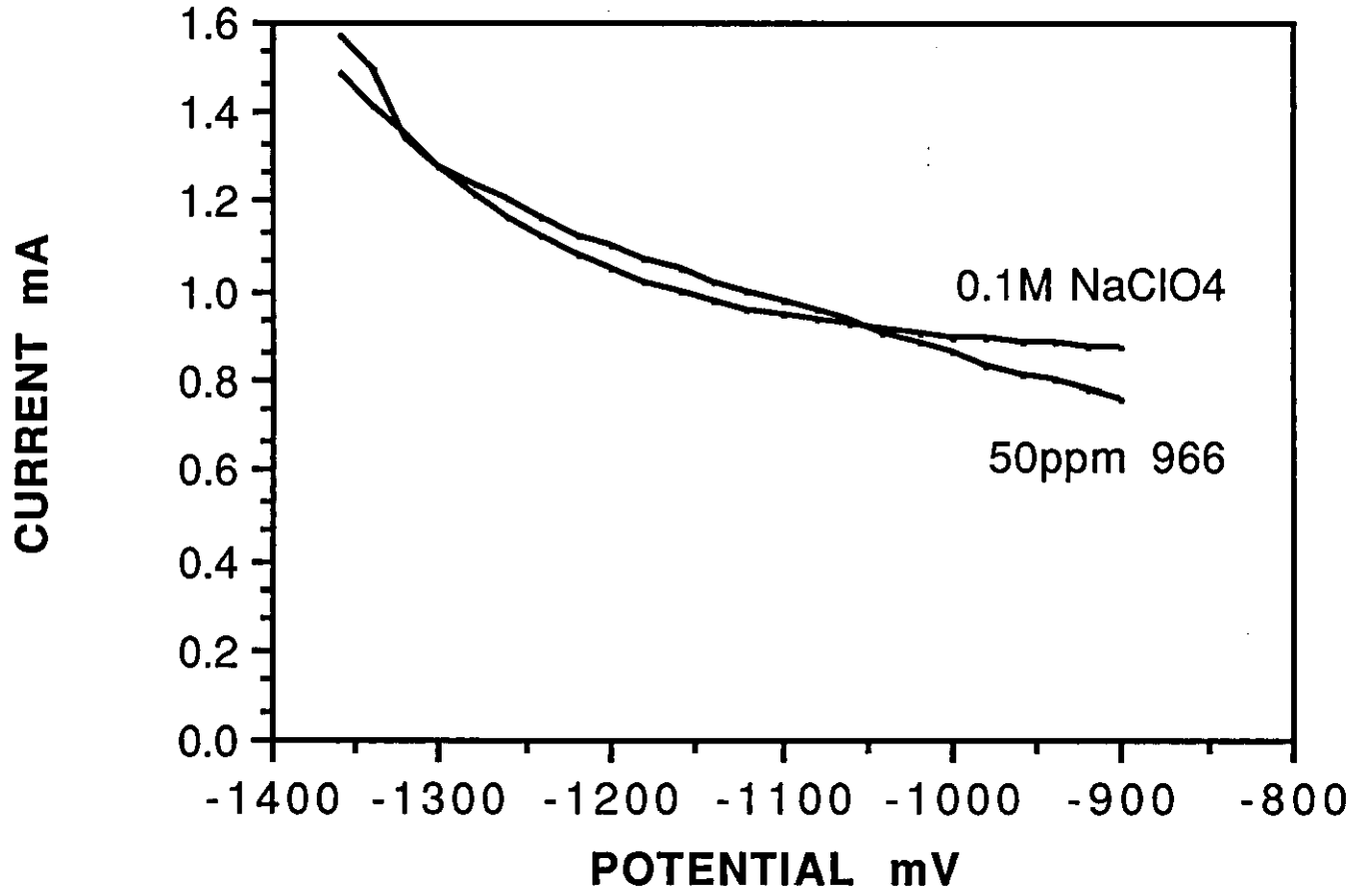

FIG.7.13 - EFFECT OF 50ppm POLYMATE 945 IN 50/50 WATER

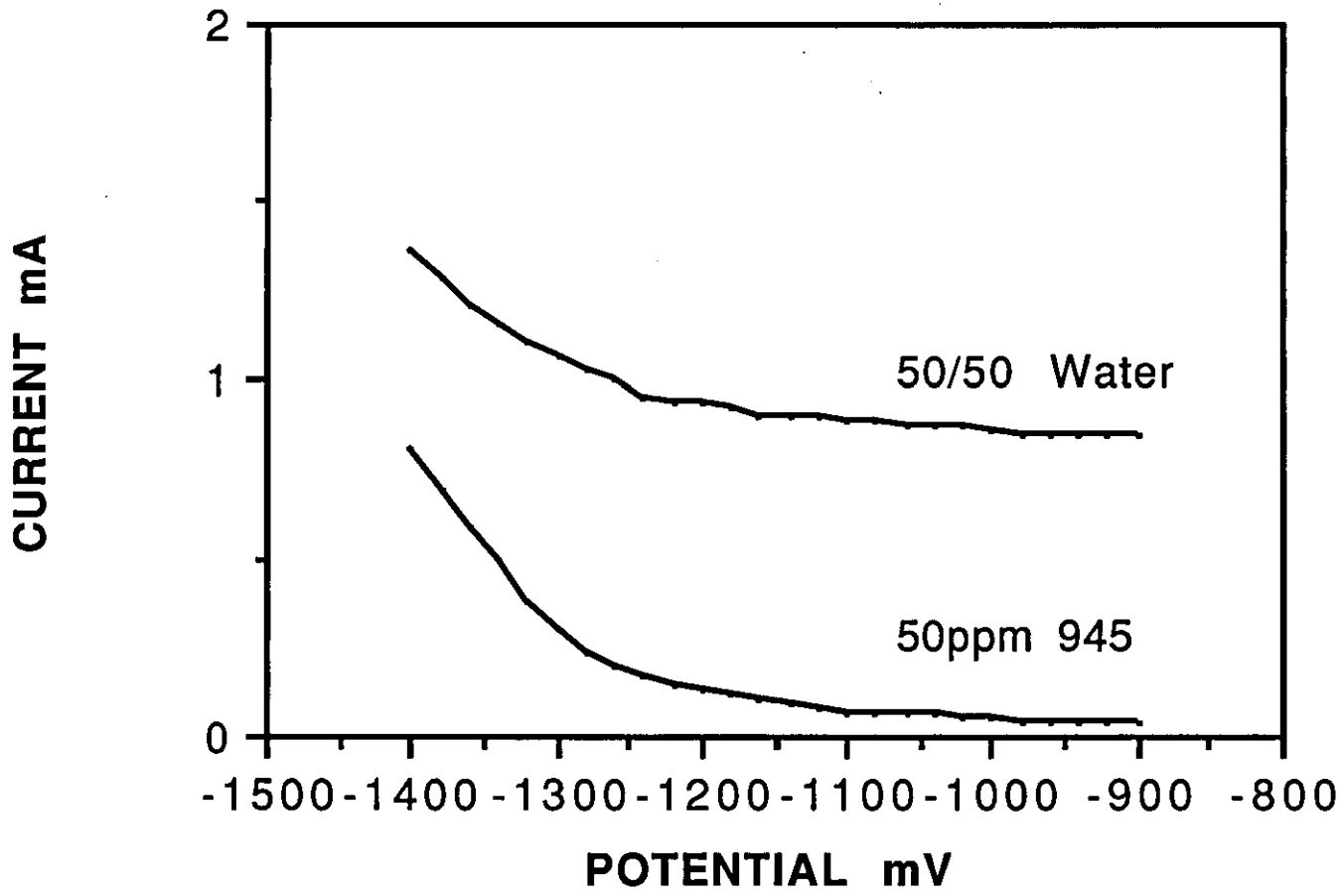

FIG.7.14 - EFFECT OF 50ppm POLYMATE 966 IN 50/50 WATER

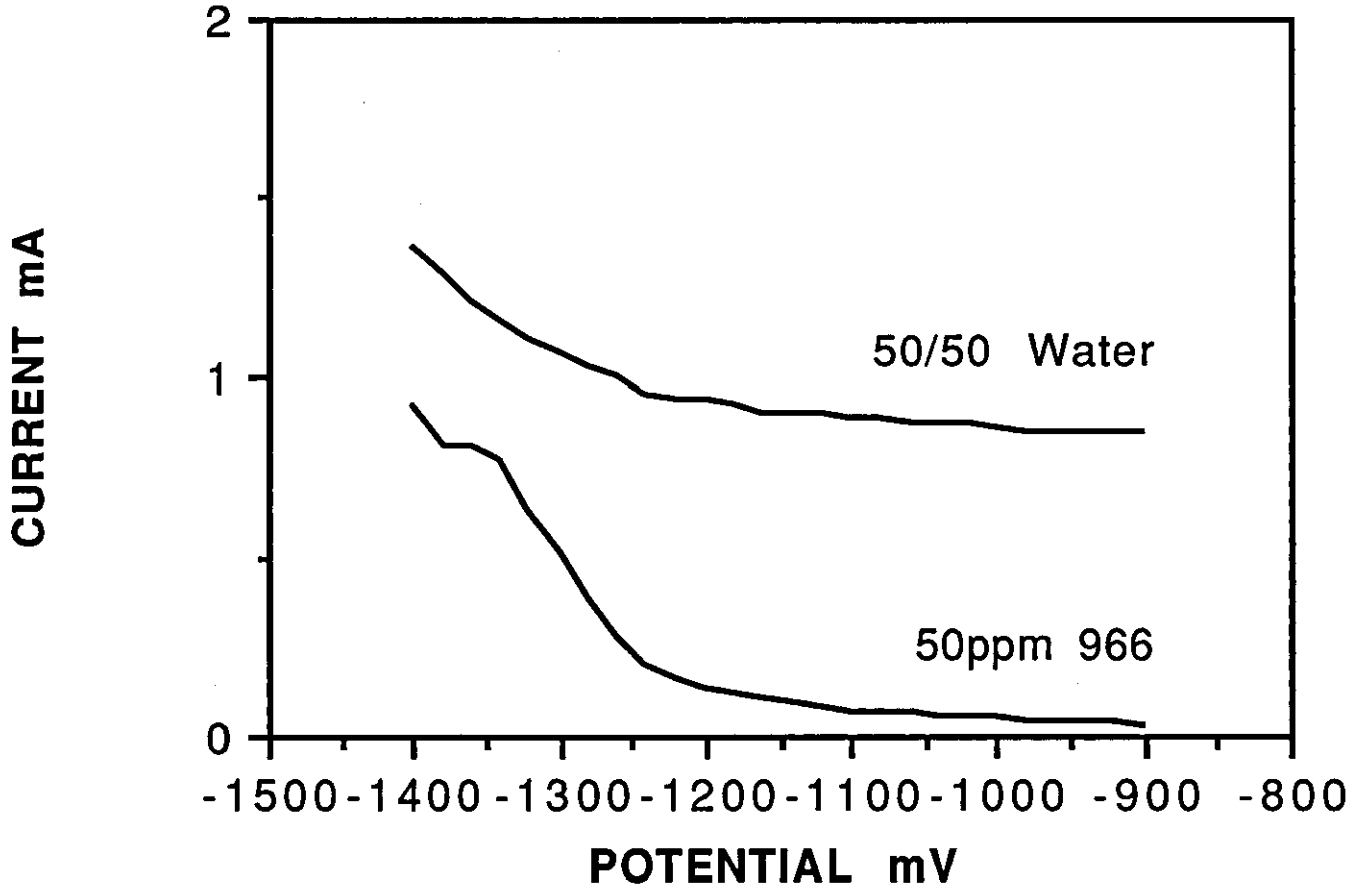

FIG.7.15 - EFFECT OF 50ppm POLYMATE 945 IN 150/150 WATER

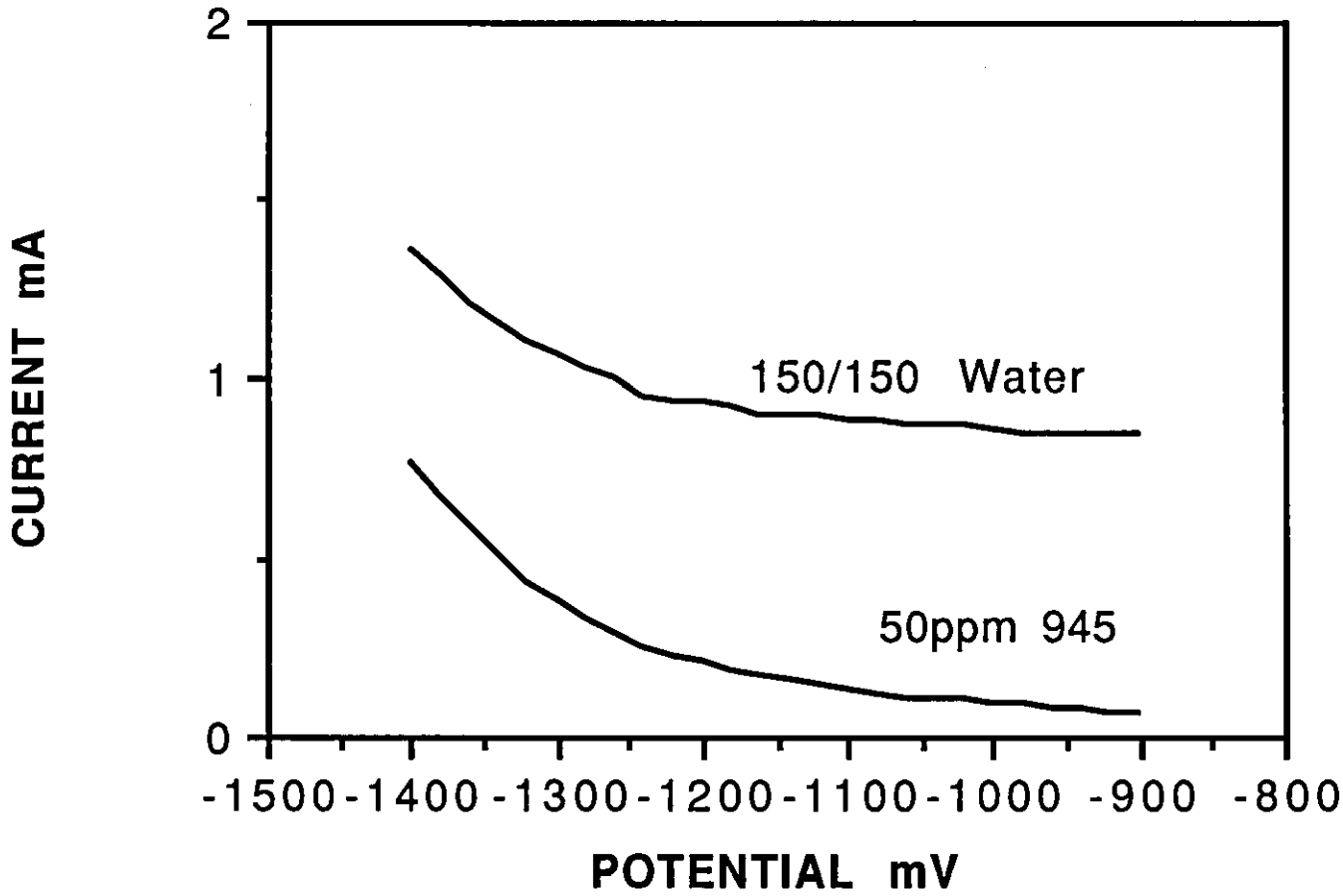

FIG.7.16 - EFFECT OF 50ppm POLYMATE 966 IN 150/150 WATER

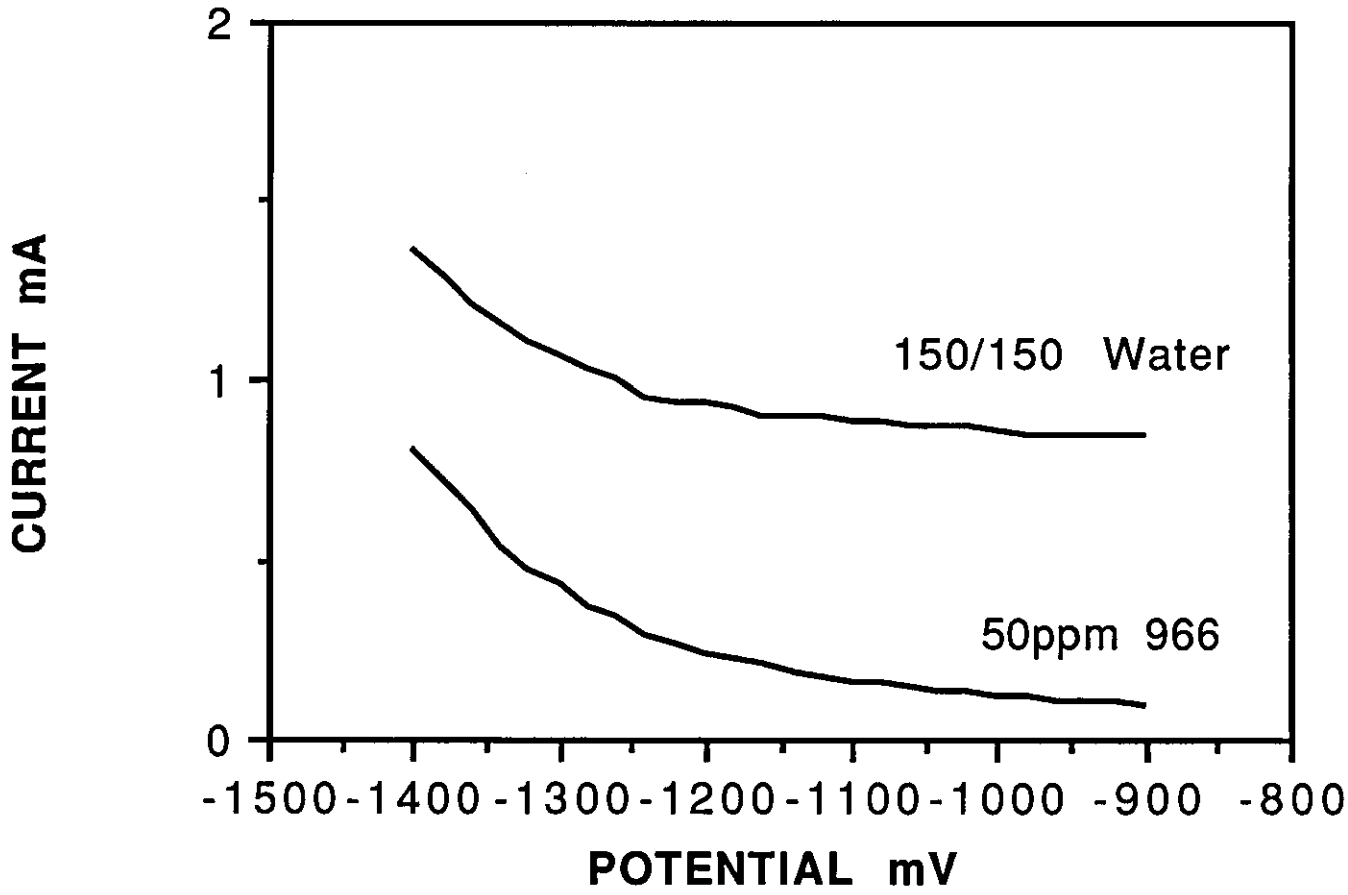

FIG.7.17 - EFFECT OF 50ppm H.P.A. IN 0.1M NaClO4

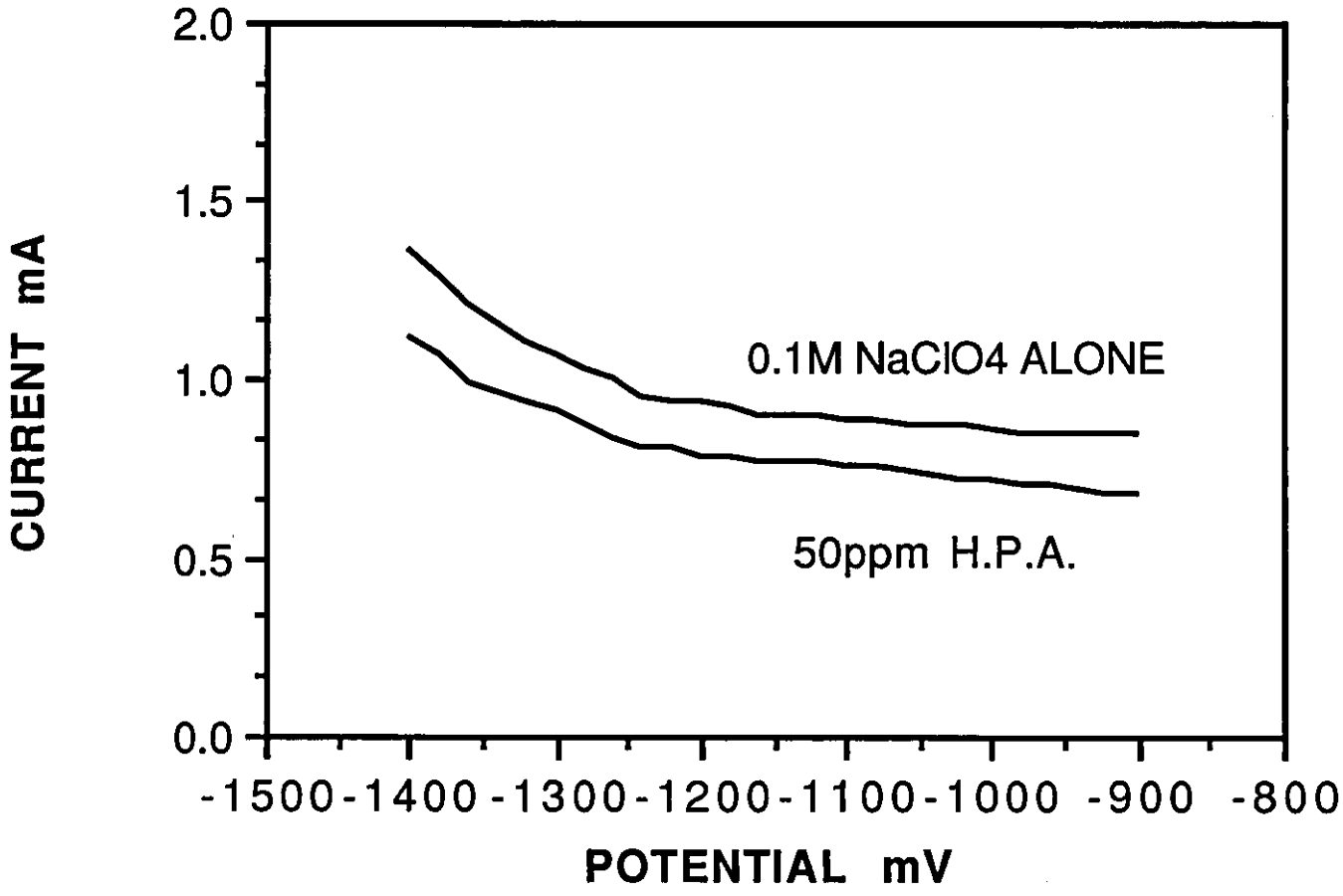

FIG 7.18 - EFFECT OF 50ppm P.C.A. IN 0.1M NaClO4

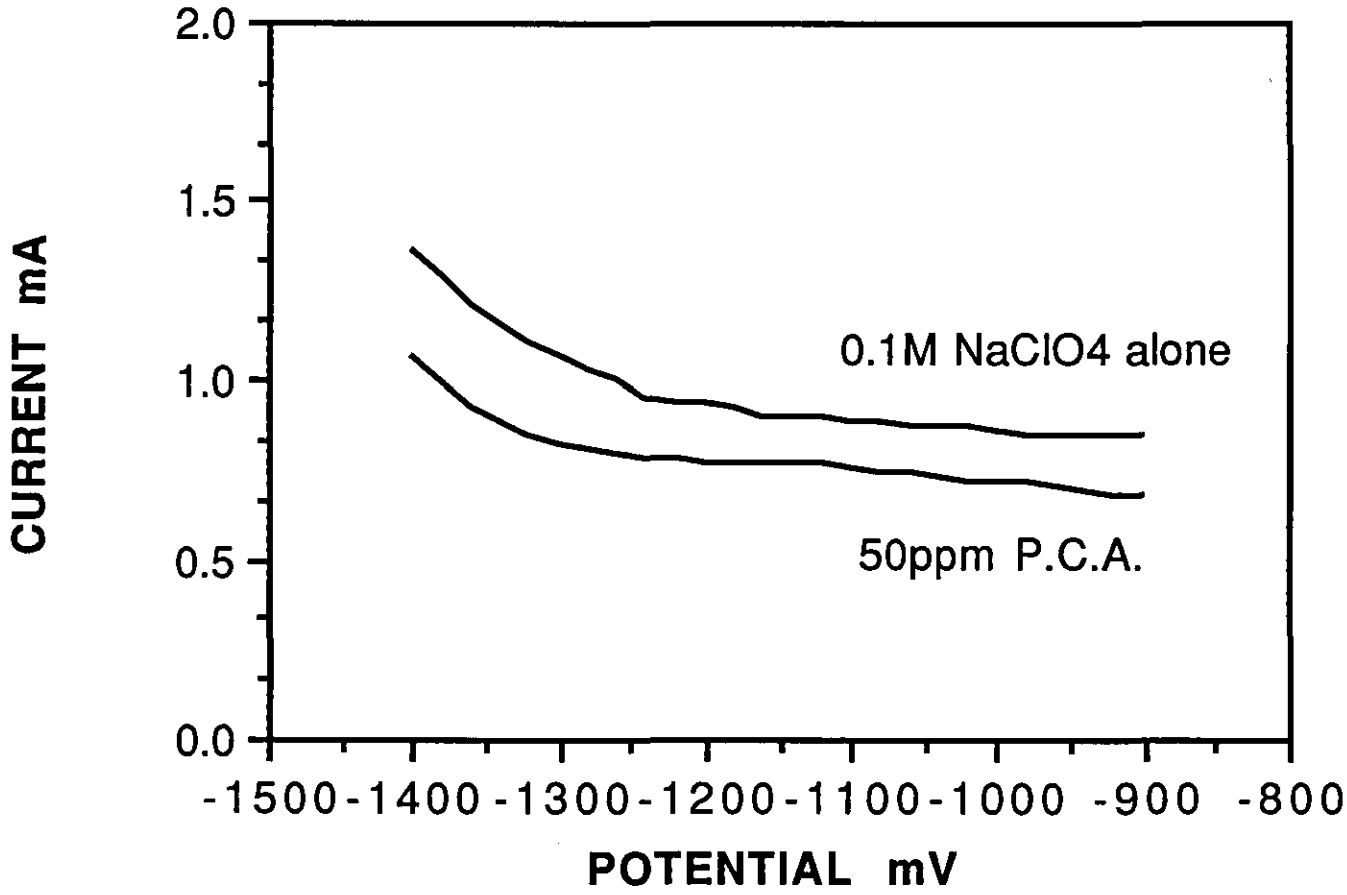

FIG. 7.19 - EFFECT 0F 50ppm H.P.A. IN 50/50 WATER

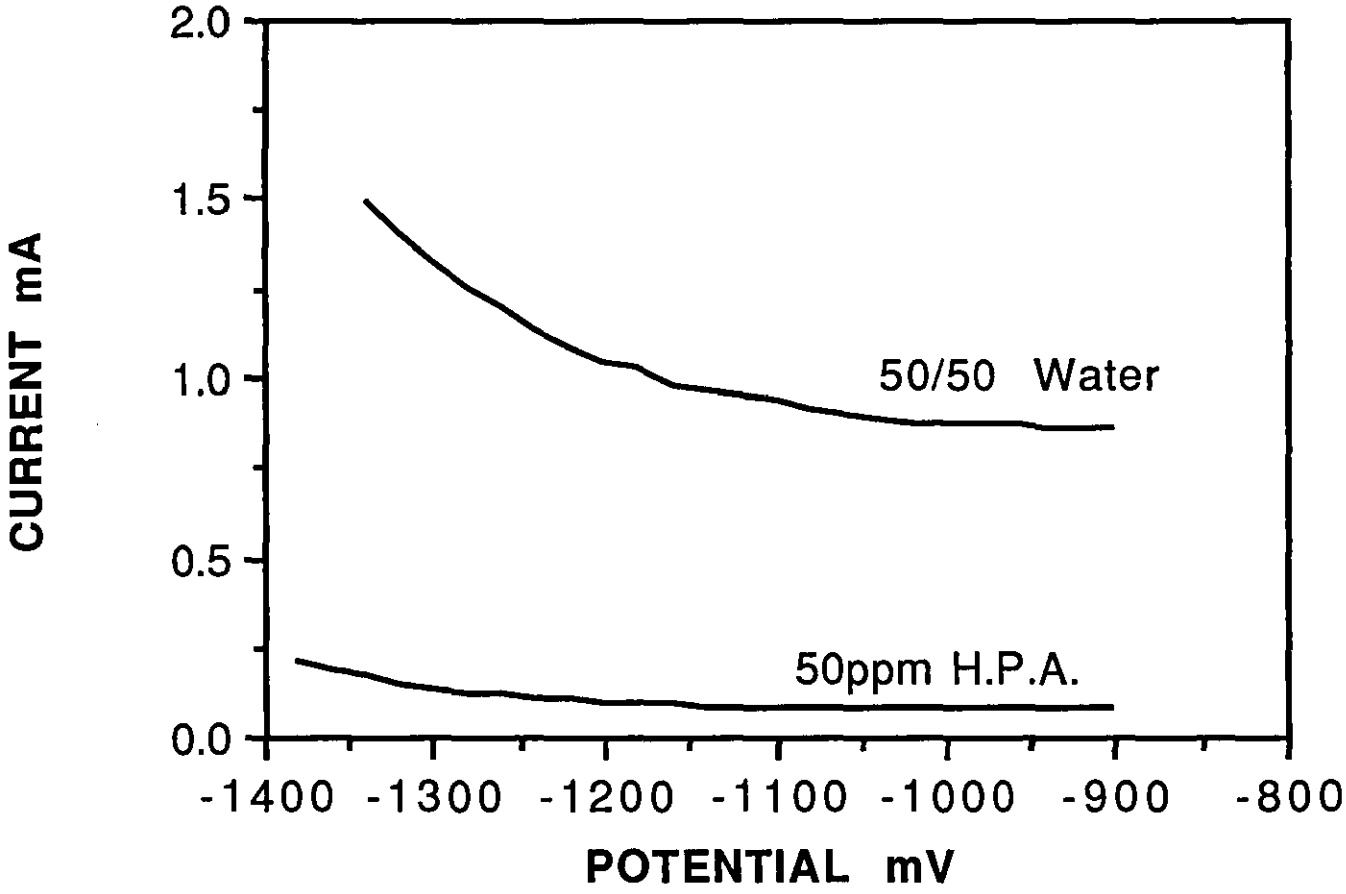

FIG.7.20 - EFFECT OF 50ppm P.C.A. IN 50/50 WATER

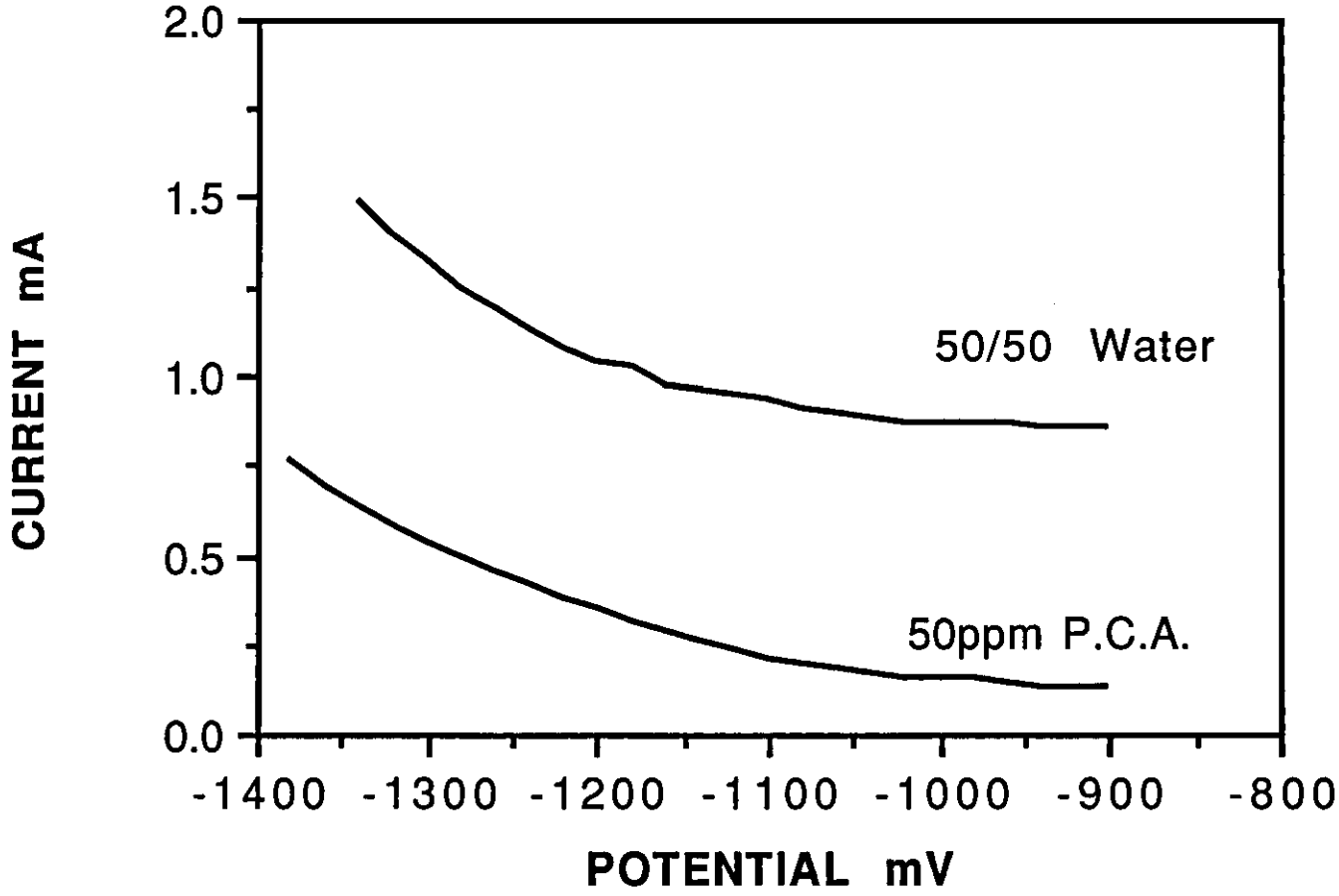

FIG.7.21 - EFFECT OF 50ppm H.P.A. IN 150/150 WATER

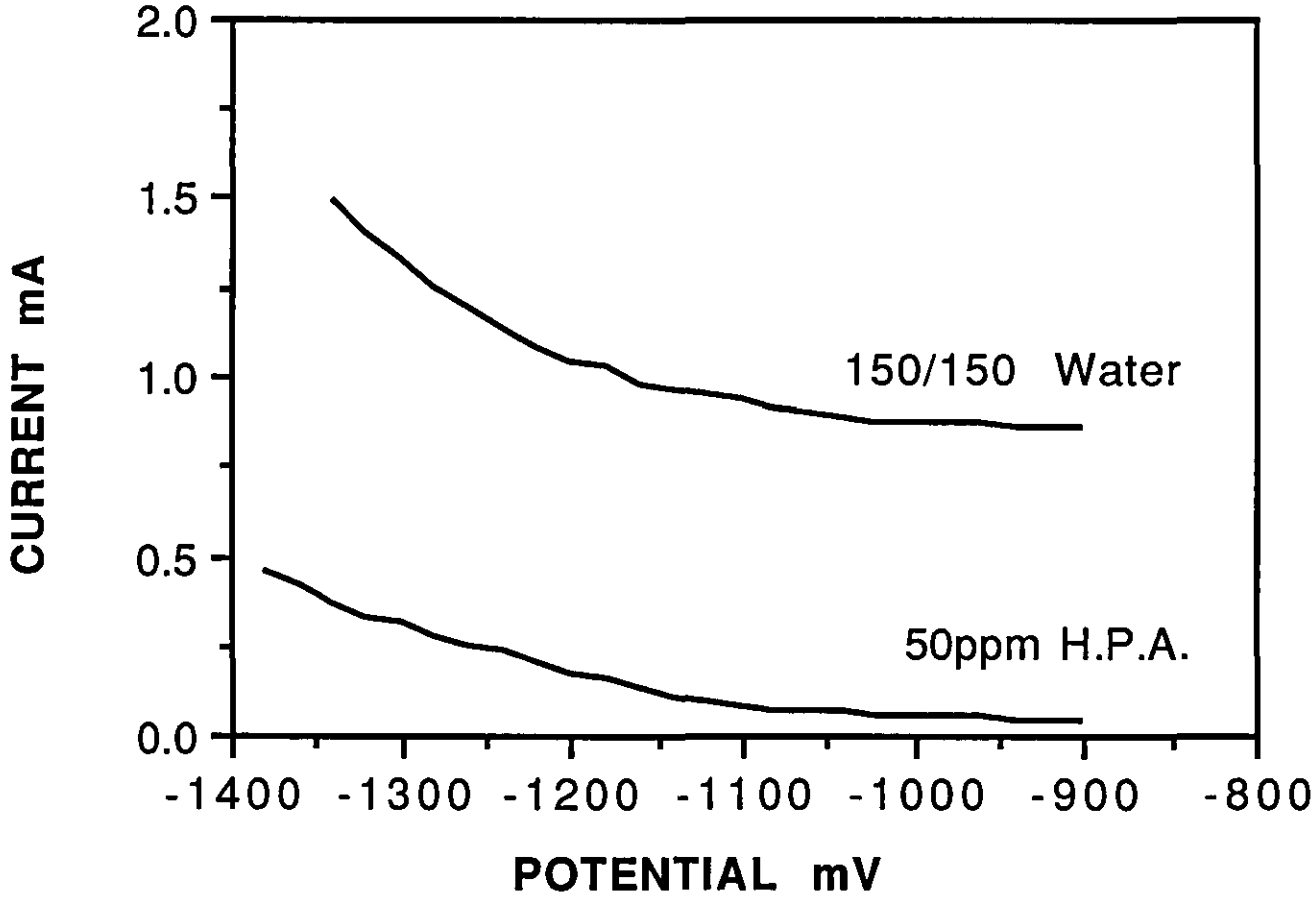

FIG. 7.22 - EFFECT OF 50ppm P.C.A. IN 150/150 WATER

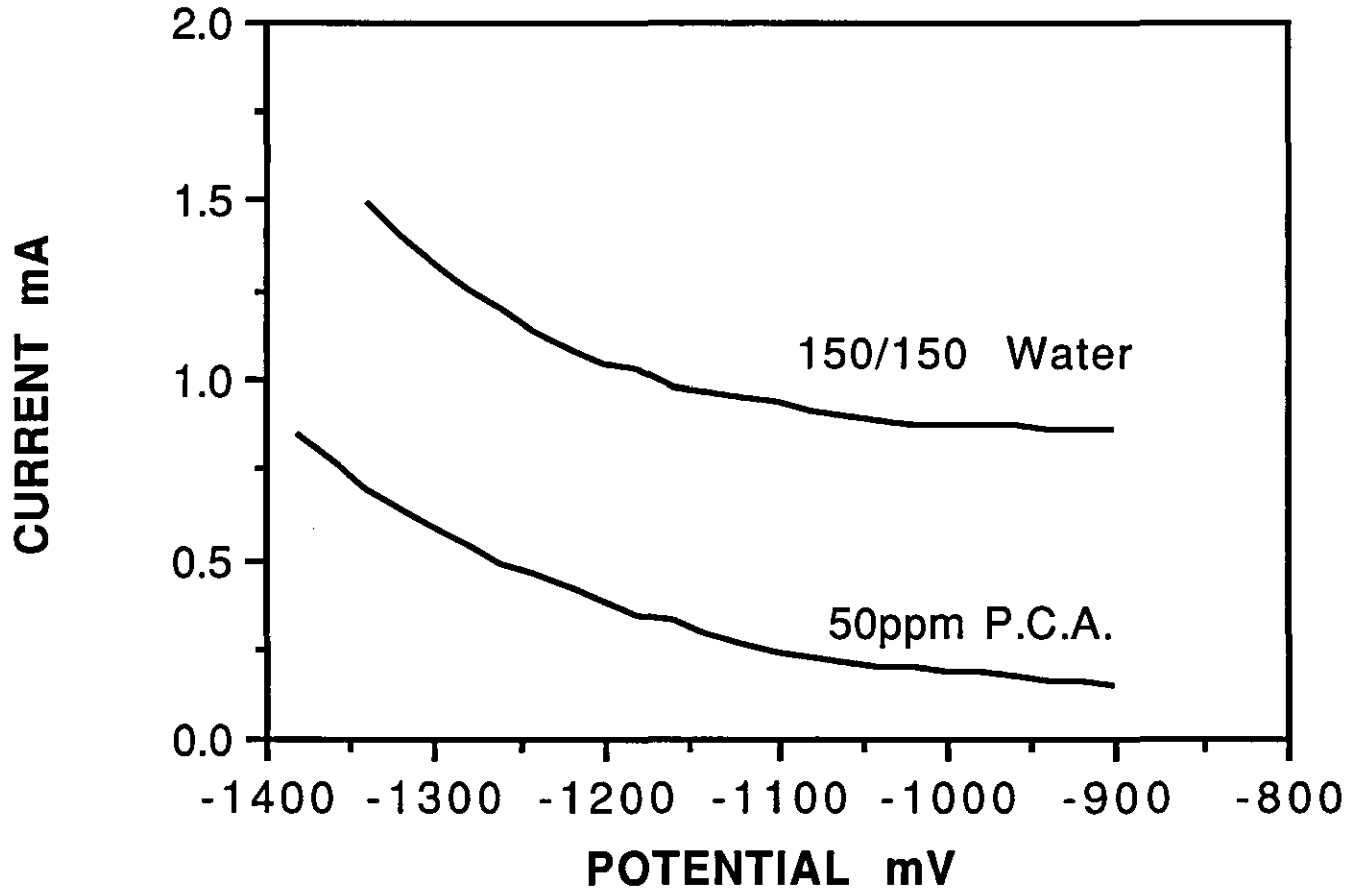

## 7.4 CONCLUSIONS

The current drop method is a simple and relatively quick technique for cathodic inhibitor evaluation. However, it is limited in that it can only be used for comparative purposes. As such, no kinetic data and very little mechanistic information can be obtained. Its value lies in its simplicity as an initial test for cathodic inhibitive action, ultimately pointing the way to efficient use of the more informative, yet time consuming test rigs. (Or other new evaluative techniques as described in Chapters 8 and 9)

# CHAPTER 8

# THE USE OF A DIFFERENTIAL AERATION CELL FOR INHIBITOR EVALUATION.

## 8.1 THEORY

The corrosion of iron, or mild steel in neutral aqueous solutions, consists of a two stage redox process at the metal surface. That is, the dissolution of iron from anodic sites:

$$Fe \text{ ------> } Fe^{2+} + 2e^-$$

believed to be areas of high surface free energy, such as defects in the crystal lattice e.g. screw dislocations and foreign atoms, and the reduction of a depolariser, in this case dissolved oxygen at the cathodic sites:

$$O_2 + 2H_2O + 4e^- \text{ ------> } 4OH^-$$

The study of corrosion is difficult since the two reactions are occurring side by side, and the opposing sites are evenly dispersed over the surface of the metal. If the two reactions could be separated and studied in isolation, then evaluation of inhibitor action at the dissociated sites would be relatively easy. Imposing a overpotential is one method of creating isolated sites, but only allows the study of one reaction at a time.

In nature, the two sites may be found separate to some extent under the conditions of differential aeration. Such a situation may arise in underground piping. If a section of the pipe is above the surface of the ground it is exposed to a much higher oxygen concentration than that of the buried pipe. This causes a imbalance in the cathodic and anodic sites. Cathodic sites predominate above the surface (i.e. at high oxygen concentrations). Hence, the number of anodic sites

below the surface increase to redress the balance and corrosion will occur underground.

The process of differential aeration was first studied by Aston[81] in 1916. He measured the voltage between two iron electrodes, one of which was aerated. He found the aerated electrode to have a negative potential with respect to the unaerated electrode. The concept was first used to study the corrosion of copper in 1919 by G.D. Bengough and O.F. Hudson[82], but it was not until 1923 that U.R. Evans[83] successfully used it to study the corrosion of iron (also copper, zinc, silver, aluminium and cadmium were studied) in KCl electrolyte. As a result of Evans's investigations, it was conclusively proved that corrosion was an electrochemical process, occurring via two half reactions. He observed the precipitation of metal hydroxide where the two products of the half reactions met. Further, in 1931[84], he attempted to quantify the rate of corrosion upon differential aeration, by measuring the current passing between the two electrodes, over a certain period of time. The current passed was found to be equivalent to the weight loss at the non-aerated electrode, proving that corrosion was effected by electrochemical factors.

When other groups attempted to reproduce the results of Evans et al difficulties were encountered. In many cases the aerated electrode suffered a greater weight loss than the non-aerated electrode. In an ideal differential aeration cell, the only reaction at the cathode should be oxygen reduction, and therefore weight loss should not occur. These observations were discussed by H.Kaesche[85] in 1964 and by U.R.Evans[86] in 1968. They found that the resistance of the ammeter used to measure the current was too high. In such a case, each electrode will react independently of the other, since no current can easily flow, and hence (as expected) the aerated electrode will corrode much quicker. Thus because of the very low currents produced by differential aeration, a "zero" resistance ammeter must be used for current measurements.

The currents produced in a differential aeration cell are not only dependent on the resistance of the ammeter, but also the oxygen concentration gradient between the two electrodes. The higher the difference in oxygen concentration between the two electrodes, the higher will be the corrosion current. This is best achieved by saturating the cathode with oxygen, whilst removing all oxygen from the anode. In order to do this practically, the two electrodes must be partitioned. In early cell designs this was not fully appreciated.

The cell fabricated by U.R.Evans[83] in 1927 used a parchment membrane to separate the two electrodes. This allowed oxygen to diffuse through to the "non-aerated" electrode and redress the balance, i.e. each electrode becomes autonomous. An improved cell design, using a cellulose acetate membrane was introduced by Evans in 1931. Cellulose acetate is less porous to oxygen than parchment, and to prevent oxygen diffusing into the electrolyte from the air, the surface was coated with a layer of viscous paraffin. However, when the two electrodes were disconnected, corrosion of the non-aerated electrode was observed. Evans reduced the degree of oxygen diffusion through the membrane further by using air rather than oxygen. Surprisingly, this did not dramatically effect the current, (probably due to the loss of cathodic sites on the anode).

In 1955, H.Grubitsch[87,88] expanded on Evans' ideas by splitting the cell into two halves (connected by a cellophane membrane), and saturating the aerated electrode with oxygen (or air) whilst using nitrogen or hydrogen to procure de-aeration. Grubitsch also discovered the need for pumping the electrolyte through the cell to remove any corrosion products which may build up at the electrode surface, and keep an homogeneous electrolyte.

Although most of the inherent problems involving the differential aeration cell have been investigated, and in some cases overcome, very few advances have been made since the 1960's. Infact very little work has been done on the technique since this time. This is somewhat surprising, since, its use as a measure of corrosion rate may be extended (with a little modification) to a technique for

inhibitor evaluation. By monitoring the current, and any changes that occur from adding inhibitors, the rate of corrosion can be calculated, and inhibitor efficiencies evaluated.

## 8.2 EXPERIMENTAL

A major problem with the differential aeration technique is the relatively small current it produces. This makes inhibitor comparison difficult because of the signal to noise ratio. To maximise the current range available for inhibitor evaluation, large circular iron electrodes were used (area = 12.5cm$^2$) and positioned as close to one another as possible (2cm apart) to minimise any IR drop through the electrolyte. The discs were positioned either side of a cellulose acetate membrane and encapsulated in a cell fabricated from four separate perspex discs, which were assembled using six locking bolts (see Figure 8.1). Cellulose acetate was chosen as the membrane because of its good conductivity and for its ability to allow efficient gas separation between each side of the cell. Alternative materials included those of the Nafion (Dupont) family. These were not adopted in this study because advantages in mechanical stability were offset by those of cost and the necessity to thoroughly de-contaminate (i.e. remove iron and inhibitor species) between each run. Cellulose acetate was simply discarded after use.

When the cell was used for prolonged periods of time, the production of hydroxide ion at the cathode (from the reduction of oxygen) caused a significant increase in pH. Furthermore, a slight decrease in pH was observed at the anode, due to the formation of ferrous hydroxide upon iron dissolution. The small cell volume (12cm$^3$) on each side of the membrane magnified these problems. To overcome these difficulties, electrolyte was recirculated through each half of the cell from two 0.5 litre reservoirs. Any corrosion products produced within the cell were diluted in this manner, and no problems were observed within the time span of the experiment. High flow rates (0.8cm$^3$ s$^{-1}$) were employed to reduce local concentration changes in the cell compartments. The use of

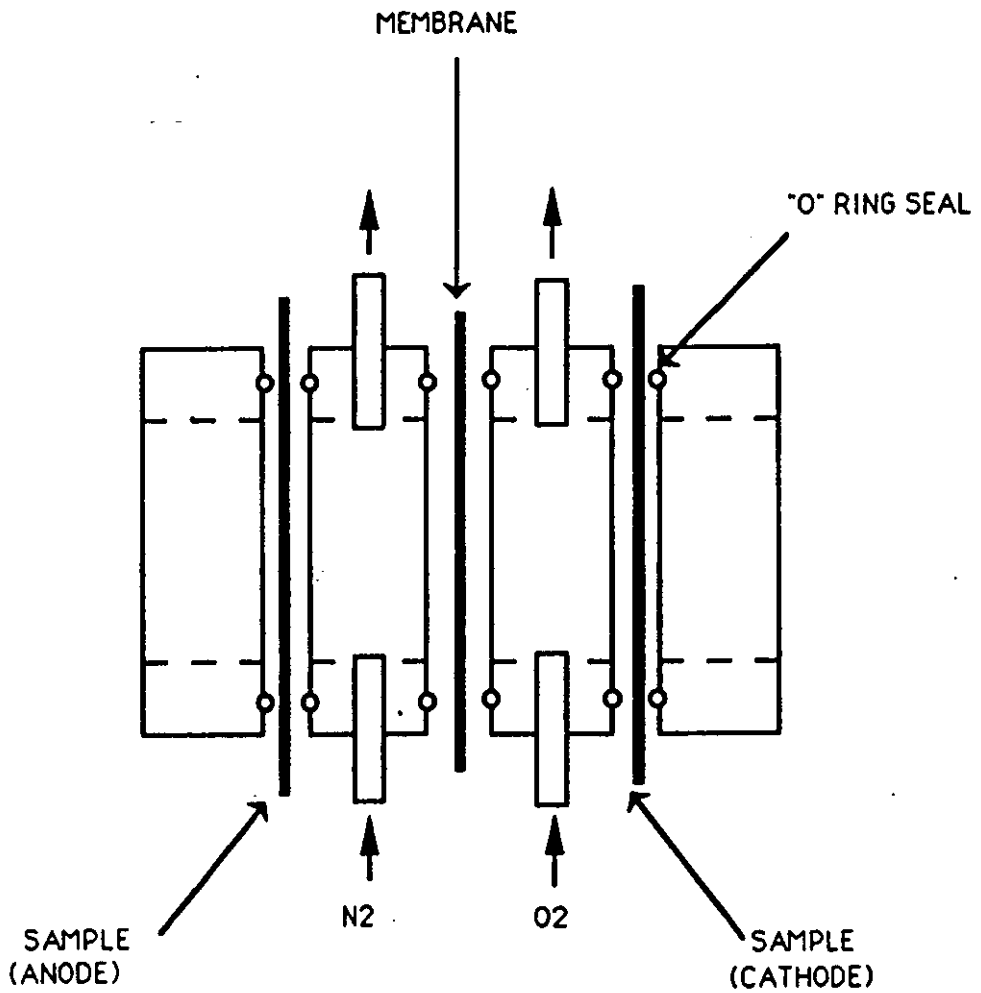


FIG.8.1 - DIFFERENTIAL AERATION CELL

reservoirs also allowed aeration/de-aeration of the electrolyte before entering the cell, and hence eliminated any possible disturbance due to bubble flow across the electrode surface. A 0.1M $NaClO_4$ solution was used as the supporting electrolyte. A 1M $NaClO_4$ solution was also assessed but was found to increase the corrosion current by only 30%. Due to economic factors this was deemed as insufficiently effective. De-aeration of the anode electrolyte compartment was provided by oxygen free nitrogen whilst oxygen was supplied to the cathodic compartment. All current measurements were made using a Hewlett Packhard "zero" resistance ammeter to minimise voltage drop in the circuit.

As stated in previous chapters surface preparation strongly effects reproducibility. The electrodes, made of iron foil (99.5% pure, 0.25mm thick) were prepared by the same method each time:

i) 30 seconds in concentrated hydrochloric acid to remove any oxide film present.
ii) washed in tri-distilled water then dried.
iii) 30 seconds in 5% nital (nitric acid / ethanol) solution.
iv) washed again in distilled water then dried.

This left the electrodes clean and free of product.

## 8.3 RESULTS AND DISCUSSION

### 8.3.1 0.1M $NaClO_4$

The first stage of experimental work was to obtain a blank, against which prospective inhibitors could be compared. A 0.1M $NaClO_4$ solution (pH=7) was used, and current readings recorded over a period of 90 minutes. This was repeated twice further and an average taken.

Figure 8.2 shows the results of three duplicate blank runs. Reproducibility was good considering new electrodes were used for each run, and that the iron surface may vary from one piece to

FIG. 8.2 - 0.1M NaClO4 ALONE

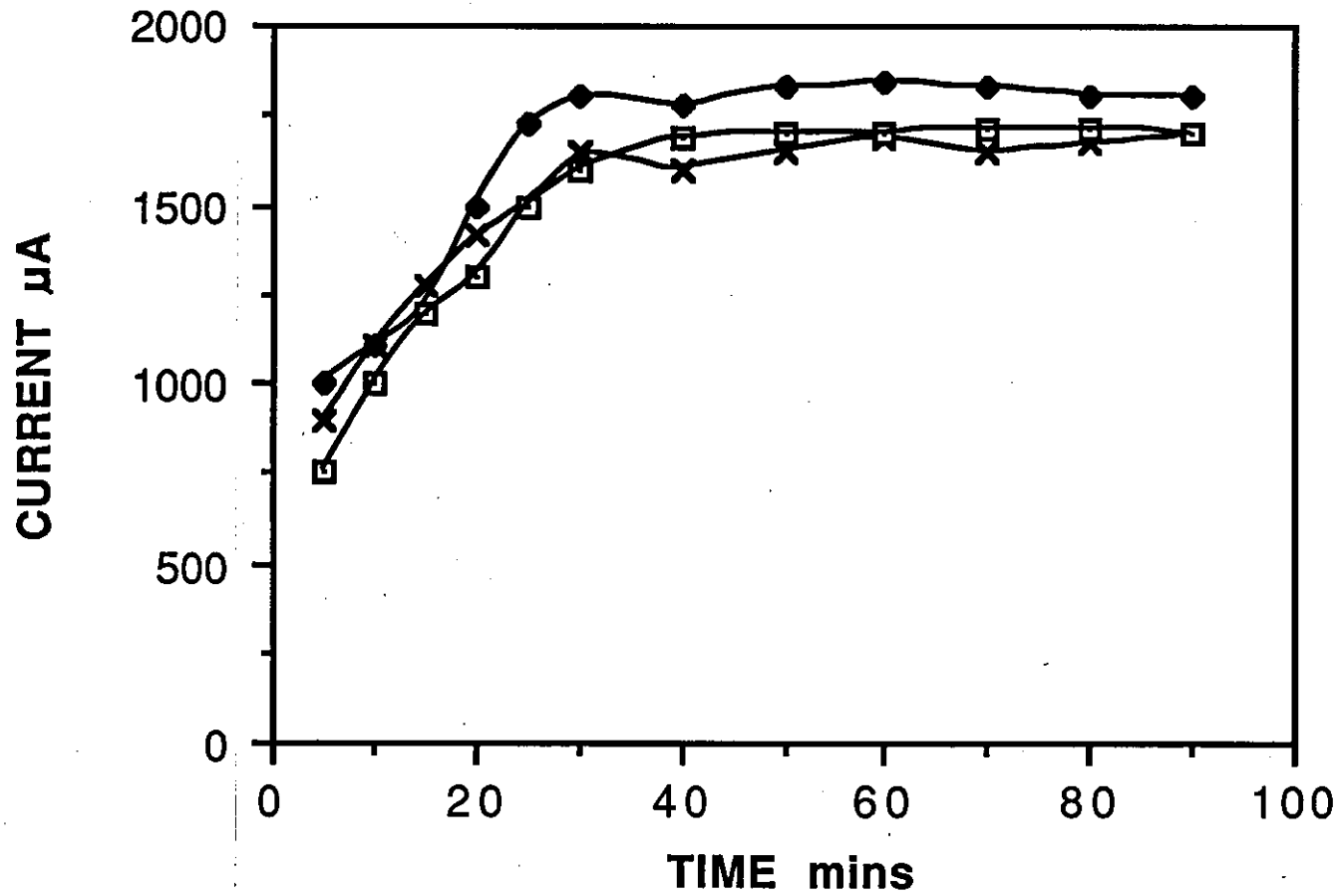

another. Initially, the current climbed for the first 30 minutes of each experiment. A plateau current was then reached at values of 1.8mA, 1.8mA and 1.7mA respectively. The experiment was terminated after 90 minutes, since previous trial runs showed a slow drop in current after a two hour period. On examination of the cellulose acetate membrane after such a two hour period, a brown colouration was observed due to iron species being adsorbed/precipitated at the membrane. This leads to blockage of the membrane pores and slowly reduces the membrane conductivity and current.

The pH of each reservoir was recorded as a function of time over a four hour period. Figure 8.3 shows that the pH in the anode compartment, fell very little over the period i.e. 7---> 6.5. Any changes in pH were probably due to the formation of iron(II) hydroxide and the associated proton liberation. The pH of the cathode changed substantially from 7--->11 over the four hour period, due to the formation of hydroxide ions upon oxygen reduction. These results suggest that the membrane functioned as required, i.e. restricting the transfer of hydroxide ions from one side to the other. The effect of this pH change was not considered a problem in the evaluation of inhibitors, as inhibitors functioned almost immediately under the experimental conditions.

### 8.3.2 ZINC.

To assess the cells effectiveness in evaluating cathodic inhibitors, zinc ions were added in the form of zinc perchlorate. Zinc ions have long been known for their cathodic inhibitive properties, and hence commonly employed in commercial inhibitor formulations. It is therefore useful to use zinc as a standard against which other cathodic inhibitors can be compared. Zinc was added in 50ppm concentration to each electrode compartment in turn, followed by simultaneous addition to both compartments. Table 8.1 gives the results obtained.

FIG. 8.3 - pH CHANGE FOR 0.1M NaClO4

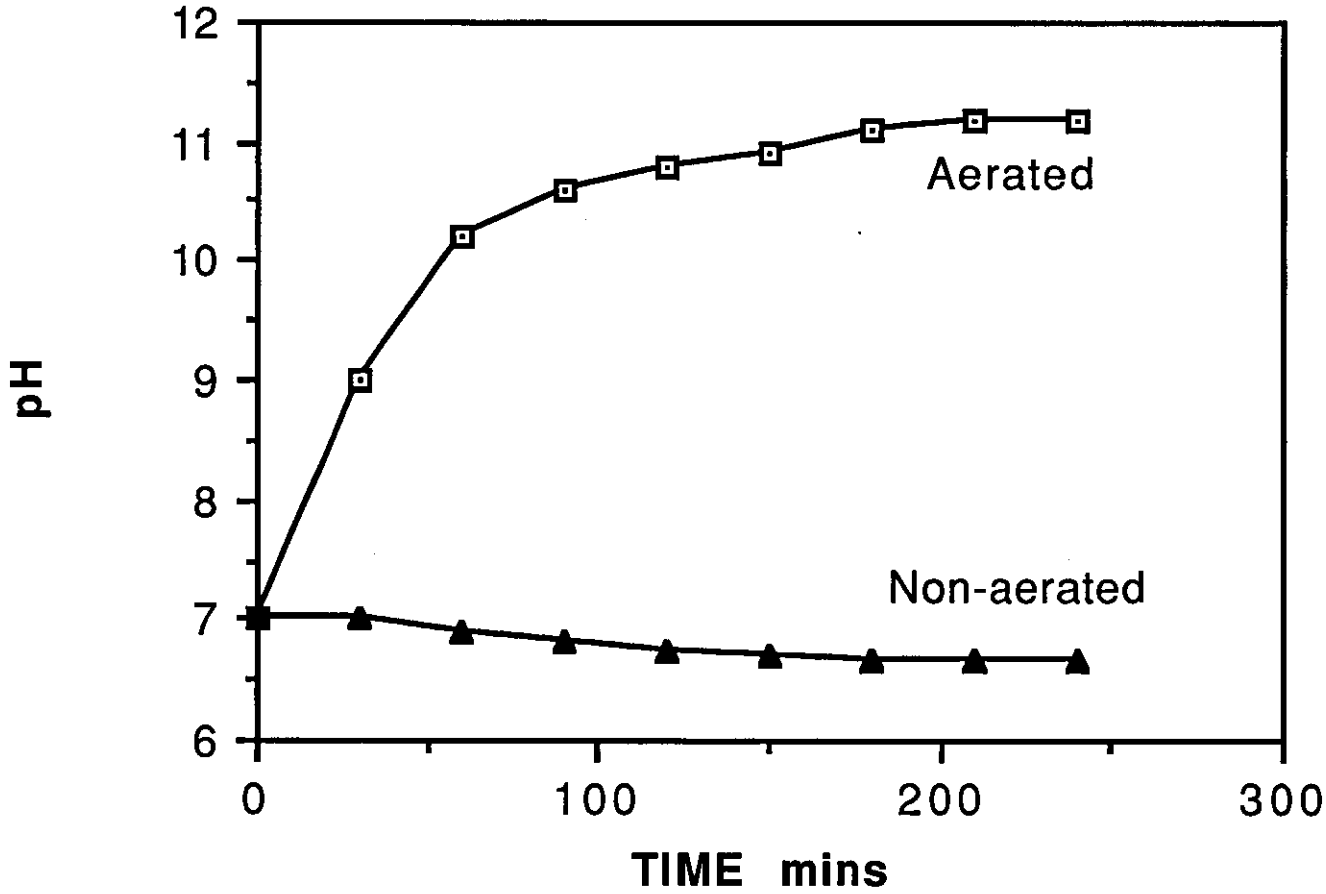

TABLE 8.1 - EFFECT OF ZINC ADDITION

| AERATED ELECTRODE | NON-AERATED ELECTRODE | CURRENT (μA) after 90mins |
|---|---|---|
| 0.1M $NaClO_4$ | 0.1M $NaClO_4$ | 1800 |
| 50ppm Zn + 0.1M $NaClO_4$ | 0.1M $NaClO_4$ | 46 |
| 0.1M $NaClO_4$ | 50ppm Zn + 0.1M $NaClO_4$ | 2800 |
| 50ppm Zn + 0.1M $NaClO_4$ | 50ppm Zn + 0.1M $NaClO_4$ | 10 |

a) Addition of Zinc to the Anode Compartment.
On the addition of zinc to the de-aerated compartment an increase in the magnitude of the current was observed. A plateau value of 2.8mA was recorded soon after addition (see Figure 8.4).

b) Addition of Zinc to the Cathode Compartment.
Figure 8.5 shows the effect of adding 50ppm zinc to the aerated electrode compartment. The current plateaued out after 20 mins, giving a value of 46μA, compared with the 1.8mA recorded for the blank.

c) Addition of Zinc to Both Electrode Compartments
Addition of zinc to both compartments resulted in the very low plateau current of 10 μA (see Figure 8.6)

The large drop in current on adding zinc to the aerated electrode suggests that under these experimental conditions, and in this dose level i.e. 50ppm, zinc is an extremely good cathodic inhibitor. Inhibition occurs almost immediately upon addition, and the rate at which a plateau value is reached suggests that the maximum effect is attained very quickly.

The subsequent increase in current when an addition is made to the anode compartment, shows that zinc has no dual properties i.e. it does not act both as an anodic and cathodic inhibitor. The subsequent increase can be explained by the formation of zinc hydroxide at cathodic sites present upon the anode. This blocking effect causes an overall increase in the observed anodic current due to iron dissolution. Oxygen reduction increases to redress the balance giving rise to a net increase in current.

When zinc was added to both compartments, the current dropped to virtually zero indicating almost complete coverage of the cathode surface. The effect upon the anode was negligible in comparison.

FIG. 8.4 - EFFECT OF 50ppm ZINC IN NON-AERATED COMPARTMENT

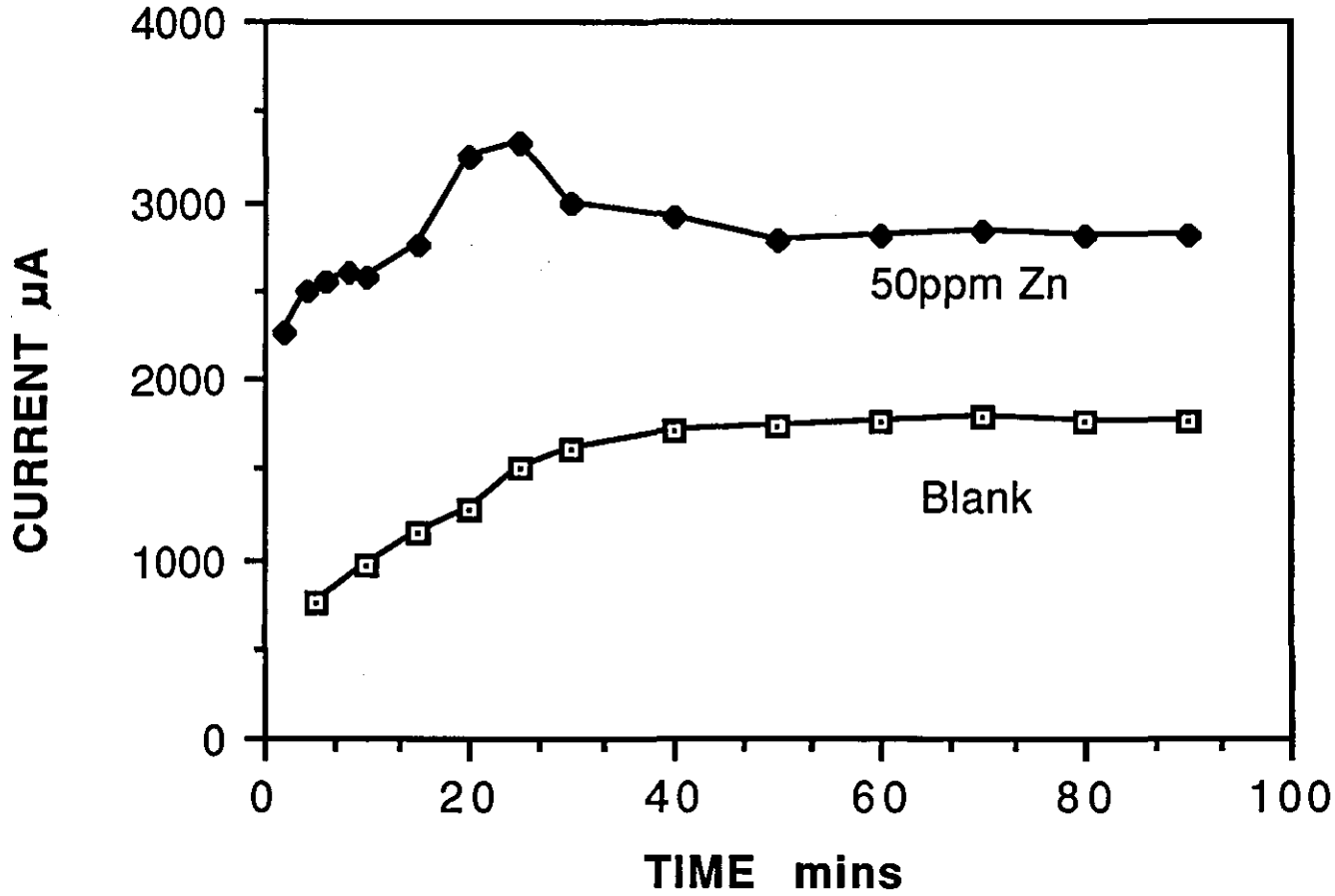

FIG. 8.5 - EFFECT OF 50ppm ZINC IN AERATED COMPARTMENT

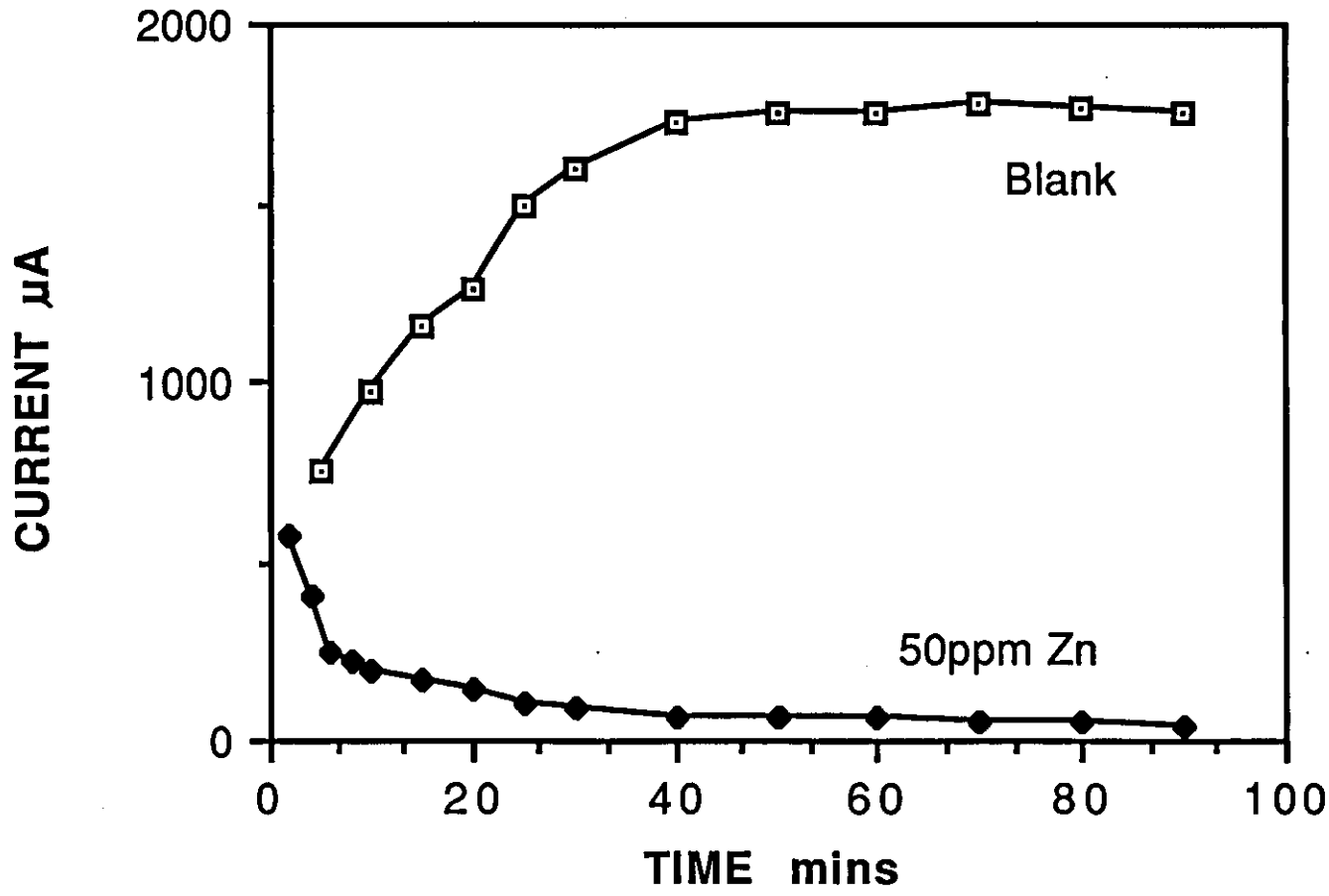

FIG. 8.6 - EFFECT OF 50ppm ZINC IN BOTH COMPARTMENTS

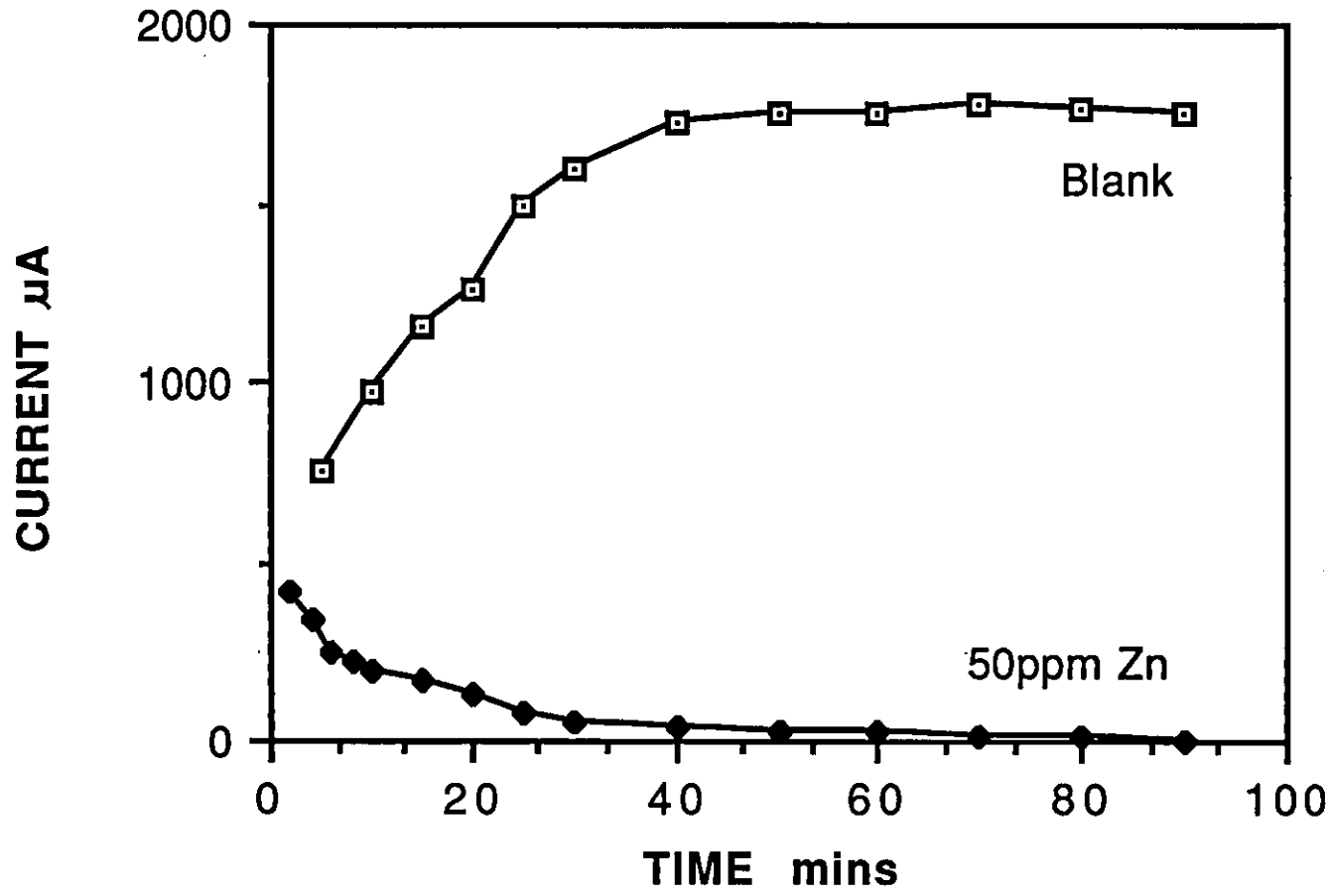

### 8.3.3 CHROMATES

To prove the effectiveness of the technique in anodic inhibitor evaluation, sodium chromate was used. Sodium chromate has long been classified as an anodic inhibitor. Two doses of 50ppm and 100ppm concentration were added to the electrolyte. Figure 8.7 shows the effect of adding 50ppm of chromate to each reservoir in turn, and then to both, the results are summarised in Table 8.2.

a) Addition to Non-aerated Electrode
When 50ppm chromate was added to the anode compartment a rapid increase in current to approx. 1700μA was observed over the first 20 minutes. The current then slowly decayed to a plateau value of 950μA.

b) Addition to Aerated Electrode
The addition of 50ppm chromate to the cathode compartment gave rise to a reduced current value of 550μA. No peak value was attained, and a plateau current formed almost immediately upon initiation of the experiment.

c) Addition to Both Electrodes Simultaneously
When 50ppm chromate was added to both compartments a small maxima of approx. 400μA was observed after 20 minutes. After 90 minutes the current had reached a value of 310μA but was still falling slowly.

If chromate is considered to be 100% anodic in its inhibitive action, one would expect a slight increase in current upon addition to the aerated electrode. However, a large decrease, even greater than that for the anode, was observed. This suggests that within the experimental conditions, chromate acts as a mixed inhibitor, being more cathodic than anodic in its action. The cathodic action of chromate may arise from the formation of a layer of chromium oxide/hydroxide at the cathodic sites. The anodic action is induced by the formation of iron chromate at the anodic sites. This could explain the maxima observed, as chromate may attack the anodic

FIG. 8.7 - EFFECT OF 50ppm CHROMATE

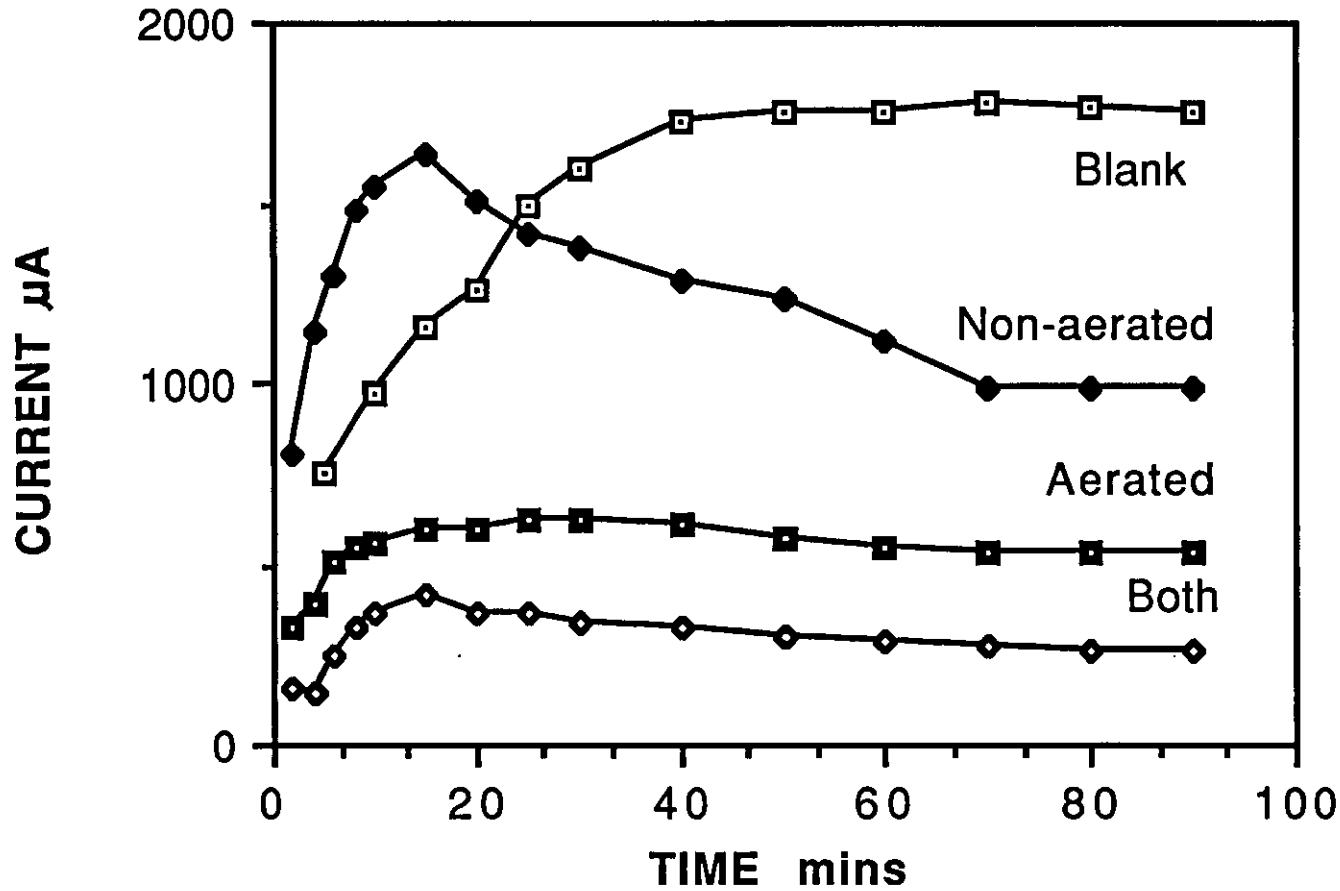

TABLE 8.2 - EFFECT OF CHROMATE ADDITION

| AERATED ELECTRODE | NON-AERATED ELECTRODE | CURRENT (μA) after 90mins |
|---|---|---|
| 0.1M $NaClO_4$ | 0.1M $NaClO_4$ | 1800 |
| 50ppm $CrO_4$ + 0.1M $NaClO_4$ | 0.1M $NaClO_4$ | 550 |
| 0.1M $NaClO_4$ | 50ppm $CrO_4$ + 0.1M $NaClO_4$ | 950 |
| 50ppm $CrO_4$ + 0.1M $NaClO_4$ | 50ppm $CrO_4$ 0.1M $NaClO_4$ | 310 |

sites prior to the formation of iron chromate. This does not explain its poor performance as a anodic inhibitor. It is known that chromate is a strong enough oxidising agent to cause inhibition without the need for oxygen. However, Cartledge[89] found that when oxygen was absent, chromate was slower in its action. This may go someway to explaining its reduced effectiveness.

Figures 8.8 and 8.9 show the effect of increasing the concentration of chromate from 50ppm to 100ppm in the non-aerated and aerated compartments respectively. The increase in dose level had very little effect on inhibition, with currents being approximately equal to those for 50ppm.

### 8.3.4 HYDROXY-PHOSPHONO CARBOXYLIC ACID ( H.P.A.)

H.P.A. is a common component in commercial inhibitor formulations where zinc is unwanted (due to its toxicity). The exact mode of action is unknown, but it is believed to have predominantly cathodic properties. However, it is known that to function efficiently, the presence of calcium ions are required. Figure 8.10 shows the effect of adding 50ppm calcium to the 0.1M $NaClO_4$ in the aerated electrode compartment. A current drop to 1500$\mu$A was observed, showing calcium to have poor cathodic properties under these conditions. Figure 8.11 shows the effect of adding 50ppm H.P.A. alone to the aerated electrode. Initially, the H.P.A. seemed to have good cathodic properties when used alone, as a current drop to 450$\mu$A was observed within the first 10 minutes. A steady increase was then observed, reaching a value of 1000$\mu$A after 90 minutes. Figure 8.12 shows the effect of using 50ppm calcium and 50ppm H.P.A. together. The current dropped to zero over the duration of the experiment.

When H.P.A. is used alone, a weak phosphonate film forms upon the iron surface but is broken down with time. With calcium present a much stronger film is produced. It is probable that calcium plugs any gaps within the phosphonate film giving rise to full surface coverage.

FIG. 8.8 - EFFECT OF CONC. OF CHROMATE ON NON-AERATED ELECTRODE

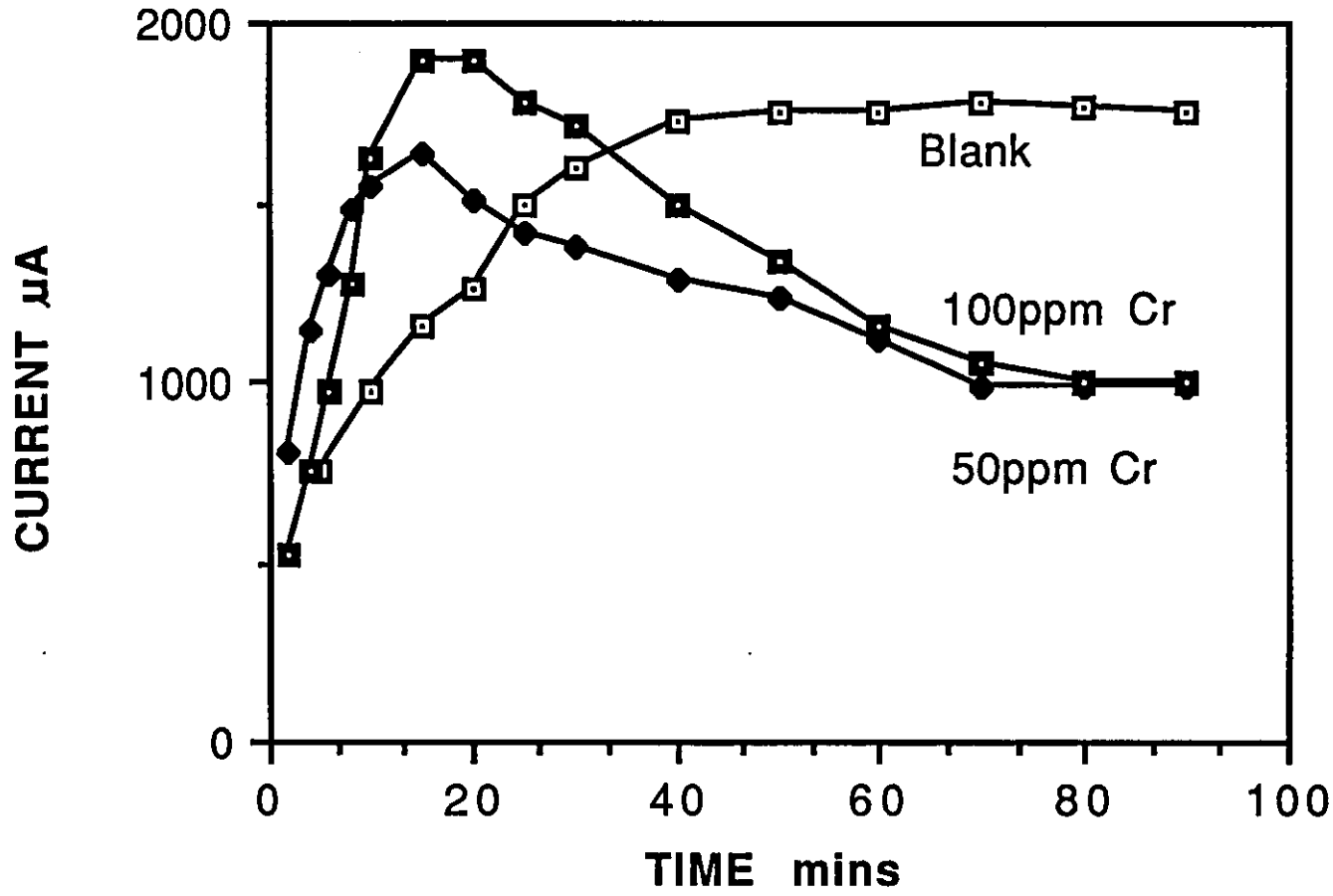

FIG. 8.9 - EFFECT OF CONC. OF CHROMATE ON AERATED ELECTRODE.

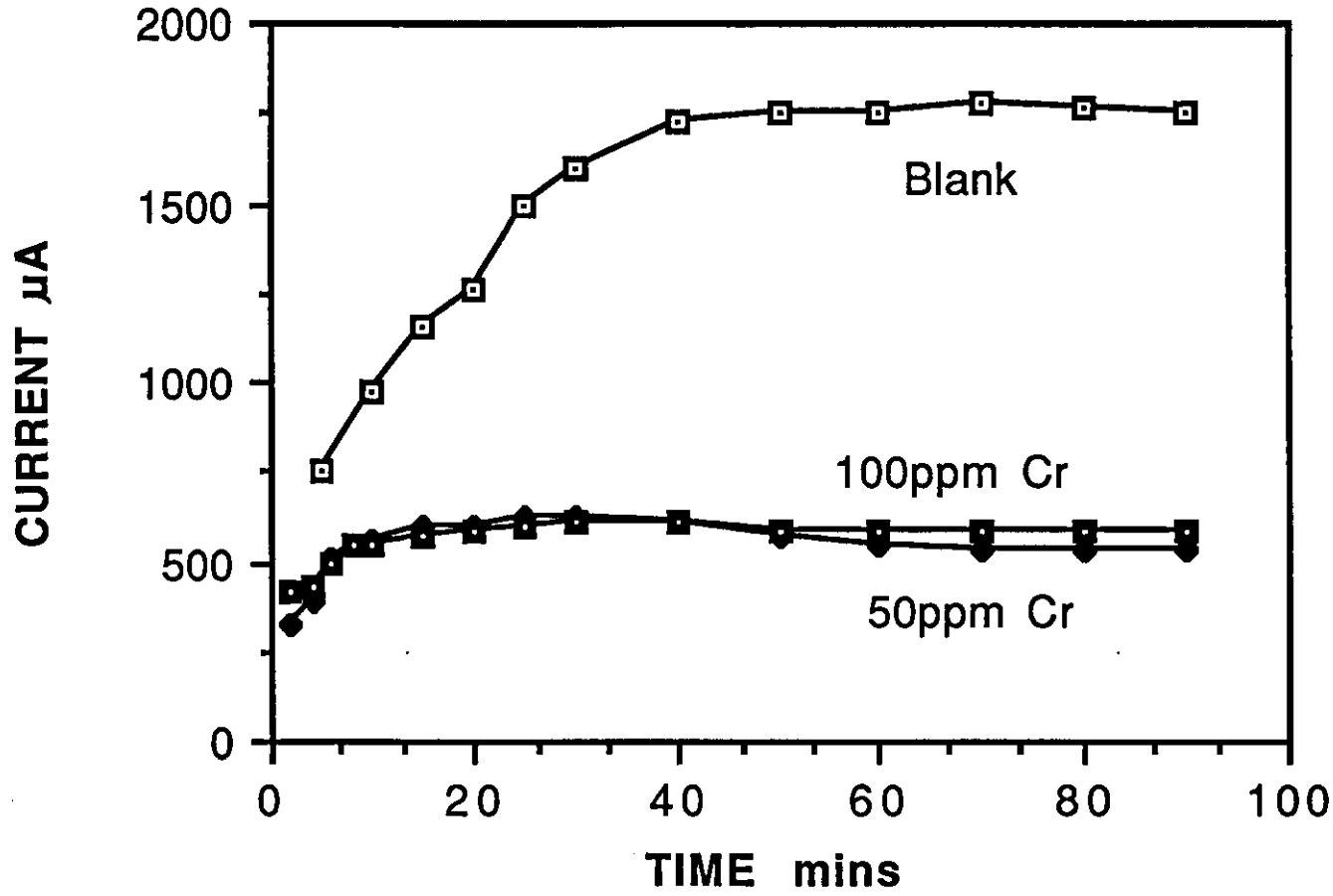

FIG. 8.10 - EFFECT OF 50ppm CALCIUM IN AERATED COMPARTMENT

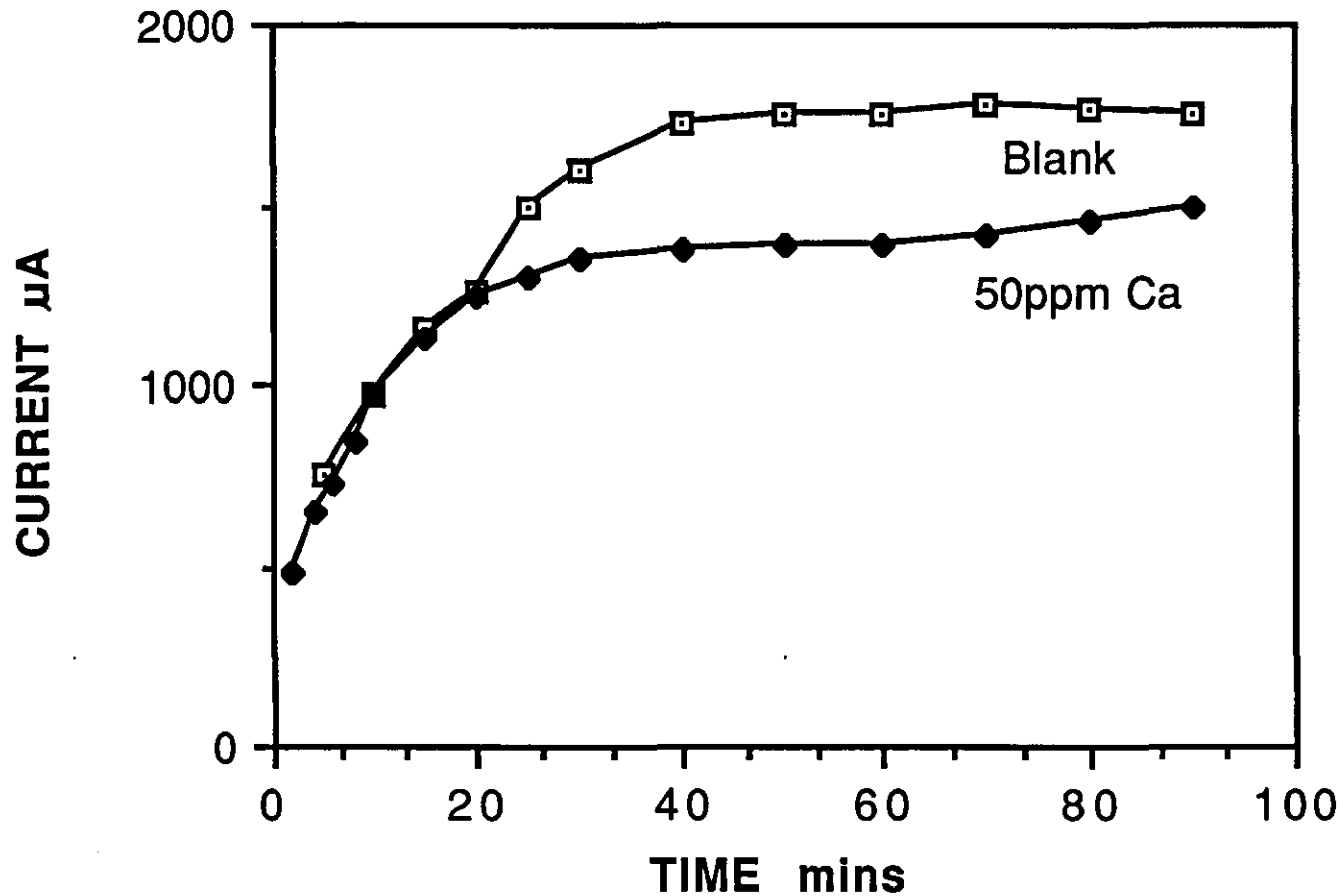

FIG. 8.11 - EFFECT OF 50ppm H.P.A. IN AERATED COMPARTMENT

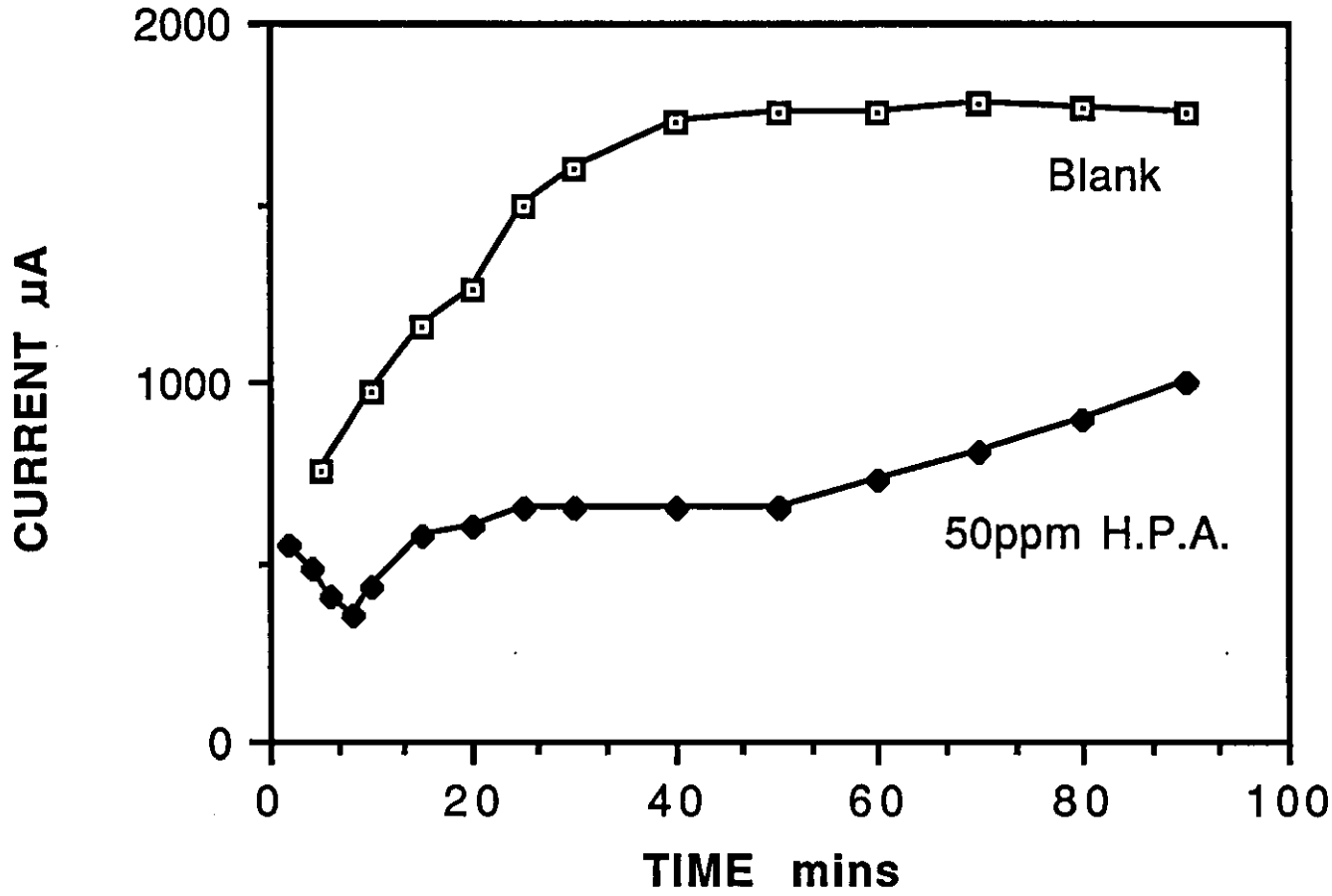

FIG. 8.12 - EFFECT OF 50ppm H.P.A. + CALCIUM IN AERATED COMPARTMENT

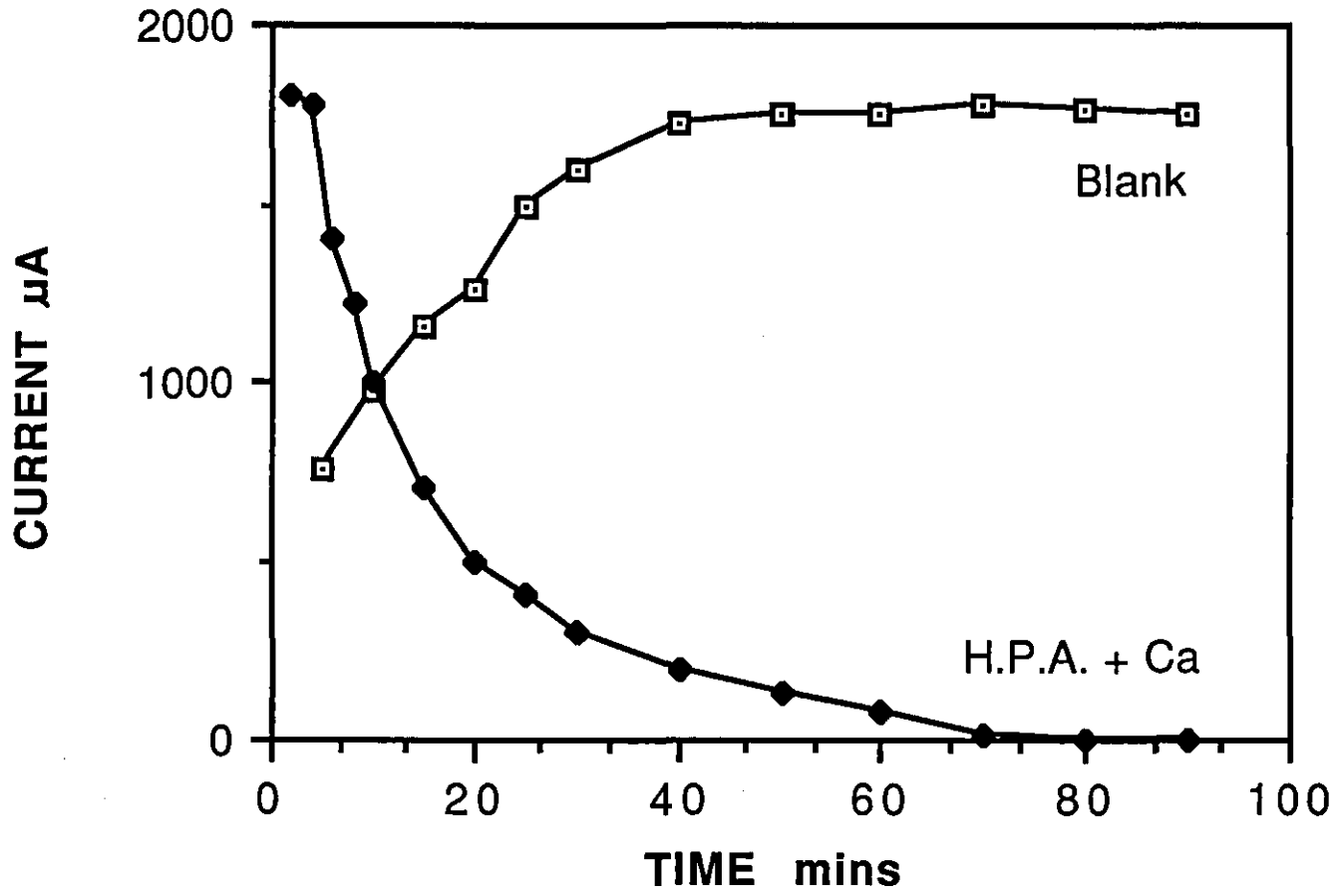

H.P.A. was then added to the non-aerated electrode, in order to investigate any anodic properties. Table 8.3 summarises the results.

a) Non-aerated Electrode (50ppm Ca each side) - A slight maxima was observed after 10 minutes followed by a steady decrease in current to 930μA - Figure 8.13. This suggest that H.P.A. works weakly upon the non-aerated electrode, showing only slight anodic properties.

b) Aerated Electrode (50ppm Ca each side) - A steady exponential decrease to zero was observed as in Figure 8.12.

The data for H.P.A. shows behaviour similar to that of chromate i.e. mixed inhibitive properties. The inhibitive behaviour is predominantly cathodic, however an improved anodic performance may be observed in the presence of oxygen.

## 8.4 CONCLUSIONS

The results from the differential aeration cell suggest that the cell design is both simple and effective. Reproducible results are obtained within the limits of the experiment, with the current reading giving a clear indication of inhibitor efficiency. Furthermore, the data obtained indicates the mode of action of the inhibitor. This is emphasised in the results obtained for chromate, which in the past has been believed to be solely anodic in its action (affecting a positive shift in potential). The data obtained suggests mixed inhibitive action, being biased towards cathodic. This was somewhat surprising, and further work is required to investigate the effect more fully.

One drawback of this technique is that the only anodic inhibitors that can be investigated are those that do not require the presence of oxygen to function i.e. having strong oxidising properties. Cathodic inhibitors suffer from no such problems and can be investigated in full.

TABLE 8.3 - EFFECT OF H.P.A. ADDITION

| AERATED ELECTRODE | NON-AERATED ELECTRODE | CURRENT (μA) after 90mins |
|---|---|---|
| 0.1M $NaClO_4$ | 0.1M $NaClO_4$ | 1800 |
| 50ppm Ca + 0.1M $NaClO_4$ | 0.1M $NaClO_4$ | 1500 |
| 50ppm H.P.A. + 0.1M $NaClO_4$ | 0.1M $NaClO_4$ | 1000 |
| 50ppm H.P.A. + 50ppm Ca + 0.1M $NaClO_4$ | 0.1M $NaClO_4$ | 0 |
| 50ppm Ca + 0.1M $NaClO_4$ | 50ppm H.P.A. + 50ppm Ca + 0.1M $NaClO_4$ | 930 |
| 50ppm H.P.A. + 50ppm Ca + 0.1M $NaClO_4$ | 50ppm Ca + 0.1M $NaClO_4$ | 0 |

FIG. 8.13 - EFFECT OF 50ppm H.P.A. + Ca IN NON-AERATED COMPARTMENT

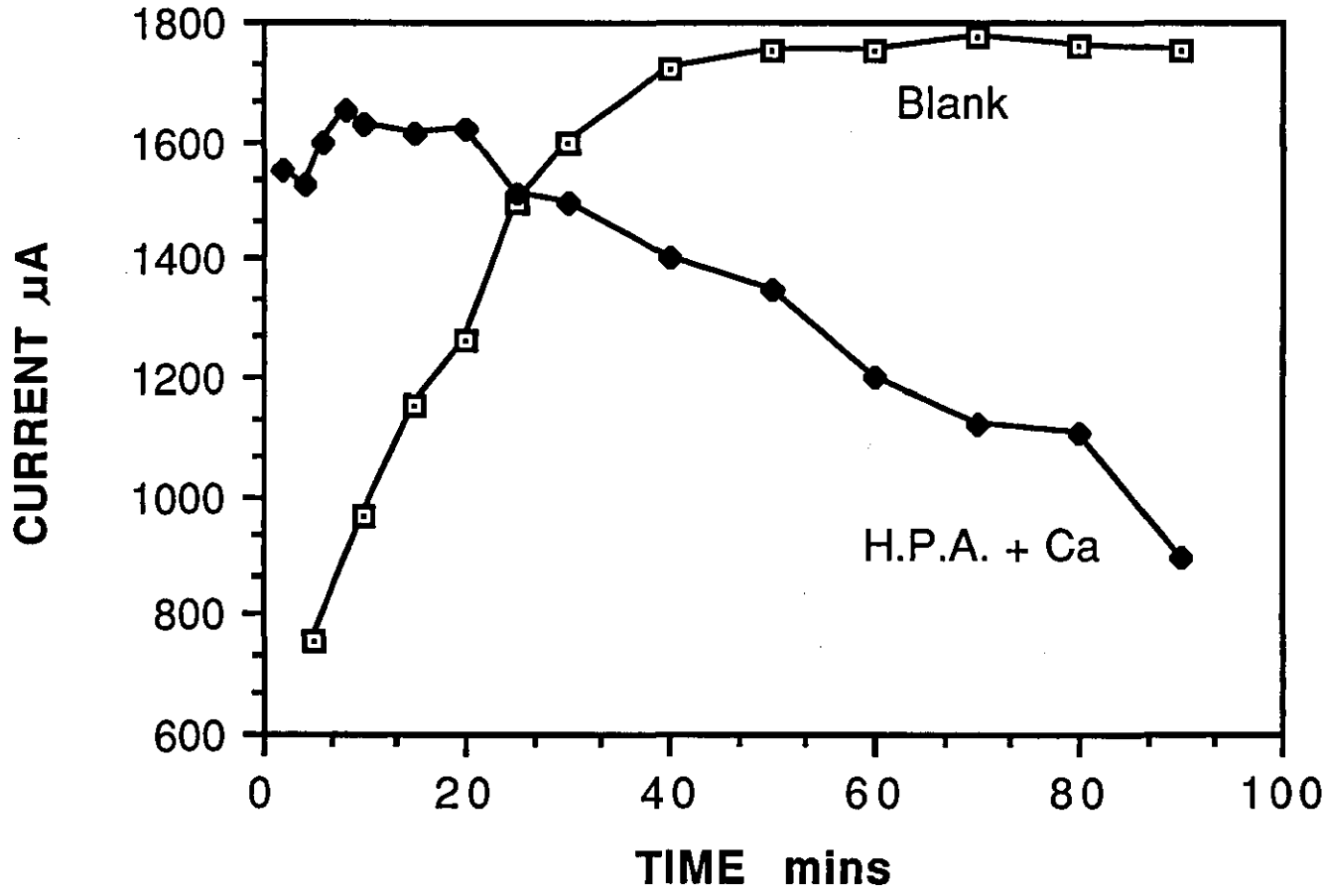

# CHAPTER 9

# FLOW-THROUGH CELLS

## 9.1 INTRODUCTION

A flow-through cell was developed with the objective of obtaining a quick and relatively simple technique for evaluating inhibitor efficacy at a surface which is not significantly shifted from its normal, dynamic equilibrium, corrosion condition. In this way, the problems arising from accentuating the cathodic reaction by polarising negative of the open circuit voltage (see rotating disc electrode experiments) should be overcome.

This target has been realised and the technique is applicable to the study of clean or pre-corroded surfaces, in inhibited neutral water systems, with both temperature and flow rate as secondary variables.

## 9.2 EXPERIMENTAL

A flow-through cell of the type shown in Figure 9.1 was used to obtain the data shown. The cell consists of three sections cut from a cylinder of perspex. Sections 1 and 2 are in the form of an annulus, whereas section 3 is a disc bored to take a platinum rod counter electrode and the glass extension arm of a saturated sodium calomel reference electrode (both set flush to the perspex surface to eliminate any turbulence in flow). When assembled, a water tight seal is effected by the use of "O" rings. This also served as a means of supporting the electrode under test. In this case an iron disc (99.99% purity - Goodfellows Metal) of active area 15.2 $cm^2$. (It has been found essential, that an electrode with a sufficiently small perimeter to area ratio is used, in order that the edge effects are kept to a minimum).

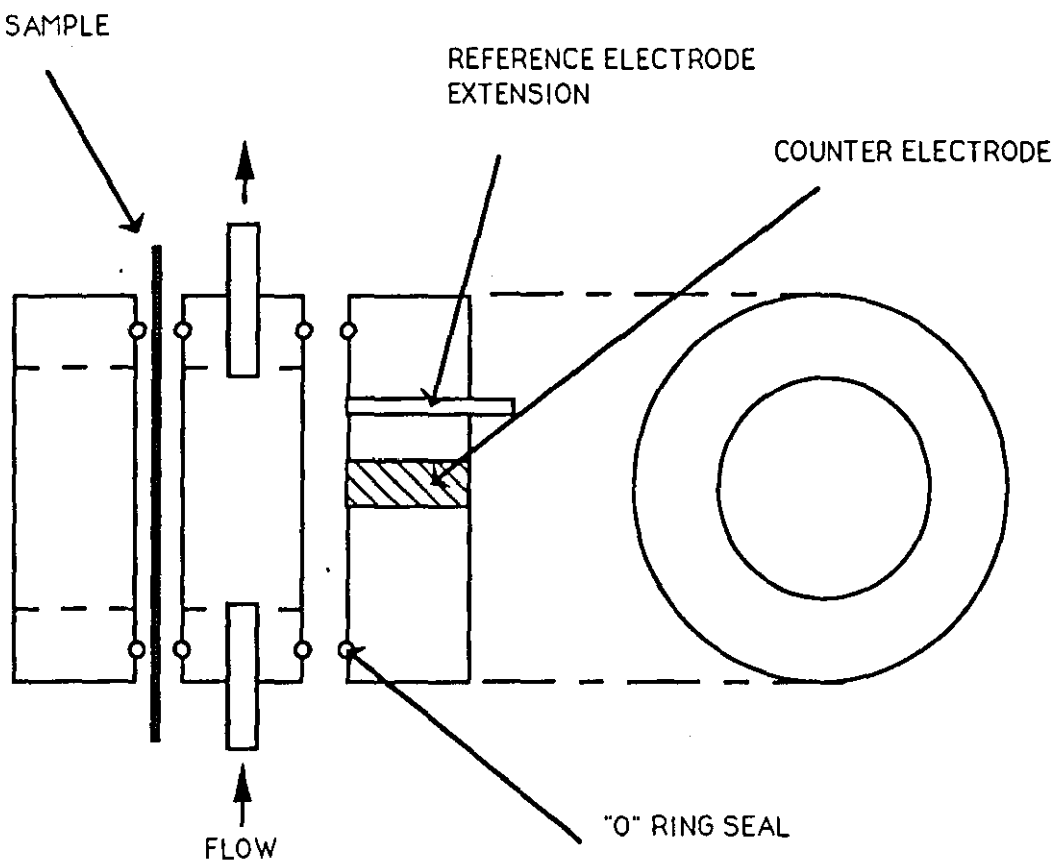


FIG. 9.1 FLOW THROUGH CELL ASSEMBLY

A peristaltic pump was used to maintain a continuous flow of electrolyte from a 500ml reservoir through the cell, across the surface of the iron disc and back to the reservoir. The inhibitor under test was either included in the electrolyte initially or added to the reservoir after the necessary pre-corroded state had been attained. Neutral, 0.1M $NaClO_4$ was employed as a supporting electrolyte, thus ensuring that the conductivity was sufficiently high for potentiostatic control to be effective. The normal experimental sequence was as follows:

The electrolyte was pre-saturated with oxygen for a period of 15 minutes. After this time the pump was switched on and the solution made to enter and continuously circulate through the cell whilst oxygen saturation was maintained. The electrode was then allowed to corrode for a period of 20 hours, during which time its steady state interfacial behaviour became established. The open circuit potential was then recorded (a constant value was attained after about 15 hours) and the system was then locked to this potential by means of a potentiostat. Nitrogen gas was then used to purge the reservoir and cell assembly of oxygen for a 2 hour period. The current which then necessarily flows through the potentiostatic circuit in order to maintain this potential (in the absence of oxygen) was finally recorded.

The experiment was carried out both in the presence and absence of inhibitor. A number of generic and commercial inhibitor formulations were tested with this simple cell arrangement. These are compared to the corrosive effect of supporting electrolyte alone and to a base line synthetic water of 50ppm hardness: 50ppm alkalinity. The temperature was maintained at $30^{o}C$ and a flow rate of $0.8cm^3/s$ was adopted. All pre-corrosion conditions were established in a 50/50 water. The iron was allowed to pre-corrode for 20 hours before the inhibitor was added. The experimental procedure was then as described above.

## 9.3 RESULTS AND DISCUSSION

### 9.3.1 CLEAN SURFACES

Table 9.1 shows the open circuit potentials and efficiency (in terms of relative current) for a number of cathodic inhibitor systems. When no inhibitor is present a current of 2120μA is required to maintain the open circuit potential (O.C.P.) of -614mV vs. SSCE. attained in oxygen saturated solution. This large current represents a very aggressive corrosion environment. This was confirmed visually by the large amount of $Fe_2O_3$ produced in the cell arrangement and reservoir.

The synthetic 50/50 water system, as expected, shows some inhibitive behaviour. The current being reduced by almost half of the previous value. The rise in open circuit voltage to -676mV is usually taken to be indicative of cathodic inhibitive properties. Since most of the cathodic inhibitors tested require the presence of calcium and/or some alkalinity to function, this solution was used as a base line for comparative purposes.

Zinc and Zinc Containing Inhibitors

Zinc, being a well known cathodic inhibitor was added in 50ppm concentration as zinc perchlorate. The amount of visible corrosion was almost negligible over the duration of the experiment, which was reflected by the very low current observed i.e. 20μA. Zinc, at concentrations greater than 50ppm showed no further decrease in corrosion current. This suggested that maximum inhibitive efficiency had been attained under the prevailing conditions. A slight positive shift in open circuit potential to -674mV vs S.S.C.E. was recorded when compared to that of 50/50 water alone. It can be concluded therefore, that any shift in potential, on addition of an inhibitor, should not be used as an indicator of its efficiency. Two commercial inhibitor formulations, both containing zinc were then tested. Polymate 945 and Polymate 966, supplied by Dearborn Chemicals

TABLE 9.1 - CLEAN ELECTRODES

| INHIBITOR | OCV (mV) | CURRENT(μA) |
|---|---|---|
| NONE | -614 | 2120 |
| 50/50 | -676 | 1105 |
| 50/50 + 50ppm Zn | -674 | 20 |
| 50/50 + 200ppm 945 | -710 | 30 |
| 50/50 + 200ppm 966 | -678 | 205 |
| 50/50 + 50ppm HPA | -725 | 85 |
| 50/50 + 25ppm HPA | -714 | 160 |
| 50/50 + 10ppm HPA | -665 | 1520 |
| 50/50 + 5ppm HPA | -678 | 1810 |
| 50/50 + 2ppm Pk205 + 5ppm HPA | -677 | 1605 |
| 50/50 + 2ppm Pk205 + 10ppm HPA | -691 | 360 |
| 2ppm Pk205 + 10ppm HPA | -672 | 1190 |

were both added in 200ppm concentration. (100ppm Polymate 945 contains 2.2ppm $Zn^{2+}$, 3ppm orthophosphate and 8.8ppm phosphonate. 100ppm Polymate 966 contains 2.2ppm $Zn^{2+}$ and 8.8ppm phosphonate). Both proved effective in reducing the corrosion rate. Polymate 945 was, however, the more efficient of the two, a current of 30μA being recorded, compared to 205μA for Polymate 966. For both, the open circuit potential was shifted in a negative direction, the largest shift occurring when Polymate 945 was employed. The only major difference between the two Polymates is that 945 contains phosphate and phosphonate whilst 966 contains only phosphonate. It can be suggested therefore that the increased efficiency of Polymate 945 when compared to Polymate 966 is due to incorporation of phosphate into the protective surface film.

Behaviour of Hydroxyphosphono-carboxylic Acid (H.P.A)

H.P.A. is of particular interest because it has been shown to exhibit good inhibitive properties in the absence of metal solution species e.g. zinc or chromate. Consequently, formulations can be devised which are of low toxicity if discharged to the environment. Figure 9.2 shows a plot of current versus concentration for Hydroxyphosphono-carboxylic acid (H.P.A.).

It can be seen that the critical effective concentration for the use of H.P.A. lies between 10ppm and 25ppm H.P.A. Both 5ppm and 10ppm H.P.A. give unacceptable corrosion protection, the rate being intermediate of that of 50/50 water and 0.1M $NaClO_4$ alone. This promotion of corrosion is probably due to the interaction between H.P.A. and the hardness/alkalinity component of the synthetic water, causing a modification and partial breakdown of the protective layer. H.P.A. is, infact, often used in inhibitor formulations where anti-scaling properties are required. Thus in low concentration i.e. less than 10ppm, H.P.A. reduces the inhibitive capacity of a 50/50 scaling water. Above 25ppm a large shift in open circuit potential is observed, and a corresponding reduction in corrosion occurs. When 50ppm H.P.A. was employed the current dropped to 85μA.

FIG. 9.2 - CURRENT vs. CONC. OF H.P.A. ADDED TO 50/50 WATER

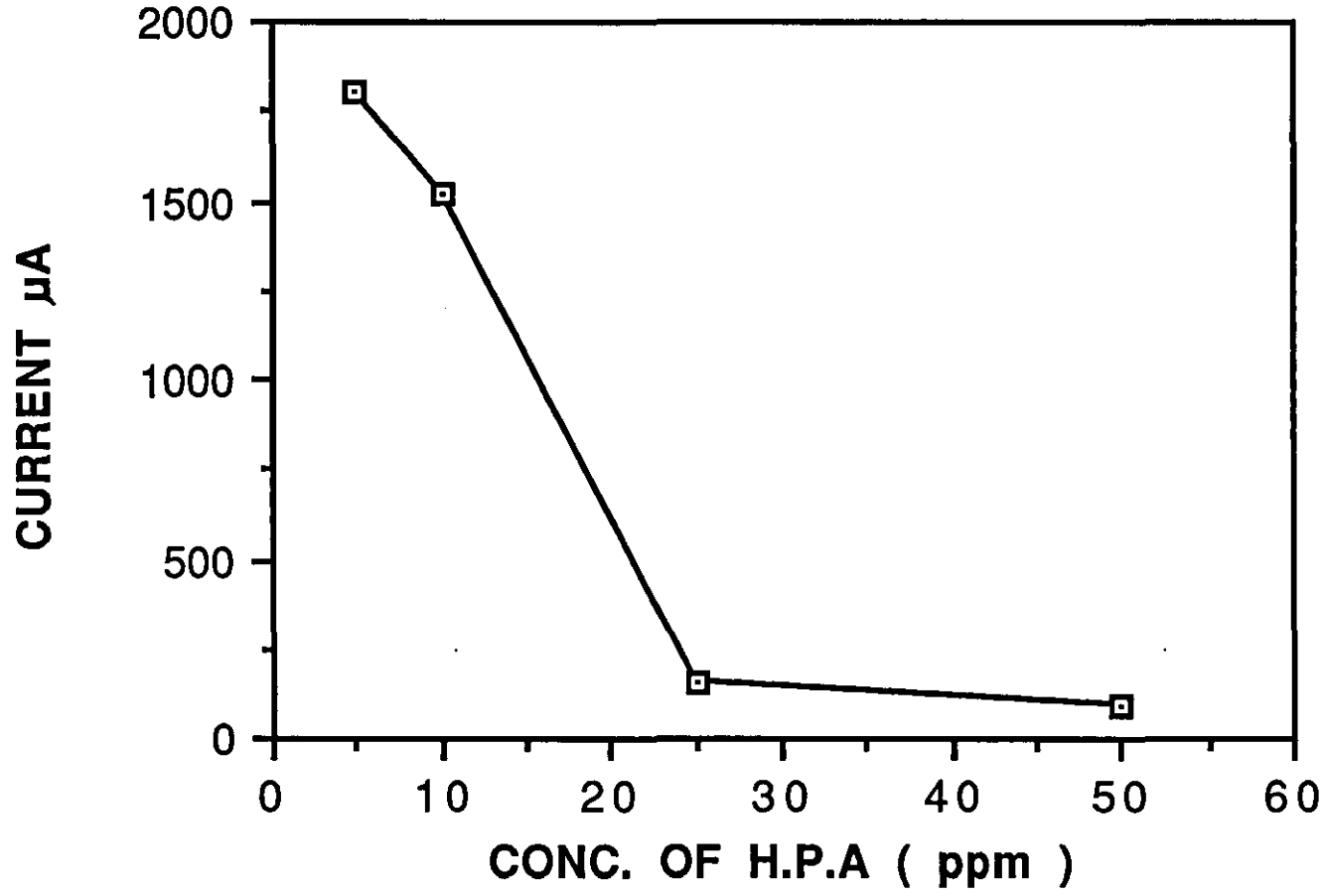

Comparison with the effect of 50ppm zinc (i.e. 20μA) shows favourable behaviour.

In order to reduce cost and comply with ever tightening environmental laws, cationic polymers have been developed to act synergistically along with H.P.A., reducing the concentration of H.P.A. required for inhibition. Figure 9.3 shows the effect of adding 2ppm of Cationic Polymer Pk 205 (as supplied by Dearborn Chemicals) to H.P.A. at 10ppm concentration.

When 10ppm H.P.A. is used with no Pk 205 present a current of 1520μA is observed. The addition of 2ppm Pk 205 to the system reduces the corrosion current to 360μA. It is apparent therefore that Pk 205 acts in conjunction with the H.P.A. to produce an effective barrier to corrosion. Grace Dearborn Chemicals have found that a ratio of 1 part cationic polymer to 5 parts H.P.A. is particularly effective . When 2ppm Pk 205 and 10ppm H.P.A. were used in the absence of any hardness/alkalinity, performance was considerably decreased giving a corrosion current of 1190μA. There is however, still some inhibitive action. This reinforces the concept that there is a necessary interaction between the inhibitive and scale forming constituents of water. It is possible that the cationic polymer is acting as an "anti-dispersant" (cf. anionic and non-ionic polymers) inducing the precipitation of colloidal scale-H.P.A. moieties. This may take place through surface adsorption and charge neutralisation (as indicated by the effective low dose level).

### 9.3.2 PRE-CORRODED SURFACES

Table 9.2 shows the corrosion currents observed when a number of inhibitors were added to a pre-corroded electrode. When compared to those values recorded with clean electrodes, all the corrosion currents are higher, yet still sufficiently low to show that inhibition is still occurring. It is possible that the time allowed for the inhibitor to regain control was too short or that a " passivating" high dose would prove to be more effective under these conditions.

FIG. 9.3 - EFFECT OF ADDING Pk205 TO 10ppm H.P.A.

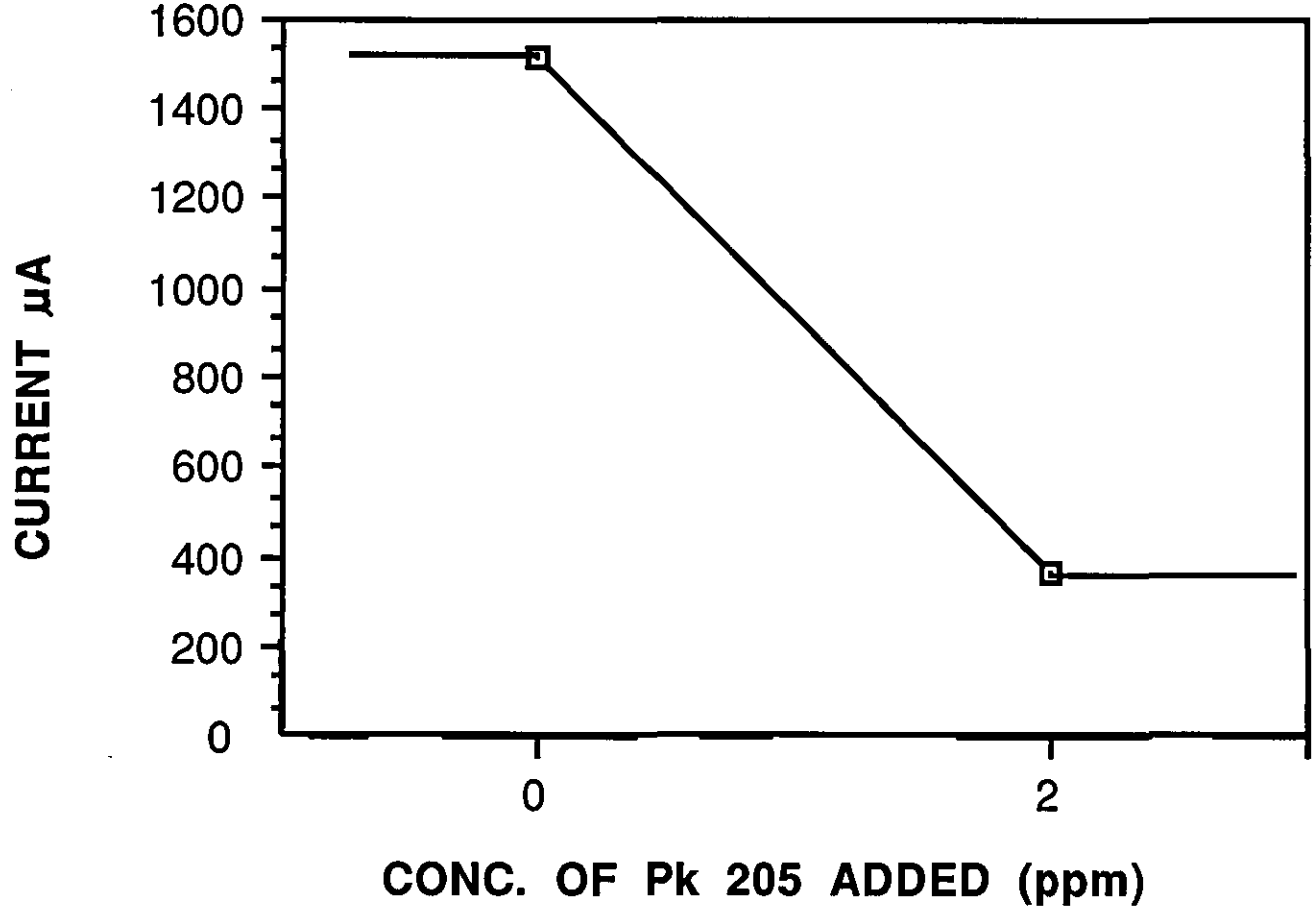

TABLE 9.2 - PRE-CORRODED ELECTRODES

| INHIBITOR | OCV(mV) | CURRENT (mA) |
|---|---|---|
| 50/50 + 50ppm Zn | -700 | 45 |
| 50/50 + 200ppm 945 | -711 | 110 |
| 50/50 + 200ppm 966 | -696 | 250 |
| 50/50 + 50ppm HPA | -694 | 190 |

## 9.4 CONCLUSIONS

It can be concluded that the flow-through cell is a quick, simple and effective method for inhibitor evaluation on both clean and pre-corroded surfaces. The results observed compare favourably with those obtained from rig tests. Furthermore, this cell set up allows studies to be conducted with varying temperature and different flow rates, with and without turbulence promotion.

Further work could include the above, and with slight modification to the experimental apparatus studies on pipe sections could be feasible. There are a large number of un-investigated parameters to the pre-corroded system which will require a considerable amount of further work.

# CHAPTER 10

## CONCLUDING REMARKS AND FURTHER WORK.

Cathodic inhibitor evaluation, was initially based upon the effect of the inhibitor on the oxygen reduction mechanism. Due to the inherent difficulties in studying oxygen reduction on a "clean" iron surface i.e. pH changes, surface defects and oxide film formation, this method was found to be impractical, giving little reproducible kinetic data. However, an insight into the difficulties incurred in a neutral pH system was gained.

Adaption of the oxygen reduction experiments lead to the "concentration step" method for cathodic inhibitor evaluation. This technique presents a simple and relatively quick evaluation method, but is limited, in that it only gives comparative results and no kinetic data. It did, however, produce some interesting results, especially when the inhibitive properties of magnesium were studied. The improved efficiency of magnesium in hard/high alkalinity waters, when compared to zinc, is worthy of further study.

The differential aeration cell proved a simple and effective evaluative technique for both anodic and cathodic inhibitors. The results proved reproducible and compare favourably with those of the "current drop" technique. The method also allows an insight into the mode of inhibitor action. The dual nature of chromate was of particular interest. Further studies on the modes of action of other well known anodic inhibitors would be of particular value, but were not possible within the time limits of the work presented here.

The flow-through cell would appear to be the best technique developed in this study for cathodic inhibitor evaluation. Its use on both "clean" and pre-corroded surfaces is of obvious value. Again, the data proved reproducible and compared favourably with the other techniques. Furthermore, some mechanistic detail was obtainable, e.g. when Pk 205 was employed. Future work on the

flow-through cell, could, involve the use of pipe sections in an high temperature environment with only a little modification to the cell design. This would allow the study of flow-rate and temperature parameters, relating to a true industrial system.

## REFERENCES


1) A. Orman Fisher, *Corrosion* , 19, 91t, (1963).

2) M. Darrin, *Ind. Eng. Chem.* 13, 755, (1941).

3) R.A. McAllister, D.H. Eastham, N.A. Dougharty and M. Hollier, *Corrosion,* 17, No.2, 579t - 588t, (1961).

4) B.W. Lifka and F.L. McGeary, in NACE Basic Corrosion Course, National Association of Corrosion Engineers, Houston, Ch.15, 1, (1973).

5) E. Schaschl, in C.C. Nathan (ed.), Corrosion Inhibitors, National Association of Corrosion Engineers, Houston, 28, (1973).

6) D.R. Robitaille, *Mater. Perform.*, 15, 263, (1976).

7) M.S. Vukasovich and D.R. Robitaille, *J. Less. Com. Met.*, 54, 437, (1977).

8) W.J. Lorenz and F. Mansfeld, *Corrosion Science*, 21, 9, 647-672, (1981).

9) H. Fischer, *Proc.3rd Euro. Synp. Corr. Inh.*, Ferrara, 15, (1970).

10) M.J. Pryor and M.Cohen, *J. Electrochem. Soc.*, 100, 203, (1953).

11) M. Stern, *J. Electrochem. Soc.*, 105, 638, (1958).

12) D.M. Brasher, *Nature*, London, 193, 868, (1962).

13) T.P. Hoar and U.R.Evans, *J. Chem. Soc.*, 2476, (1932).

14) I.L. Rozenfeld, Corrosion Inhibitors, McGraw-Hill Inc., Chapter 5, 151-153, (1981).

15) G.O. Okamoto, N. Nagayomo and Y. Mitami, *J. Electrochem. Soc.* (Japan), 24, (1956).

16) M. Darrin, *Ind. Eng. Chem.*, 38, 368, (1946).

17) M. Cohen, *J. Phys. Chem.*, 56, 451, (1952).

18) J.P. Hancock and J.E. Mayne, *J. Appl. Chem*, 9, 345, (1959).

19) G.B. Hatch and O. Rice, *Ind-Eng. Chem*, 32, 1572, (1940).

20) G. Butler, *Proc. 3rd Euro. Symp. Corr. Inhib.*, Ferrara, 753, (1970).

21) H.H. Uhlig, D.N. Triadis and M. Stern, *J. Electrochem. Soc.*, 102, 59, (1955).

22) G.B. Hatch, *Ind. Eng. Chem.*, 44, 445, (1952).

23) J.C. Lamb and R. Eliassen, *J. Am.Water Wks. Ass.*, 46, 445, (1954).

24) H. Gatos, *Comptes Rendus 1er Symp. Eur. Inhib. Corr.*, 1960, Univ.Ferrara, 257, (1961).

25) D.M. Brasher and A.D. Mercer, *Br. Corrosion J.*, 3, 121, (1978).

26) W.D. Robertson. *J. Electrochem. Soc.*, 98, 94, (1951).

27) D.R. Robitaille and J.G. Bilek. *Chemical Engineering* , 83, 77, (1976).

28) L.Lehrman and H.L.Shuldener, *Ind. Eng. Chem.*, 44, 451, (1952).

29) I.L. Rozenfeld, Corrosion Inhibitors, McGraw-Hill Inc, (1981).

30) E.F. Duffer and D.S. McKinney, *J. Electrochem. Soc.*, 103, 645, (1956).

31) O. Lahodry-Sarc. and L. Kastelan, Proc.4th, *Euro. Symp. Corr. Inhib.*, Ferrara, 223, (1975).

32) O. Lahodry-Sarc. and L. Kastelan, *Corrosion Science*, 21, 265, (1981).

33) H. Helmholtz, *Wied. Ann.*, 7, 377, (1879).

34) A. Gouy, *J. Phys.*, 9, 457, (1910).

35) D.L. Chapman, *Phil. Mag.*, 25, 475, (1913).

36) O. Stern, *Zeit. Elektrochem.*, 30, 508, (1924).

37) D.C. Grahame, *Chem. Rev.*, 41, 1441, (1947).

38) M.A.V. Devanathan, J. O'M Bockris and K. Muller, Proc. Roy. Soc., 55, A 274, (1963).

39) W. Nernst, *Z. Physik. Chem.*, 4, 129, (1889).

40) T. Erdey-Gruz and M. Volmer, *Z. Physik. Chem.*, 105A, 203, (1930).

41) J. Tafel, *Z. Physik. Chem.*, 50, 641, (1905).

42) A. Fick, *Pogg. Ann.*, 94, 59, (1855).

43) W. Nernst, *Z. Physik. Chem.*, 105A, 203, (1930).

44) H.R. Valentine, *Applied Hydrodynamics*, London: Butterworths Scientific Publications, (1959).

45) V.G. Levich, *Physicochemical Hydrodynamics*, New Jersey: Prentice-Hall, (1962).

46) V.G. Levich, *Acta Physicochim. URSS.*, 17, 257, (1942).

47) V. Yu Filinovsky and Yu V. Pleskov, *Prog. Surf. Membr. Science*, 10(2) , 27, (1976).

48) R.N. Adams, Electrochemistry at Solid Electrodes, Dekker, N.Y. (1969).

49) R.S. Nicholson and I. Shain, *Anal. Chem.*, 36, 706, (1964).

50) A.J. Ba rd and L.R. Faulkner, Electrochemical Methods, Wiley (1980).

51) H. Vaidyanathan, N. Hackerman, *Electrochim. Acta*, 16, 2193, (1971).

52) A. Damjanovic and P.G. Hudson, *J.Electrochem Soc.*, 135, (9), 2269-2273, (1988).

53) E.S. Brandt., *J. Electroanal. and Interfacial. Electrochem.*, 150 (1-2), 97-100, (1983).

54) R.R. Adzic, N.H. Markovic and V.B. Vesovic, *J. Electroanal. and Interfacial. Electrochem.*, 165 (1-2), 105-120, (1984).

55) R.R. Adzic, N.H. Markovic and V.B. Vesovic, *J. Electroanal. and Interfacial. Electrochem.*, 165 (1-2), 121-133, (1984).

56) J.M. Martinovic, D.B. Sepa, M.V. Vijnovic and A. Damjanovic, *Electrochim. Acta*, 33, (10), 1267-1272, (1988).

57) R.R. Adzic, N.A. Anastasijevic and Z.M. Dimitrijevic, *Electrochim. Acta*, 31, (9), 1125-1130, (1986).

58) J. O'M. Bockris, D. Drazic, and A.R. Despic, *Electrochim.Acta*, 4, 325, (1961).

59) K.E. Heusler, in "Encyclopedia of Electrochemistry of the Elements," Vol. IX, A.J. Bard, Editor, p.299, Marcel Dekker, New York (1977).

60) J. O'M. Bockris, B.T. Rubin, A. Despic, and B. Lovrecek, *Electrochim. Acta*, 17, 923, (1972).

61) I. Epelboin, C. Gabrielli, M. Keddam, and H. Takenouti, in "Comprehensive Treatise of Electrochemistry", J. O'M. Bockris, B.E. Conway, E. Yeager, and R.E.White, Editors,151, Plenum Press, New York (1981).

62) H.C. Kuo and K. Nobe, *J. Electrochem. Soc.*, 125, 853, (1978).

63) H.J. Cleary and N.D. Greene, *Corrosion Science*, 9, 603, (1969).

64) Ch. Fabjan, M.R. Kazemi and A. Neckel, *Ber. Bungsenges. Phys. Chem.*, 84, 1026, (1980).

65) D.J. Schiffrin, *Specialist Periodical Reports* - Electrochemistry Vol.8, 131, (1983).

66) B. H. J. Bielski, *Photochem. Photobiol.*, 28, 645, (1978).

67) Z.A. Foroulis, *Corrosion*, 35, 340, (1979).

68) P. Delahay, *J. Electrochem. Soc.*, 97, 198, 205, (1950).

69) D.T. Sawyer and E.T. Seo, *Inorganic Chemistry*, 16, (2), 501, (1977).

70) H.S. Wroblowa, Y-C. Pan, and G. Razumney, *J. Electroanal. Chem. Interfacial. Electrochem.*, 69, 195, (1976).

71) J. Chevalet, F. Rouelle, L. Gierst, and J.P. Lambert, *J. Electroanal. Chem. Interfacial. Electrochem.*, 39, 201, (1972).

72) N.I. Dubrovina and L.N. Nekrasov, *Elektrokhimiya*, 8, 1503, 1972; *Sov. Electrochem. (Engl. Transl.)*, 8, 1466, (1972).

73) a) B. Kastening and G. Kazemifard, *Ber. Bunsenges. Phys. Chem.*, 74, 551, (1970).
b) J. Divisek and B. Kastening, *J. Electroanal. Chem. Interfacial Electrochem.*, 65, 603, (1975).

74) V. Jovancicevic and J. O'M. Bockris, *J. Electrochem. Soc.*, 9, 1797, (1986).

75) J.P. Hoare, in "Encyclopedia of Electrochemistry of the Elements", Vol.II, A. J. Bard, Editor, p. 220, Marcel Dekker, New York (1974).

76) K.I. Noninski and E.M. Lazarov, *Elektrokhimiya*, 9, 673, (1974); 11, 1103, (1975).

77) M.R. Tarasevich and V.A. Bogdanovskaya, *Elektrokhimiya*, 7, 1072, (1971).

78) Ku Ling-Ying, N.A. Shumilova, and V.S. Bagotskii, *ibid.*, 3, 460, (1967).

79) M.R. Tarasevich, A. Sadowski and E. Yeager, in " Comprehensive Treatise in Electrochemistry", Vol. 7, J. O'M Bockris, B.E. Conway, E. Yeager, S.U.M. Khan, and R.E. White, Editors, p.301, Plenum Press, New York (1983).

80) M. Pourbaix, Atlas of Electrochemical Equilibria. Pergamon Press (1966).

81) J. Aston, *J. of the American Electrochem. Soc.*, 29, 449, (1916).

82) G.D. Bengough and D.F. Hudson, *J. Inst. Metals*, 21, 122, (1919).

83) U.R. Evans, *J. Inst. Metals*, 30, 239, (1923).

84) U.R Evans, L.C. Bannister, and S.C. Britton, *Proc. Royal Soc.*, 131A, 355, (1931).

85) H. Kaesche, *Werkst. u. Korrosion*, 15, 379, (1964).

86) U.R. Evans, Corrosion and Oxidation of Metals, First Supplementary Addition, Edward Arnold, 51, (1968).

87) H. Grubitsch, *Monatshefte fur Chemie*, 86, 752, (1955).

88) U.R. Evans, Corrosion and Oxidation of Metals, Edward Arnold, 129, (1960).

89) G.H. Cartledge, *Corrosion*, 18 ,316t, (1962).